IMPLEMENTATION OF NORTHFINDING TECHNIQUES

A THESIS SUBMITTED TO
THE GRADUATE SCHOOL OF NATURAL AND APPLIED SCIENCES
OF
MIDDLE EAST TECHNICAL UNIVERSITY

BY

PINAR OĞUZ

IN PARTIAL FULFILLMENT OF THE REQUIRMENTS
FOR
THE DEGREE OF MASTER OF SCIENCE
IN
ELECTRICAL AND ELECTRONICS ENGINEERING

JUNE 2006

Approval of the Graduate School of Natural and Applied Sciences.

Prof. Dr. Canan Özgen

Director

I certify that this thesis satisfies all the requirements as a thesis for the degree of Master of Science.

Prof. Dr. İsmet Erkmen

Head of Department

This is to certify that we have read this thesis and that in our opinion it is fully adequate, in scope and quality, as a thesis for the degree of Master of Science.

Assoc. Prof. Dr. T. Engin Tuncer

Supervisor

Examining Committee Members

Prof. Dr. Kemal Leblebicioğlu	(METU, EE)	
Assoc. Prof. Dr. T. Engin Tuncer	(METU, EE)	
Assist. Prof. Dr. Çağatay Candan	(METU, EE)	
Assist. Prof. Dr. Afşar Saranlı	(METU, EE)	
Dr. Tolga Sönmez	(TÜBİTAK-SAGE)	

I hereby declare that all information in this document has been obtained and presented in accordance with academic rules and ethical conduct. I also declare that, as required by these rules and conduct, I have fully cited and referenced all material and results that are not original to this work.

Name, Last name: Pınar Oğuz

Signature :

ABSTRACT

IMPLEMENTATION OF NORTHFINDING TECHNIQUES

Oğuz, Pınar

MS, Department of Electrical and Electronics Engineering

Supervisor: Assoc. Prof. Dr. T.Engin Tuncer

June 2006, 131 pages

The fundamental problem of navigation is to find the initial north angle of the body with respect to the reference frame. Determination of the north angle of the body frame is required in spacecraft, aircraft, sea-craft, land-craft and missile control and guidance.

This thesis discusses implementation and comparison of four northfinding techniques. These are GPS (Global Positioning System) based with integer search, GPS based with Kalman filter, accelerometer based and IMU (Inertial Measurement Unit) based techniques. The north angle is determined by the processing of difference measurements of the GPS carrier phase between two antennas at GPS based northfinding techniques. Carrier phase ambiguity resolution is the main problem in GPS based techniques. Since, GPS receiver measures only the fractional part of the carrier phase. Therefore, integer part remains unknown. Two distinct ideas are applied to solve carrier phase ambiguities in two techniques. One of them is integer search on single phase difference. Suitable integer sets are checked on the cost function which is constructed from the single phase difference between two antennas. The other technique uses integer estimator and attitude estimator with Kalman filter rely on double difference phase measurements which are obtained from carrier phase differences of two antennas and two satellites at one instant. To test the GPS based techniques, a realistic GPS emulator is implemented. GPS emulator provides typical GPS raw navigation data including satellite positions, pseudoranges and carrier phases. Accelerometer based northfinding technique is composed of a vertically placed linear accelerometer on a rotating platform. The north angle is found by Coriolis acceleration due to Earth and platform rotation. Implementation problems of this technique in practice are discussed. IMU based northfinding technique has inertial sensor components such as gyroscopes and accelerometers to sense the Earth rotation rate and gravitational force respectively. The north angle is found by the processing of these inertial sensors output. Real set-up is established to test the IMU based technique.

Keywords: northfinding, GPS carrier phase measurements, single phase difference, double phase difference, carrier phase ambiguity, integer search, Kalman Filter, GPS Emulator, Coriolis Effect, accelerometer, gyroscope.

ÖZ

KUZEY BULMA TEKNİKLERİNİN GERÇEKLENMESİ

Oğuz, Pınar
Yüksek Lisans, Elektrik ve Elektronik Mühendisliği Bölümü
Tez Yöneticisi: Doç. Dr. T.Engin Tuncer
Haziran 2006, 131 sayfa

Seyrüseferin temel problemi gövde çerçevesi ve referans sistemi arasındaki kuzeyle yapılan ilk açıyı bulmadır. Kuzeyle yapılan açının belirlenmesi uzay araçları, hava araçları, deniz araçları, kara araçları ve füze sistemlerinin kontrolü ve yönlendirilmesinde gereklidir.

Bu tez dört tane kuzey bulma tekniğinin gerçeklenmesi ve karşılaştırılmasını ele almaktadır. Bunlar GPS tabanlı tamsayı aramaya dayanan, GPS tabanlı Kalman filtreye dayanan, ivmeölçer tabanlı ve AÖB (Ataletsel Ölçüm Birimi) tabanlı tekniklerdir. GPS tabanlı tekniklerde kuzeyle yapılan açı iki anten arasındaki GPS taşıyıcı fazlarının farklarının işlenmesi ile belirlenir. GPS tabanlı tekniklerdeki temel problem taşıyıcı faz belirsizliğidir. Çünkü GPS alıcısı taşıyıcı fazın sadece kesirli kısmını ölçer ve tamsayı kısmı belirsiz kalır. Taşıyıcı faz belirsizliğini çözmek için iki teknikte iki farklı fikir uygulanmıştır. Bir tanesi tek faz farkına uygulanan tamsayı aramadır. Uygun tamsayı setleri iki anten arasındaki tek faz farkından oluşturulan maliyet fonksiyonunda sınanır. Diğer teknik ise bir andaki iki anten ve iki uydu arasındaki faz farklarından oluşturulan ikili faz farkı ölçümlerine dayanan Kalman filtreli tamsayı tahmincisi ve yönelim tahmincisidir. GPS tabanlı teknikleri sınamak için, gerçekçi bir GPS benzetimcisi gerçeklenmiştir. GPS benzetimcisi GPS'in uydu pozisyonu, sözde uzaklık ve taşıyıcı faz gibi tipik ham seyrüsefer bilgilerini sağlar. İvmeölçer tabanlı kuzey bulma tekniği dönen bir platforma dik olarak konulan lineer bir ivmeölçerden oluşmaktadır. Kuzeyle yapılan açı dünyanın ve platformun dönmesi nedeniyle oluşan Coriolis ivmesinden bulunmaktadır. Bu yöntemin pratikteki gerçeklenme problemleri incelenmiştir. AÖB tabanlı kuzey bulma yöntemi dünyanın dönü hızını ve yerçekimi kuvvetini ölçmek için sırasıyla dönüölçer ve ivmeölçer gibi ataletsel ölçerleri içerir. Kuzeyle yapılan açı bu ataletsel ölçerlerin çıktılarının işlenmesiyle bulunur. AÖB tabanlı kuzey bulma tekniğini test etmek için gerçek bir düzenek kurulmuştur.

Anahtar Sözcükler: kuzey bulma, GPS taşıyıcı fazı ölçümleri, tek faz farkı, ikili faz farkı, taşıyıcı faz belirsizliği, tamsayı arama, Kalman Filtre, GPS Benzetimcisi, Coriolis Etkisi, ivmeölçer, dönüölçer.

To my Mum and Dad,

For all their love and support of me in all of my endeavors

ACKNOWLEDGEMENTS

I wish to express my special thanks to my supervisor Assoc. Prof. Dr. T. Engin Tuncer for his guidance, support and suggestions.

I also wish to thank to my colleagues at TÜBİTAK SAGE, especially to Dr. Tolga Sönmez and Ezgi Günaydın for their support and advices.

Besides, I would like to thank to my family, my sister, my fiancé and my friends for their love, support and encouragements.

Finally, the support provided by TÜBİTAK-SAGE to this thesis is greatly acknowledged.

TABLE OF CONTENTS

LIST OF TABLES

LIST OF FIGURES

CHAPTER 1

INTRODUCTION

The focus of this thesis is to implement northfinding techniques. As an introduction, thesis objective, northfinding concept and its importance, literature survey on this subject and the thesis outline are presented.

1.1 Thesis Objective

Main objective of this study is to implement several northfinding techniques. However, in order to achieve this main objective, this thesis has certain additional targets as outlined:

1. GPS (Global Positioning System) structure is implemented to construct a simulation environment for GPS based northfinding techniques. Therefore, this thesis includes detailed information about GPS structure.

2. Attitude determination or northfinding is the process whereby the orientation of the axes of a vehicle system is determined with respect to the reference axis system. Therefore, transformations of coordinate systems are thoroughly explored.

3. Carrier phase measurements of GPS, single-phase difference, double-phase difference, triple-phase difference, cycle ambiguity

problem, integer search, Kalman filter concepts are surveyed and discussed in this thesis.

4. Working principles of inertial sensors such as accelerometers and Coriolis effect are investigated to understand the subject better. Practical usage of accelerometer based northfinding technique is discussed

5. Inertial navigation system concept is discussed. IMU (Inertial Measurement Unit) based northfinding technique is tested with real data obtained from an IMU placed in three-axis motion simulator. This simulator and inertial sensor characteristics are presented in this thesis.

1.2 Northfinding Systems

Attitude determination or northfinding is the process of estimating and computing the system orientation relative to the reference frame of interest, such as inertial frame or local frame. The attitude determination process typically involves various types of sensors and sophisticated algorithms for data processing. The algorithm, the hardware and the data processing determine the accuracy limit. Attitude determination or northfinding has drawn intensive research interest due to its importance in control, guidance and navigation. Numerous results related to attitude determination have been reported in the literature.

The most important problem of a navigated vehicle is determining its position and attitude. Systems that calculate the position, velocity and attitude of a navigated vehicle in a known coordinate system are named as navigation systems. Modern navigation systems are divided mainly into two groups.

First group which is inertial navigation systems determine information about position and attitude by internal means; without external signals. In general, inertial navigation is described as measuring accelerations of the vehicle and taking integral of these measurements to find position, velocity and attitude in a defined coordinate system. In the subject of inertial navigation system: to satisfy the need for attitude information, many attitude sensors have been developed for different platforms and applications. For space vehicles, star trackers, horizon scanners, sun sensors, or magnetometers have been used. Magnetic or electromagnetic compasses provide land or marine vehicles with their heading information. Gyroscopes are used in many kinds of vehicles, including airplanes, land vehicles, marine or submarine and space vehicles. To measure attitude, every attitude sensor or combination of sensors have advantages and disadvantages in terms of system cost, accuracy etc.

On the contrary, second group needs external signal such as electromagnetic signals to calculate position and attitude. For instance, GPS supplies necessary information to the user by using signals from GPS satellites. The role of a GPS receiver as an attitude sensor has attracted a great deal of attention recently due to its many advantages over other sensors that have been available for long time. The greatest advantage of using a GPS receiver as an attitude sensor is that it is very cost-effective. A GPS attitude sensor can produce high accuracy attitude information that is otherwise only possible by using expensive conventional attitude sensors. In addition to the attitude information, a GPS attitude sensor can produce position information too, and can also work as a time reference. Due to this multi-functional capability, one GPS receiver can augment many conventional sensors on vehicle, resulting in a significant savings in a system cost. However, one major drawback of GPS, in particular in military applications, is that it is under the control of a single country. Therefore, the GPS signal can easily be disabled and is not usable.

In this thesis, four northfinding systems are discussed. First one is the GPS based northfinding technique with integer search and second one is the GPS based northfinding technique with Kalman filter. These techniques get their inputs from external signals. Third technique is the accelerometer based northfinding technique. The last one is IMU based northfinding technique. Third and fourth types of northfinding techniques obtain their inputs from internal means.

1.3 Literature Survey on Northfinding Systems

Let us investigate the history of northfinding systems based on GPS. The earlier works on the GPS-based attitude determination can be found in [1, 2]. However, navigation engineers showed great interest in this new concept at the end of the 1980's [3]. A great deal of effort on this GPS application has been concentrated on integrating GPS-based attitude sensors with INS (Inertial Navigation Systems) [4, 5]. GPS based attitude determination systems have been applied to various platforms in various applications. Results on the application of a GPS based attitude sensor to land vehicles are published in [6]. Application of the system to ships is discussed in [7, 8, 9]. Application of the system to determine the attitude of aircraft is reported in [10, 11, 12]. Results of the application of the system to spacecraft are published in [13, 14].

Let us classify the GPS literature according to GPS based northfinding algorithms. Many algorithms are improved in time to increase the accuracy and decrease the computational effort.

First method is exhaustive search [15, 16, 17, 18, 19]. This technique relies on checking all possible integer sets to minimize the properly chosen cost function, while finding the north angle and solving the integer ambiguity. In this method, several updates are done to reduce the search space.

Second method is motion-based [20, 15, 21]. This technique assumes that a certain amount of motion has occurred during the data collection, from either vehicle body rotation or GPS line of sight motion.

Third method is double difference [22, 23, 24, 25, 26, 27, 28, 29]. All existing literature on this technique use the double differences of GPS carrier phases as observables. However, while finding rough initial attitude, integer ambiguity or the north angle, they use different processes. For example, in references [22, 25, 26, 28], Kalman filter is applied on double phase differences to find the integer ambiguity and the north angle. In addition, initial condition, which is rough initial attitude, is calculated from triple phase differences. In references [23, 24, 29], least square error approach is applied on double phase differences. In reference [27], the artificial neural network is applied.

Fourth method is dual baseline [30, 31]. In this technique, three antennas or in other words two baselines are used. One of the baselines is short and the other one is long. Using short baseline, rough initial attitude is determined. Then, using longer baseline and rough initial attitude in filter process, integer ambiguity is solved and attitude of the vehicle is determined.

For the above methods, different number of antennas or satellites or different filtering techniques can be considered. Other than these methods, new methods are developed everyday for different applications.

The concept of accelerometer based northfinding systems is very new [32, 33, 34]. Therefore, there are not many sources on these systems. However, as more accurate accelerometers are created and more practical set-ups are prepared, these systems will provide low-cost and light northfinding. These systems use a rotating platform, one or two accelerometers which are placed vertically and horizontally to detect the Coriolis effect arises from rotation of platform and Earth.

IMU based northfinding method is another surveyed method. Inertial navigation systems are arranged easily to yield the north angle of the vehicle with respect to reference frame [35, 36]. Strapdown inertial navigation systems are composed of inertial sensors, which are gyroscopes and accelerometers. Gyroscopes and accelerometers measure vehicle angular accelerations and linear accelerations respectively. By using these measurements and algebra, the north angle of the vehicle can be found.

1.4 Thesis Outline

This thesis consists of six chapters including the introduction chapter.

Chapter-2 presents GPS and GPS signal structure, implementation of a GPS emulator to test and to construct inputs of GPS based northfinding technique. Satellite constellation, raw GPS data creation, elevation and azimuth angle of satellites for a given user position and orientation are discussed. In addition, coordinate frames are presented.

Chapter-3 presents GPS based northfinding technique with exhaustive search for single-phase difference. In this chapter, carrier phase measurements, single-phase difference, cycle ambiguity resolution and integer search are presented. Advantages and disadvantages of the technique are given.

Chapter-4 introduces GPS based northfinding technique with Kalman Filter for double phase difference. Double difference, triple difference and cycle ambiguity resolution with Kalman filter are introduced. Advantages and disadvantages of the technique are given. Chapters-3 and 4 present the northfinding techniques, which get inputs from external signals or means.

Chapter-5 provides information about accelerometer based northfinding technique. Coriolis effect, accelerometer structure and working principles of accelerometers are presented. An overview of the technique is given to be compared with the other methods.

Chapter-6 gives detailed information about IMU based northfinding technique. IMU structure and types, inertial sensors and simulation environment characteristics are provided. Advantages and disadvantages of the technique are given. Chapters 5 and 6 present the northfinding techniques, which get inputs from internal means (inertial sensors). Conclusion is the last chapter of the thesis to present the importance and the results of this study.

CHAPTER 2

GPS SIGNAL AND GPS EMULATOR

The Global Positioning System (GPS) has been developed for enabling accurate positioning and navigation anywhere on or near the surface of the earth. It is envisaged that GPS receivers will be embarked on many aircraft and spacecraft in the future for navigation purposes, supplying mainly position and time information. Therefore, there has been an increasing interest in the development of additional applications of this navigation system as it is attitude determination. Although originally developed as a means for navigation, GPS has since been shown to be an abundant source of attitude information as well.

A GPS Emulator is developed in order to simulate navigation scenarios such as integrated navigation systems or attitude determination. GPS emulator calculates pseudoranges, carrier-phases, orbit information, elevation, azimuth angles and PRN (pseudo-random) numbers of the visible satellites seen by the user. The emulator implements the stochastic error sources in the GPS system such as atmospheric errors, satellite clock errors, receiver clock errors.

This chapter includes the detailed information about GPS Signal and the GPS Emulator. Firstly, overview of GPS and GPS signals are presented. Afterwards, the GPS Emulator is implemented to test the correctness of the GPS based northfinding algorithm and examination of errors. Detailed descriptions on GPS Emulator implementation such as setting the satellite constellation, finding satellite azimuth and elevation angle, satellite selection and errors on GPS Emulator, are given.

2.1 GPS

The GPS is a space-based, all-time, all-weather navigation system developed by the Department of Defense of USA to determine position, velocity, and time for a user that is on (or near) the earth. The system consists of three segments: space segment, control segment, and user segment.

The space segment consists of 24 satellites that form the constellation deployed in six evenly spaced planes with an inclination of 55^{o} and 4 satellites per plane, as shown in Figure 1.

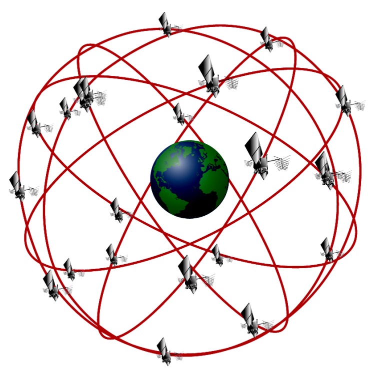

Figure 1. GPS Satellite Constellation

The distance between a satellite and the surface of earth is about 20200 km. Each satellite vehicle transmits two microwave carrier signals, in L1 frequency (1575.42 MHz) and in L2 frequency (1227.60 MHz). The L1 frequency carries the navigation message and code signal for the Standard

Position Service, which is a positioning and timing service; while the L2 frequency is used to measure the ionospheric delay for Precise Position Service (PPS). Three binary codes shift the L1 and/or L2 carrier phase. C/A (Coarse Acquisition) code is 1.023 MHz Pseudo Random Noise (PRN) Code that is uniquely defined for each satellite to identify the satellite vehicle and the transmission time between each satellite vehicle and the GPS receiver. The Precise P(Y)-Code is a 10.23 MHz PRN code for PPS by authorized users. The navigation message is a 50 Hz signal consisting of data bits that describe the GPS satellite orbits, clock corrections, and other system parameters. C/A Code is modulated on the L1 carrier only, while P(Y) Code and Navigation Message are modulated on both the L1 and the L2 carriers, as indicated in Figure 2.

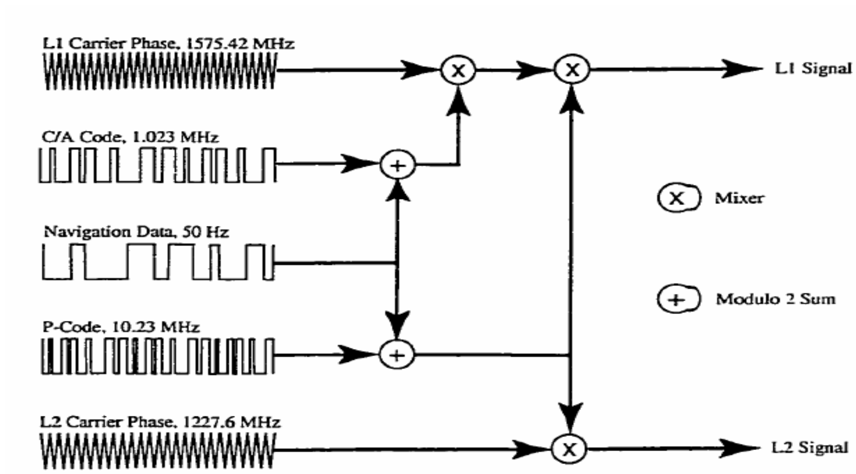

Figure 2. GPS Satellite Signals

The control segment consists of a master control station, five monitor stations, and ground stations with the main operational tasks of uploading the message to the satellites and tracking the satellites for orbit determination, orbit prediction, and time synchronization.

At the user segment, both military and civilian users use GPS receivers to determine the position, velocity, and time. GPS receivers measure time delays and decode messages from in-view satellites to determine the information necessary to complete position and time bias calculations. The military PPS GPS receivers have the ability to output all the C/A Code, P(Y) code, carrier L1, and carrier L2, and navigation messages. However, the civilian users can only reach the C/A Code pseudorange, carrier L1, carrier L2, and navigation messages [37, 38].

2.2 GPS Emulator

In this section, a realistic GPS emulator is developed. GPS emulator calculates typical raw navigation data from available satellites for a given receiver position and attitude at a given time.

GPS emulator inputs are the receiver's latitude, longitude, height, orientation (roll, pitch and yaw angles) and the receiver time. GPS emulator calculates pseudoranges, carrier-phases, orbit informations, elevation, azimuth angles and PRN (pseudo-random) numbers of the visible satellites seen by the user [39].

Pseudorange measurements, provided by GPS satellites, contain errors such as atmospheric and clock delays. In this GPS emulator, stochastic models of the pseudorange error sources are considered in order to provide the pseudorange measurements as realistic as possible. Pseudorange stochastic error models will be described in detail later.

Carrier phase measurements are constructed from non-erroneous pseudorange measurements by dividing pseudorange measurements with carrier wavelength. Afterwards, multipath error can be added into carrier phase measurement to get realistic measurements.

GPS Emulator finds out the visible satellites and their positions for a given user position and orientation at a given time. Coordinate conversions between different frames are applied in gathering the satellite information [40]. Furthermore, elevation and azimuth angles of the GPS satellites and the user orientation are computed since these angles are the decision criteria for the determination of the visible satellites. In addition, mathematical representation for the decision criteria is developed.

2.2.1 Coordinate Systems

In this part, coordinate systems are introduced for the understandability of the following chapters. Coordinate systems (reference frames) are established such that information can be exchanged between interfacing systems in a consistent manner. These reference frames are orthogonal and right-handed. In the following, reviews of the definitions of some commonly used coordinate systems.

2.2.1.1 ECI (Earth Centered Inertial) Frame

ECI frame has its origin at the centre of the Earth and axes are non-rotating with respect to the fixed stars, defined by the axes x_{ECI} , y_{ECI} , z_{ECI} with z_{ECI} coincident with the Earth's polar axis (which is assumed to be invariant in the direction)

2.2.1.2 ECEF (Earth Centered Earth Fix) Frame

ECEF frame has its origin at the center of the Earth and axes which are fixed with respect to the Earth, defined by the axes x_{ECEF} , y_{ECEF} , z_{ECEF} with z_{ECEF} along the Earth's polar axis. The axis x_{ECEF} lies along the intersection of the plane of the Greenwich meridian with the Earth's equatorial plane. The earth frame rotates, with respect to the inertial frame, at a rate w_e about the axis z_{ECI} . ECI Frame and ECEF Frame are shown in Figure 3.

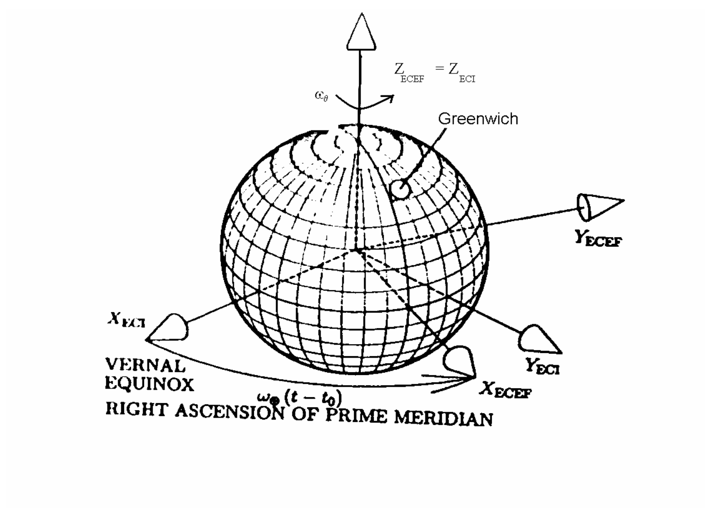

Figure 3. ECI and ECEF Frames

2.2.1.3 Navigation Frame

On Earth, the coordinate system is typically defined to be locally level. The positive x-axis is pointed north, the positive y-axis is pointed east, and the positive z-axis is pointed down. In Figure 4, navigation frame E-N-U (East-North-Up) is seen.

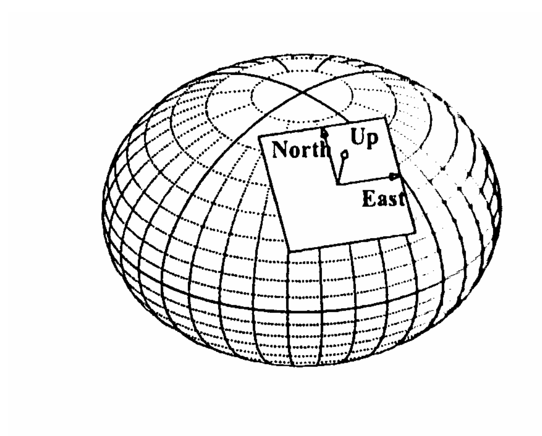

Figure 4. Locally Level Coordinate System (E-N-U)

2.2.1.4 Body Frame

The body frame is an orthogonal axis set, which is aligned with the roll, pitch and yaw axes of the vehicle. For the body (for example aircraft) coordinate system, the positive x-axis is directed towards the nose, the positive y-axis points along the right wing, and the positive z-axis is directed towards the floor of the aircraft as seen in Figure 5.

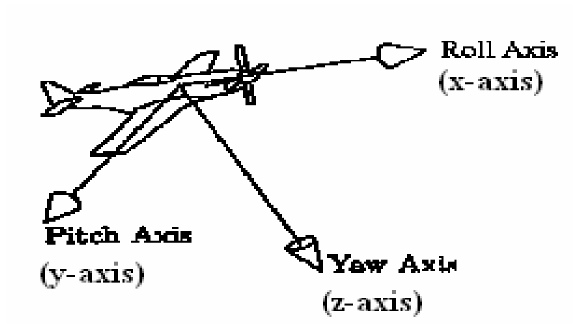

Figure 5. Body Frame

2.2.2 Satellite Constellation

There are 24 GPS satellites around the world and the satellites are placed at 6 orbits (4 satellites per orbit). Satellite constellation is defined by using different argument of perigee, inclination angle and right ascension angle for each satellite. Therefore, first step of the algorithm is to appoint the argument of perigees, inclination angles and right ascension angles of all 24 satellites (for the definition of these terms see Figure 6).

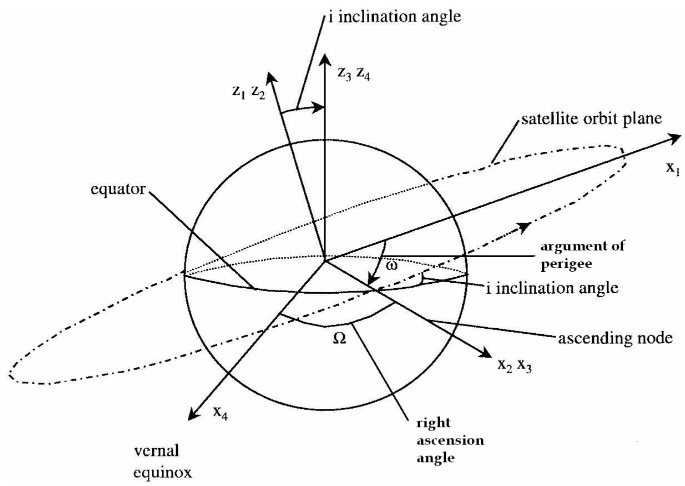

Figure 6. Earth Equator and Orbit Plane

Argument of perigee (ω) is found for each satellite by multiples of 45° plus a phase difference. Inclination angle (i) is 55° for each satellite. The right ascension angle (Ω) of six different orbits are 60° apart from each other. These are typical GPS parameters [41].

The next step is to compute the position of each satellite in ECEF by using w, i, Ω, initial time and the receiver time. To find the position of each satellite, true anomaly (v), the distance r from the satellite to the center of the earth should also be known. General view of the satellite geometry in the two dimensional orbital frame is shown in Figure 7.

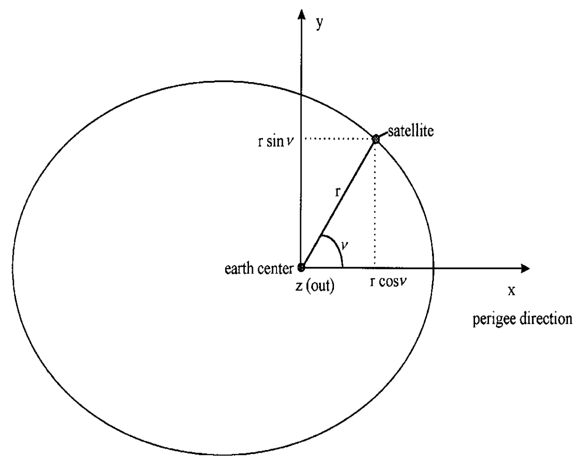

Figure 7. Satellite Geometry

Analytically, the position of the satellite on the two dimensional orbital plane can be calculated as in Equation 2.1.

$$\begin{aligned} x &= r \cos v \\ y &= r \sin v \\ z &= 0 \end{aligned} \qquad (2.1)$$

Where:

x, y, z : Satellite position in two dimensional orbital frame

v : True anomaly (parameter related with the period of the satellite)

r: Distance from the satellite to the center of the earth

These coordinates has to be converted to a common three-dimensional coordinate frame for the calculations. To transform this 2 dimensional orbital frame to ECI frame, it has to be rotated with w, Ω, i around appropriate axes according to Figure 6. After these rotations, coordinates of satellite in ECI become as in Equation 2.2.

$$\begin{bmatrix} x_{eci} \\ y_{eci} \\ z_{eci} \end{bmatrix} = C_3^4 C_2^3 C_1^2 \begin{bmatrix} r\cos v \\ r\sin v \\ 0 \end{bmatrix} = \begin{bmatrix} r\cos\Omega \quad \cos(v+\omega) - r\sin\Omega \quad \cos i \sin(v+\omega) \\ r\sin\Omega\cos(v+\omega) + r\cos\Omega\cos i\sin(v+\omega) \\ r\sin i\sin(v+\omega) \end{bmatrix} \qquad (2.2)$$

Where:

x_{eci}, y_{eci}, z_{eci}: Satellite position in ECI frame,

C_i^j: Direction cosine matrix corresponding to the transformation from *i* frame to *j* frame,

ω: Argument of perigee,

i: Inclination angle,

Ω: Right ascension angle.

After these transformations, position of satellite is in the ECI frame, and does not rotate with the earth. In order to refer a certain point on the surface of the earth, the rotation of the earth must be taken into consideration. This coordinate system is referred to as ECEF frame. To consider the earth rotation, Equation 2.3 is used.

$$\Omega_{er} = \Omega - \dot{\Omega}_{ie}\, t_{er} \qquad (2.3)$$

Where:

$\dot{\Omega}_{ie}$: Earth rotation rate,

t_{er} : When t_{er} =0 Greenwich meridian aligns with the vernal equinox.

Hence, the overall transform of satellite position from orbital frame to ECEF frame is shown in Equation 2.4.

$$\begin{bmatrix} x_{ecef} \\ y_{ecef} \\ z_{ecef} \end{bmatrix} = C_3^4 C_2^3 C_1^2 \begin{bmatrix} r\cos v \\ r\sin v \\ 0 \end{bmatrix} = \begin{bmatrix} r\cos\Omega_{er}\cos(v+\omega) - r\sin\Omega_{er}\cos i\sin(v+\omega) \\ r\sin\Omega_{er}\cos(v+\omega) + r\cos\Omega_{er}\cos i\sin(v+\omega) \\ r\sin i\sin(v+\omega) \end{bmatrix} \quad (2.4)$$

GPS emulator operates in ECEF frame. User position (ϕ-latitude, λ-longitude, h–height) in navigation frame is transformed to ECEF frame (x_u, y_u, z_u) as shown in Equations 2.5, 2.6 and 2.7 [38].

$$x_u = \left(\frac{r_e}{\sqrt{(1-\varepsilon^2 \sin^2 \phi)}} + h \right) \cos\phi \cos\lambda \qquad (2.5)$$

$$y_u = \left(\frac{r_e}{\sqrt{(1-\varepsilon^2 \sin^2 \phi)}} + h \right) \cos\phi \sin\lambda \qquad (2.6)$$

$$z_u = \left(\frac{r_e\left(1-\varepsilon^2\right)}{\sqrt{(1-\varepsilon^2 \sin^2 \phi)}} + h \right) \sin\phi \quad (2.7)$$

Where:

x_u, y_u, z_u: User position in ECEF frame,

ε : Eccentricity of the earth,

ϕ : Latitude of user in navigation frame,

λ : Longitude of user in navigation frame,

h : Height of user in navigation frame.

A typical satellite track obtained from GPS Emulator in ECI and ECEF coordinate frames are shown in Figure 8 and Figure 9. In inertial frame, a GPS satellite orbit is almost circular. However, relative to earth, its track is quite different.

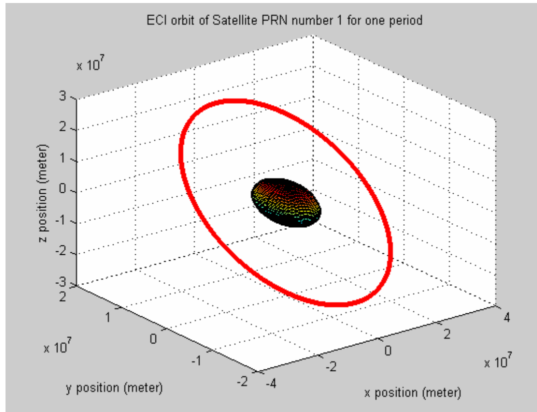

Figure 8. Satellite Orbit in ECI Frame

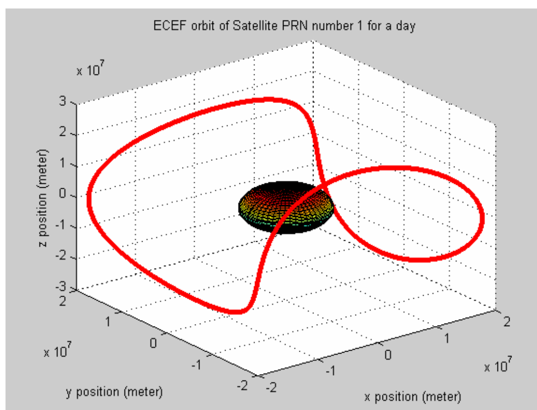

Figure 9. Satellite Orbit in ECEF Frame

2.2.3 Satellite Elevation and Azimuth Angles

By using the receiver (user) position and satellite positions (x_{ecef} y_{ecef} z_{ecef}) in ECEF frame, elevation and azimuth of each satellite can be found as in Figure 10.

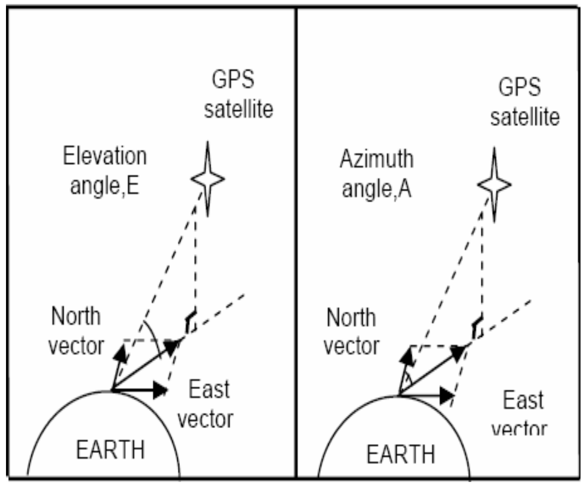

Figure 10. Elevation and Azimuth Angles of GPS Satellites

The Local East, North and Up unit vectors at the receiver position are

$$\text{East} = (-y_u / p, x_u / p, 0) \quad (2.8)$$

$$\text{Up} = (x_u / R, y_u / R, z_u / R) \quad (2.9)$$

$$\text{North} = (-x_u z_u / (pR), -y_u z_u / (pR), p / R) \quad (2.10)$$

Where:

$p = \sqrt{(x_u^2 + y_u^2)}$,

$R = \sqrt{(x_u^2 + y_u^2 + z_u^2)}$.

The unit line of sight vector V from the user to the satellite is

$$V = (\frac{(x_{ecef} - x_u)}{D}, \frac{(y_{ecef} - y_u)}{D}, \frac{(z_{ecef} - z_u)}{D}) \quad (2.11)$$

$$D = \sqrt{((x_{ecef} - x_u)^2 + (y_{ecef} - y_u)^2 + (z_{ecef} - z_u)^2)} \quad (2.12)$$

From the geometry in Figure 10, elevation angle E and the azimuth angle A can be found as:

$$\sin(E) = V \cdot \mathrm{Up} \qquad (2.13)$$

$$\tan(A) = \frac{(V \cdot \mathrm{East})}{(V \cdot \mathrm{North})} \quad (2.14)$$

2.2.4 Satellite Selection

The orientation of the receiver (roll, pitch and yaw) and the positions of the 24 GPS satellites are processed to find detectable satellites. The first criterion is that the available satellites have to be above the horizon; otherwise, the receiver can not get any signal from that satellite.

Criterion 1: $E > 0$

Secondly, only the satellites that have a line of sight within $90°$ with respect to antenna direction can be detected.

Criterion 2: $0° < \arcsin(V \cdot u_{antenna}) < 90°$

Where:

$u_{antenna}$: Antenna direction in ECEF frame which can be calculated from roll, pitch and yaw angles.

The satellites that pass these criteria used for further processing.

2.2.5 Pseudorange Measurement

In order to make a position fix, the distance from the antenna to the satellite has to be known. Distance measurement is achieved by calculating the travel time of the GPS signal from satellite to antenna. This should be very precise as the signal propagates at the speed of light. In GPS terminology, this distance is called pseudorange. The word "pseudo" is used since this measurement includes errors such as GPS satellite clock error, atmospheric errors and receiver clock bias. Equation 2.15 defines pseudorange simply as the Euclidean distance between the satellite and the receiver.

$$\rho = \sqrt{((x_i - x_u)^2 + (y_i - y_u)^2 + (z_i - z_u)^2)} \qquad (2.15)$$

Where:

ρ : Pseudorange,

(x_i, y_i, z_i) : i^{th} satellite position,

(x_u, y_u, z_u) : Receiver (user) position.

In GPS emulator, pseudorange measurement output is provided by adding the errors to ρ as Equation. 2.16:

$$\rho_{output} = \rho + \tau_{ion} + \tau_{tro} + \Delta t_{satellite} + \Delta t_{user} \quad (2.16)$$

Where:

ρ_{output} : GPS emulator pseudorange output,

τ_{ion}, τ_{tro} : Ionosphere and troposphere errors,

$\Delta t_{satellite}$: GPS satellite clock error,

Δt_{user} : GPS user clock error.

2.2.5.1 Satellite Clock Error:

Satellite clock error bias is defined uniquely for each satellite. Moreover, white noise is added to this bias. In GPS emulator, satellite clock error is defined as white noise having 2.0 m bias with 0.7 m standard deviation [42]. Satellite clock error is modeled as shown in Figure 11.

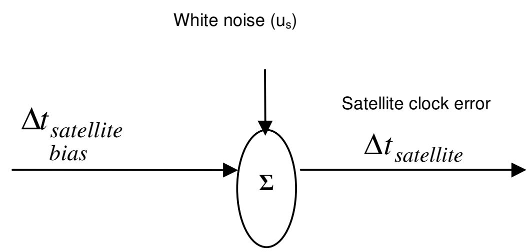

Figure 11. Satellite Clock Error Model

2.2.5.2 Ionosphere Error

Ionosphere error model used in GPS emulator is the GPS ionosphere model. According to this model, the form of the single-frequency GPS user ionosphere correction algorithm requires the user's approximate geodetic latitude, longitude, elevation and azimuth angles to the satellite and the ionosphere correction coefficients. It is important that at a given time ionosphere correction parameters are same for all the tracked satellites. As a result of the correction algorithm, low elevation satellites have larger ionosphere error.

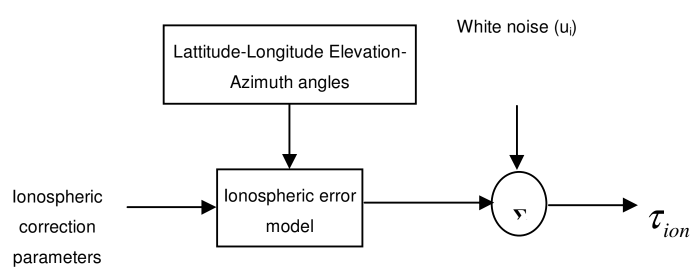

Figure 12. Ionosphere Error Model

White noise is added to the calculated ionosphere error in order to include the indefiniteness of the used model. Described approach is illustrated in Figure 12. In GPS emulator, u_i is defined as zero mean with having 0.5 m standard deviation [42].

2.2.5.3 Troposphere Error

Compared with the ionosphere effect, the troposphere effect is about an order of magnitude less. There are many models to calculate the effect. The simple model as shown in Equation 2.17 is used in this thesis.

$$\Delta_{tro} = \frac{2.47}{\sin(E) + 0.0121} \qquad (2.17)$$

Where:

Δ_{tro} : Calculated troposphere error,

E : Elevation angle.

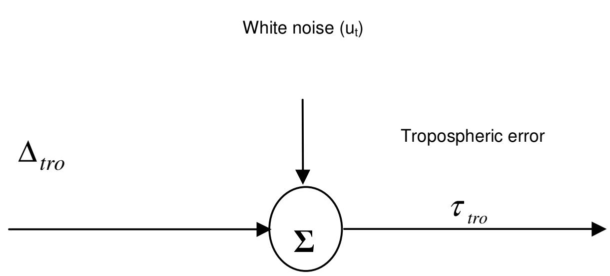

Figure 13. Troposphere Error Model

In GPS emulator, troposphere error is defined as Δ_{tro} plus zero mean 0.5 m standard deviated white noise [42]. White noise is added as shown in Figure 13.

2.2.5.4 User Clock Bias Error

GPS user clocks are not as stable as the satellite atomic clocks. Hence, clock bias is observed directly in the pseudorange. Clock bias and clock drift change from receiver to receiver. The clock model is given in Figure 14.

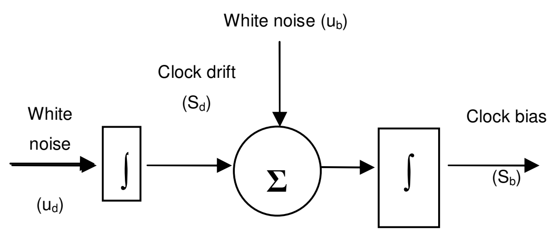

Figure 14. User Clock Bias Error Model

2.2.6 Carrier Phase Measurement

GPS based northfinding techniques use carrier phase measurement obtained from GPS satellite as fundamental observables. In this work, carrier phase measurements are constructed from non-erroneous pseudorange measurement by dividing pseudorange measurement with carrier wavelength. In this way, carrier cycles are created. Since GPS receivers only measure the fractional component of phase cycles, *rem* function in MATLAB is applied to phase cycles to get fractional component. Afterwards, fractional component is subtracted from the whole to form integer part, which is the critical part to be solved by GPS based northfinding algorithm. Afterwards, multipath error can be added into carrier phase measurement to get realistic measurements seen in Figure 15.

As a rule of thumb, multipath error on carrier phase measurement can be considered to have a variance as follows [43, 15, 20, 28].

$$\sigma^2_{multipath\_error}(cycle) = (0.5cm/\lambda)^2 \qquad (2.18)$$

Where:

λ: Wavelength (cm)

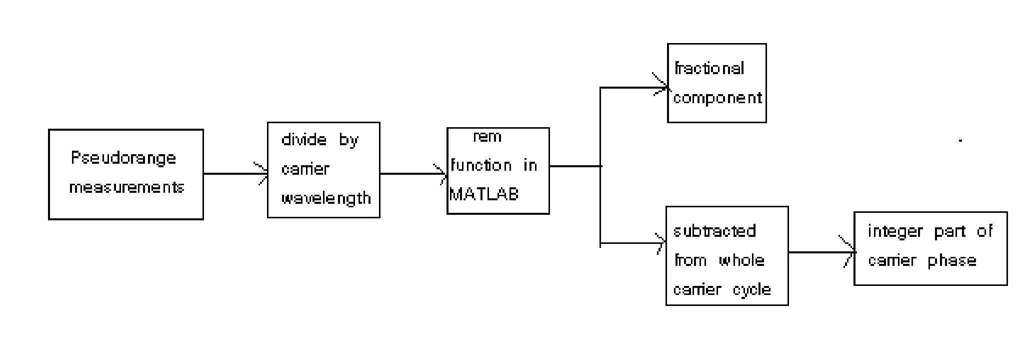

Figure 15. Construction of Carrier Phase in GPS Emulator

2.2.7 User Position Calculation

GPS based northfinding techniques use GPS emulator outputs to calculate the user position. User position calculation from GPS emulator outputs is given in this part for the sake of completeness. User position is calculated from pseudorange measurements and GPS satellite positions as in Equation 2.19 [41].

$$\rho_i = \sqrt{((x_i - x_u)^2 + (y_i - y_u)^2 + (z_i - z_u)^2)} + b_u \qquad (2.19)$$

Where:

ρ_i : Pseudorange from satellite *i*,

(x_i, y_i, z_i) : i^{th} satellite position,

(x_u, y_u, z_u) : Receiver (user) position,

b_u : User clock bias error.

It is difficult to solve Equation 2.19, since it is a nonlinear equation. However, it can be linearized. In this equation, user position and user clock bias error are unknown. Differentiate this equation with respect to user position and user clock bias error,

$$\delta\rho_i = \frac{(x_i - x_u)\delta x_u + (y_i - y_u)\delta y_u + (z_i - z_u)\delta z_u}{\sqrt{((x_i - x_u)^2 + (y_i - y_u)^2 + (z_i - z_u)^2)}} + \delta b_u$$

$$\delta\rho_i = \frac{(x_i - x_u)\delta x_u + (y_i - y_u)\delta y_u + (z_i - z_u)\delta z_u}{\rho_i - b_u} + \delta b_u \qquad (2.20)$$

In Equation 2.20, δx_u, δy_u, δz_u and δb_u can be considered as the only unknowns. x_u, y_u, z_u, b_u are treated as known values, since one can assume some initial values for these quantities. From these initial values a new set of δx_u, δy_u, δz_u and δb_u can be calculated. These values are used to modify the original x_u, y_u, z_u, b_u to find another new set of solutions. This new set of x_u, y_u, z_u, b_u can be considered again as known quantities. This process continues until the absolute values of δx_u, δy_u, δz_u and δb_u are very small and within a certain predetermined limit. The final values of x_u, y_u, z_u, b_u are the desired solution. This method is often referred to as the iteration method.

With δx_u, δy_u, δz_u and δb_u as unknowns, Equation 2.20 becomes a set of linear equation. This procedure is often referred to as linearization. For four satellites, Equation 2.20 can be written in matrix form as

$$\begin{bmatrix} \delta\rho_1 \\ \delta\rho_2 \\ \delta\rho_3 \\ \delta\rho_4 \end{bmatrix} = \begin{bmatrix} \alpha_{11} & \alpha_{12} & \alpha_{13} & 1 \\ \alpha_{21} & \alpha_{22} & \alpha_{23} & 1 \\ \alpha_{31} & \alpha_{32} & \alpha_{33} & 1 \\ \alpha_{41} & \alpha_{42} & \alpha_{43} & 1 \end{bmatrix} \begin{bmatrix} \delta x_u \\ \delta y_u \\ \delta z_u \\ \delta b_u \end{bmatrix} \qquad (2.21)$$

Where:

$$\alpha_{i1} = \frac{(x_i - x_u)}{\rho_i - b_u},\ \alpha_{i2} = \frac{(y_i - y_u)}{\rho_i - b_u},\alpha_{i3} = \frac{(z_i - z_u)}{\rho_i - b_u} \qquad (2.22)$$

Equation 2.21 can be written in more compact form as

$$\delta\rho = \alpha\delta x \qquad (2.23)$$

Assuming more satellites, the solution of Equation 2.23 is as follows

$$\delta x = \left[\alpha^T \alpha\right]^{-1} \alpha^T \delta\rho \qquad (2.24)$$

In order to find desired user position solution, Equation 2.24 must be used repetitively in an iterative way. A quantity is often used to determine whether the desired result is reached and this quantity can be defined as in Equation 2.25.

$$\delta v = \sqrt{\delta x_u^2 + \delta y_u^2 + \delta z_u^2 + \delta b_u^2} \qquad (2.25)$$

When this value is less than a certain predetermined threshold, the iteration will stop. In this iterative process, initial values for x_u, y_u, z_u, b_u are zero. $\delta\rho_i$ is calculated from the difference between measured and calculated pseudorange measurements. In addition, calculated value ρ_i is used to calculate $\alpha_{i1}, \alpha_{i2}, \alpha_{i3}$ at each step.

2.3 Summary

Here, a realistic stochastic model for a general-purpose GPS receiver is developed to test navigation scenarios such as attitude determination in MATLAB environment. Twenty-four satellite tracks are simulated and the emulator reports the satellites that are detectable in a real time scenario. Two basic criteria for satellite detection are defined; other constraints can also be implemented in the emulator. Moreover, realistic errors of GPS are considered on pseudorange measurements and carrier phase measurements. In addition, calculation of user position is given.

CHAPTER 3

GPS BASED NORTHFINDING TECHNIQUE WITH EXHAUSTIVE SEARCH

The goals of this chapter and the next chapter are to utilize the precise positioning potential of GPS for attitude determination or in other words northfinding. In GPS based northfinding algorithm, attitude or the north angle is determined by processing difference measurements of the GPS carrier phase between two or more antennas. In this thesis, two antennas are used. Carrier phase difference measurements are ambiguous because of the unknown number of GPS signal cycles received. GPS receiver senses only the fractional component of the GPS carrier phase. Therefore, resolution of the GPS signal cycle ambiguity becomes a necessary task before determining the attitude or the north angle for a stand-alone GPS attitude sensing system [22].

Two techniques used in solving carrier phase cycle ambiguities are described in this chapter and in the next chapter. The first idea is to use exhaustive integer search on single-phase difference of the GPS carrier phase. The other one is the triple phase difference with a Kalman filter for minimizing the attitude estimate error.

In this chapter, GPS based northfinding algorithm based on single-phase difference with integer search is presented. Detailed descriptions of the set up and the algorithm are given. Concept of the GPS carrier phase measurement is introduced. Afterwards, cycle ambiguity resolution method, integer search on single-phase difference, is explained. Then, errors in GPS based northfinding algorithm with integer search are examined. In northfinding algorithm, errors such as multipath on carrier phase are considered in order to simulate the measurements as realistic as possible. Afterwards, application scheme and program results are explained. All the simulations are done in MATLAB. GPS Emulator is used for the simulation of northfinding algorithm. In the northfinding algorithm, GPS emulator outputs such as pseudorange and carrier phase measurements, baseline vector are used. Finally, overview of this GPS based northfinding technique is considered in order to give a general idea to the reader.

3.1 Concept of GPS Based Northfinding Technique

In this section, development of GPS based northfinding algorithm and the set up are explained.

3.1.1 Set Up

Attitude is defined by the transformation, which relates a coordinate system fixed in space to a coordinate system fixed in the body. Locally level navigation frame and the body frame are related through the antenna locations since the antennas construct a baseline and a pointing vector, which defines the attitude or the north angle of the body. The antenna locations in two coordinate systems are related as follows:

$$R_n = AR_b \qquad (3.1)$$

Where:

R_n: Matrix containing the locations of the antennas in locally level coordinate frame

R_b: Matrix containing the locations of the antennas in the body coordinate frame

A: Attitude transformation matrix.

Matrix A is defined as the product of three rotation matrices, each of which specifies a rotation about a certain body coordinate system axis.

When the body frame is rotated about the heading axis by the heading angle ψ,

$$A_1 = \begin{bmatrix} \cos(\psi) & \sin(\psi) & 0 \\ -\sin(\psi) & \cos(\psi) & 0 \\ 0 & 0 & 1 \end{bmatrix} \qquad (3.2)$$

rotated about the pitch axis by the pitch angle θ,

$$A_2 = \begin{bmatrix} \cos(\theta) & 0 & -\sin(\theta) \\ 0 & 1 & 0 \\ \sin(\theta) & 0 & \cos(\theta) \end{bmatrix} \qquad (3.3)$$

rotated about the roll axis by the roll angle ϕ,

$$A_3 = \begin{bmatrix} 1 & 0 & 0 \\ 0 & \cos\phi & \sin\phi \\ 0 & -\sin\phi & \cos\phi \end{bmatrix} \qquad (3.4)$$

The resulting attitude matrix A can be shown as follows:

$$A = A_3 A_2 A_1 = \begin{bmatrix} \cos\theta\cos\psi & \cos\theta\sin\psi & -\sin\theta \\ -\cos\phi\sin\psi + \sin\phi\sin\theta\cos\psi & \cos\phi\cos\psi + \sin\phi\sin\theta\sin\psi & \sin\phi\cos\theta \\ \sin\phi\sin\psi + \cos\phi\sin\theta\cos\psi & -\sin\phi\cos\psi + \cos\phi\sin\theta\sin\psi & \cos\phi\cos\theta \end{bmatrix}$$

(3.5)

Calculating attitude transformation matrix A gives the attitude or the north angle of the body. A set up, which is constructed from two antennas and a single baseline, is placed on the body axis towards to nose of the vehicle in practice. This system is shown in Figure 16.

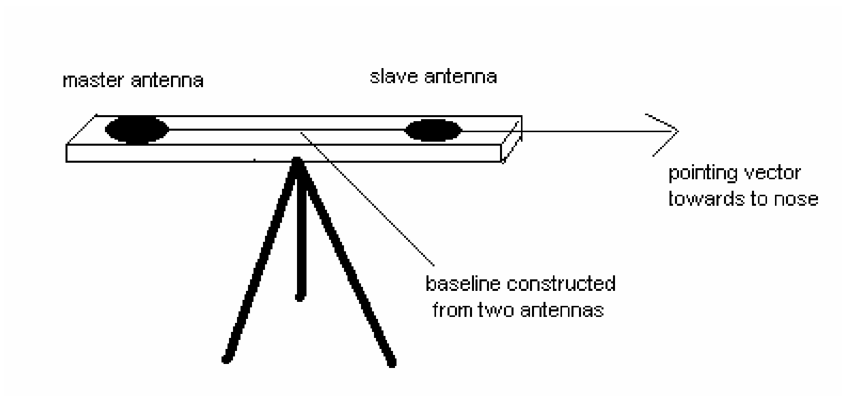

Figure 16. GPS Based Northfinding with Two Antennas

To calculate the attitude of the vehicle, the relative phase difference of the GPS carrier is measured between the pair of antennas spaced about some distance apart, which is discussed in the next part.

3.1.2 Carrier Phase Measurement and Algorithm

In GPS based northfinding algorithm, two GPS receivers or antennas are used. The main measurement used for attitude determination is the phase difference of the GPS signals received from two antennas separated by a baseline. The phase difference between antennas is also referred to as a single-phase difference.

The distance between the antennas and a GPS satellite is much larger than the baseline length between two antennas, such that the GPS carrier signal can be treated as a plane wave [20]. A signal traveling at the speed of light arrives at the antenna closer to the satellite slightly before reaching the other as seen in Figure 17. By measuring the difference in carrier phase between the antennas, a receiver can determine the relative range between the pair of antennas. With the addition of carrier phase between the antennas from multiple satellites using two antennas, the receiver can estimate the north angle of the vehicle [43].

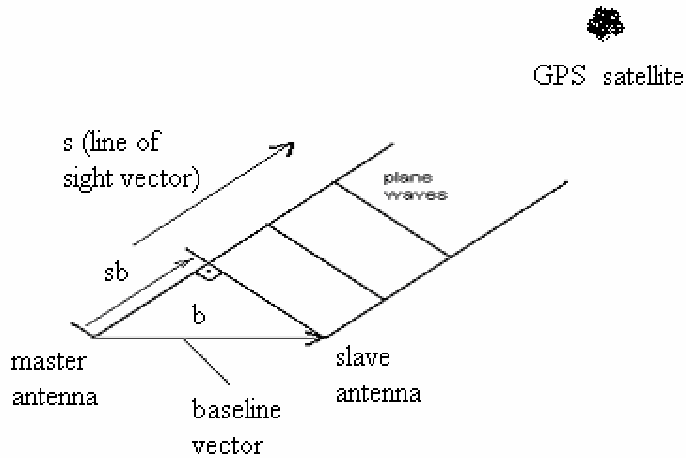

Figure 17. Carrier Phase Measurement

The measured differential phase, $\Delta\Phi$ (measured in wavelengths), is proportional to the projection of the baseline vector b(3x1), (measured in wavelengths), into the line of sight unit vector to the satellite, $\hat{s}$(3x1), for baseline i and satellite j. The GPS receiver measures the fractional part of the differential phase. The integer component k must be resolved through independent means before the differential phase measurement can be interpreted as a differential range measurement. The above expressions are in Equation 3.6.

$$\Delta\Phi_{ij} = \hat{s}_j^T b_i - k_{ij} + v_{ij} \qquad (3.6)$$

Where:

v_{ij} : Additive, time-correlated measurement noise from the relative ranging error sources,

$\hat{s}_j$: Line of sight unit vector to the satellite j,

b_i : Baseline vector i,

k_{ij} : Integer ambiguity.

To clarify the presentation, it is first assumed that the cycle ambiguities are already known. If the integers are known, then the differential phase measurement can be treated explicitly as differential range measurements through the relationship in Equation 3.7.

$$\Delta r = \Delta\Phi + k \qquad (3.7)$$

An optimal attitude solution for a given set of range measurements Δr_{ij} taken at a single instant for baseline *i* and satellite *j* is obtained by minimizing the quadratic attitude determination cost function in Equation 3.8.

$$J(A) = \sum_{i=1}^{m}\sum_{j=1}^{n}(\Delta r_{ij} - b_i^T A\hat{s}_j)^2 \qquad (3.8)$$

Where:

m: Number of baselines,

n: Number of satellites,

$b_i\,(3x1)$: Baseline vector defined in the body frame,

$\hat{s}(3x1)$: Line of sight to the GPS satellite given in the local horizontal frame,

A (3x3): Right handed, orthonormal attitude transformation matrix (det*A*=1, $A^T A = I$) from the local horizontal frame to the body frame (variable to be used in minimization).

Given a trial attitude matrix A_0, a better estimate may be obtained by linearizing cost function in Equation 3.8 about trial solution and solving for a correction matrix δA. Solving for the best correction matrix during iteration *p* yields a new and better trial matrix for iteration *p+1*, so that

$$A_{p+1} = \delta A_p A_p \qquad (3.9)$$

Where:

δA_p : Correction matrix at iteration *p,*

A_p : Trial matrix at iteration *p.*

A simple correction matrix can be constructed of small-angle rotations as in Equations 3.10.

$$\delta A(\delta\theta) \cong I + \Theta^x \qquad (3.10)$$

Where:

I (3x3): Identity matrix,

$\delta\theta$ (3x1) : Vector of small angle rotations about the three body frame axes as in Equations 3.11:

$$\delta\theta = \begin{bmatrix} \delta\theta_{x'} \\ \delta\theta_{y'} \\ \delta\theta_{z'} \end{bmatrix} \qquad (3.11)$$

In addition, Equation 3.12 is the skew-symmetric matrix associated with the vector $\delta\theta$.

$$\Theta^x = \begin{bmatrix} 0 & -\delta\theta_{z'} & \delta\theta_{y'} \\ \delta\theta_{z'} & 0 & -\delta\theta_{x'} \\ -\delta\theta_{y'} & \delta\theta_{x'} & 0 \end{bmatrix} \qquad (3.12)$$

Using Equations 3.9 and 3.10, the attitude cost function becomes as in Equation 3.13.

$$J(\delta\theta)|_{A_0} \cong \sum_{i=1}^{m}\sum_{j=1}^{n}\left[\Delta r_{ij} - b_i^T (I+\Theta^x) A_0 \hat{s}_j\right]^2 = \sum_{i=1}^{m}\sum_{j=1}^{n}\left(\delta r_{ij} - b_i^T \Theta^x A_0 \hat{s}_j\right)^2 \qquad (3.13)$$

Where:

$$\delta r_{ij} \equiv \Delta r_{ij} - b_i^T A_0 \hat{s}_j \qquad (3.14)$$

$$b_i^T \Theta^x A_0 \hat{s}_j = \hat{s}_j^T A_0^T \Theta^x b_i = \hat{s}_j^T A_0^T B_i^x \delta\theta \qquad (3.15)$$

Linearizing about trial matrix A_0, the linearized cost function may be written as in Equations 3.16:

$$\delta J(\delta\theta)\,|_{A_0} = \left\| H\delta\theta - \delta r \right\|_2^2 \qquad (3.16)$$

Where:

δr **:** Vector formed by stacking all phase difference measurements,

H: Observation matrix formed by stacking the measurement geometry for each separate measurement as in Equation 3.17.

$$H = \left[\hat{s}_j^T A_0^T B_i^x \right] \qquad (3.17)$$

At trial matrix A_0, Equation 3.16 is assumed to be zero to find small angle rotations. Therefore, small angle rotations are calculated as in Equation 3.18.

$$\delta\theta = (H^T H)^{-1} H^T \delta r \qquad (3.18)$$

The estimation for A is then refined iteratively until the process converges to the numerical precision of the computer. Afterwards, the north or azimuth angle of the vehicle can be determined some tangent process applied to the attitude transformation matrix A. Since examining Equation 3.5, the matrix components *A (1, 1)* and *A (1, 2)* are related with azimuth angle of the vehicle directly.

3.2 Cycle Ambiguity Resolution Technique: Integer Search

In this section, integer search on single-phase difference technique is presented to solve cycle ambiguity. The estimated attitude is ambiguous since carrier phase difference measurements are ambiguous because of the unknown number of GPS signal cycles received. GPS receiver measures only the fractional component of the GPS carrier phase. Therefore, resolution of the GPS signal cycle ambiguity becomes a necessary task before determining the attitude or the north angle for a stand-alone GPS attitude sensing system. Therefore, cycle ambiguity resolution is the process of determining the integer number of wavelengths that lie between a given pair of antennas along a particular line of sight as seen in Figure 18 [43]. It is the key initialization step that must be performed before attitude determination using GPS can start [44].

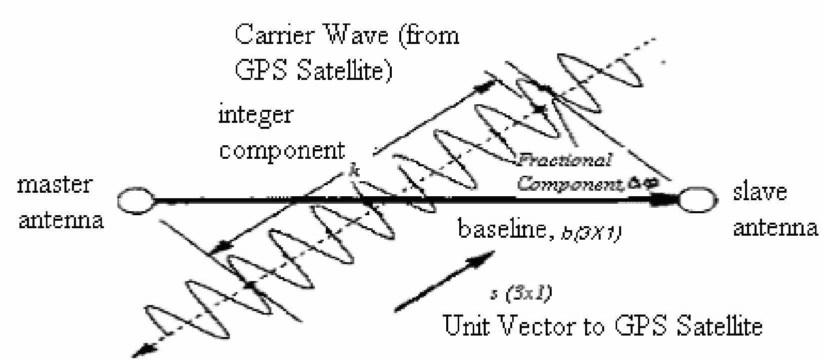

Figure 18. Cycle Ambiguity

One of the techniques which is commonly used to rapidly resolve the ambiguities is the ambiguity search technique which selects the most likely ambiguity from all possible combinations. Using search techniques, it is possible to obtain centimeter level accuracy in minutes, especially in good conditions, e.g. lots of satellites and low multipath [44].

In integer search, all possible combinations of candidate integers are systematically checked against a cost function until the correct set is found.

Considering unknown integer values, new cost function is employed as in Equation 3.19.

$$J(A^{(1)}, A^{(2)}, ..., A^{N}, k) = \sum_{l=!}^{N} \sum_{i=1}^{m} \sum_{j=1}^{n} (\Delta\Phi_{ij}^{(l)} + k_{ij} - b_i^T A^{(l)} \hat{s}_j^{(l)})^2 \quad (3.19)$$

Where:

A(l): Attitude matrix at each time *l*,

k: Vector of the cycle ambiguities for all the baseline and antenna combinations.

The problem is to find the independent attitude matrices at each time and the set of integers that minimize the stated cost function.

In this part of the thesis, four GPS satellites are used for position calculations and three GPS satellites are used for attitude determination. Integer sets are chosen according to the baseline length. Integer sets, which are triple combination of [-1 0 1], are used for baseline length from 0 wavelength to one wavelength. Since, at most one cycle can be passed between two antennas in positive or negative direction according to the satellites position and antennas attitude. Similarly, integer sets, which are triple combination of [-2 -1 0 1 2], are used for baseline length from one wavelength to two wavelength. Since, at most two cycles can be passed between two antennas in positive or negative direction according to the satellites position and antennas attitude. Triple combinations of these integers are formed, as three satellites are used and one integer is to be determined for each satellite. Moreover, iteration number of this algorithm or number of integer sets depend on the number of GPS satellites and the baseline length. This is defined in Equation 3.20.

$$iteration\_number = (m)^n \qquad (3.20)$$

Where:

m: Number of integers depends on baseline length,

n: Number of satellites.

As the baseline length gets longer or more GPS satellites are used, iteration number grows very fast as seen from the Equation 3.20.

3.3 Errors on Carrier Phase Measurement

There are several errors on carrier phase measurement due to multipath, troposphere, receiver-specific errors or satellite geometry. By far the largest error source in northfinding is multipath. Multipath occurs when the signal arrives at the antenna from reflected surfaces in addition to the line-of-sight source. The reflected signal is phase shifted with respect to the original transmission and appears as additive noise at the antenna. The description of the multipath effect is seen in Figure 19.

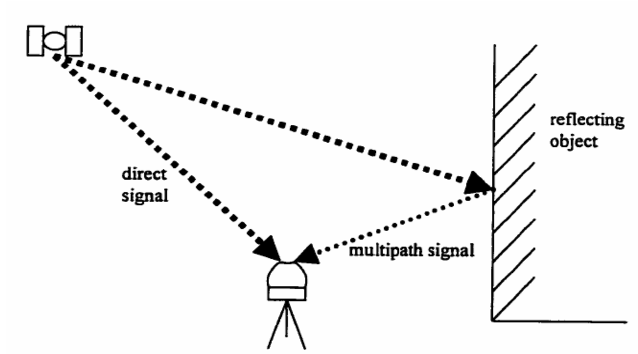

Figure 19. Receiver Multipath from Satellite

Since the antenna locations are different, multipath signature at each antenna is unique and the error does not have a common model [44]. However, the approximate rule of thumb that the differential ranging error between a pair of antennas is about 5 mm. Therefore, a zero mean Gaussian measurement error with standard deviation (5 mm/wavelength) in cycle is a typical multipath phase noise [20].

As multipath usually dominates all other error sources, an approximate and general rule of thumb for northfinding angular accuracy (in radians) for a representative baseline length of L (in cm) is simply as follows [43]:

$$\sigma_{\theta}(radians) \cong \frac{0.5cm}{L(cm)} \qquad (3.21)$$

Accuracy depends on baseline length as seen from Equation 3.21. As baseline length is longer, iteration number and ambiguousness increase due to increase in number of unknown integer cycle. However, the north angle measurement gets more accurate.

3.4 Application Scheme

GPS emulator can be used to provide input data to the north (azimuth) finder systems. In Figure 20, flow of data in an azimuth finder system is shown. Receiver time, orientation of the platform, latitude, longitude and height of the antennas are given to the GPS emulator. GPS emulator calculates the pseudorange, satellite position and carrier phase for each visible satellite according to the orientation of the observer. Then, azimuth finder takes baseline vector and GPS emulator outputs as inputs and calculates the azimuth of the platform by using afore mentioned techniques.

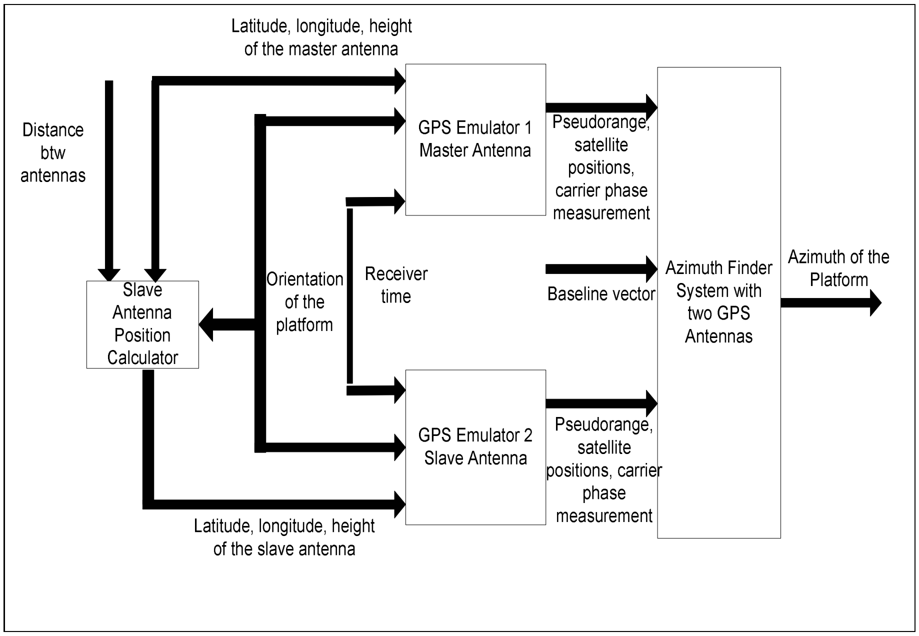

Figure 20**.** Simulation Scheme for Azimuth Finder Systems

Let us systematically define the aforementioned technique inside the azimuth finder block in Figure 20:

Step 1: Take the pseudorange measurements, carrier phase measurements, satellite positions from GPS Emulator and accurate measurement of baseline vector at one instant.

Step 2: Calculate antenna positions and line of sight vectors for each satellite, constitute possible integer sets, which will be checked in the algorithm.

Step 3: Put line of sight vectors, one of the integer set which are integer ambiguity, baseline vector, carrier phase difference between the antennas and initial attitude matrix, which is identity matrix into cost function in Equation 3.19. Get cost function value and compare it with a determined cost function limit. If the cost function value is smaller than this limit, exit the program or do the following steps.

Step 4: Calculate a new difference range measurement using carrier phase measurement, attitude determination matrix, line of sight vector and integer set as in Equation 3.14

Step 5: Calculate observation matrix using baseline vector, line of sight vector and attitude determination matrix as in Equation 3.17.

Step 6: Calculate small angle rotations using difference range measurement and observation matrix as in Equations 3.16, 3.17, 3.18.

Step 7: Calculate simple correction matrix using small angle rotation as in Equation 3.10.

Step 8: Calculate new trial attitude determination matrix as in Equations 3.9 and go to step 3 to calculate new cost function value.

3.5 Simulation Results

In this part, some simulation results are discussed. This part is divided into two sections. Firstly, simulation scheme, which is demonstrated at IDEF (International Defense Industry Fair) 2005, September and its solutions are showed. Secondly, GPS based northfinding algorithm solution and errors are examined.

3.5.1 Simulation Results 1

In Figure 21, green northfinder platform, which can be assumed as an aircraft or any vehicle, is seen. Axes of E-N-U (East-North-Up) coordinate frame are shown as red line, green line and white line respectively. Two antennas, which are rectangular, are placed on the platform (aircraft) towards to nose or x-axis of the vehicle. With the help of a joystick, baseline length and the attitude of the platform can be changed and GPS based northfinding system calculates north angle of the platform. As a result, program shows input azimuth angle, calculated azimuth angle, change of baseline length and the error to the user.

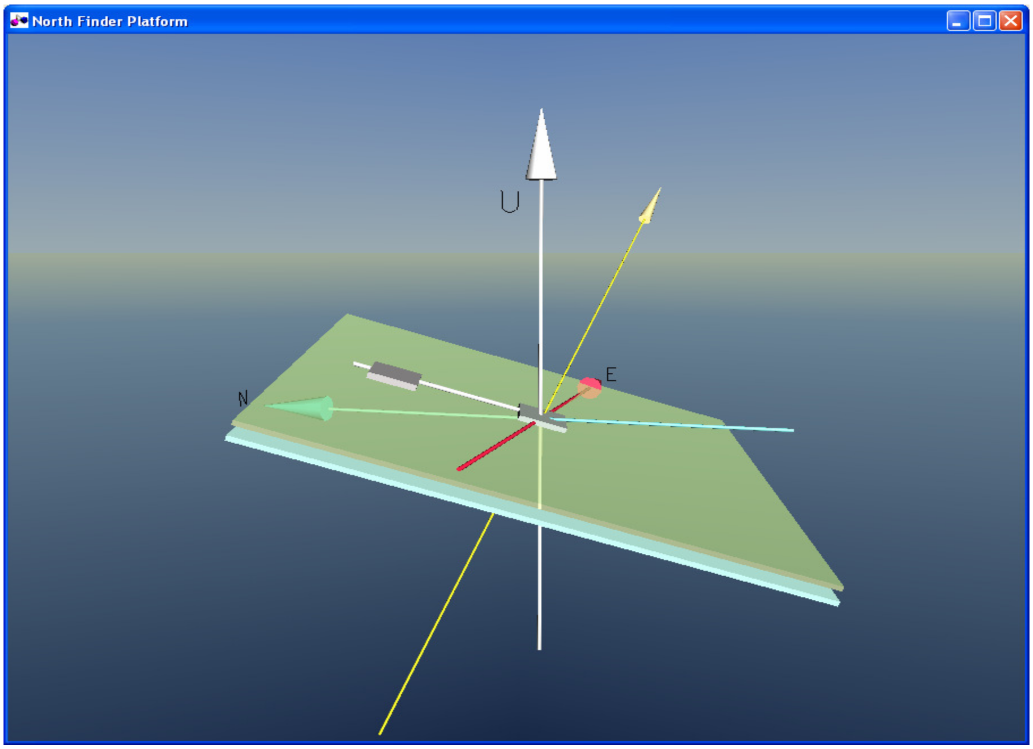

Figure 21. Northfinder Platform, Antennas and Axes of Coordinate Frames

These typical results for the azimuth finder system are shown in Figure 22, Figure 23, Figure 24 and Figure 25. The data is collected while the platform is moving. The real orientation of the platform is shown in Figure 22. This orientation information is given as input to the GPS emulators and slave antenna position calculator as seen in the diagram in Figure 20. In Figure 23, azimuth of the platform, which is calculated by Azimuth Finder System, is shown. In Figure 24, the error between the real orientation of the platform and the calculated orientation of the platform can be seen. The error is nearly zero. In this application also distance between antennas are changed to see the precision of the azimuth finder algorithms. Therefore, in Figure 25 changing of antenna distances are seen. Yaw input is written at the figures. Yaw, azimuth or north are in the same meaning.

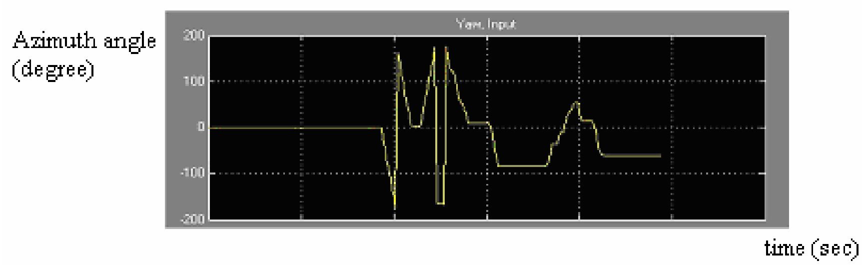

Figure 22. Real Azimuth of the Platform

Figure 23. Calculated Azimuth of the Platform

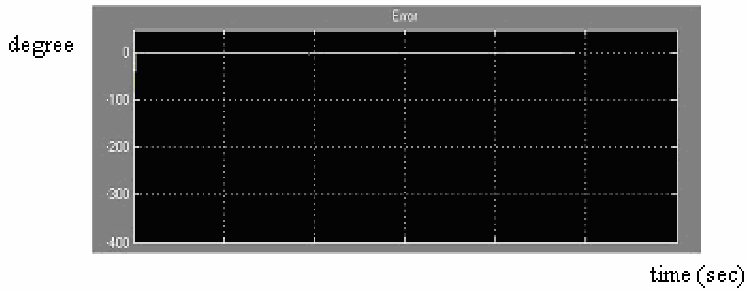

Figure 24. Error between Calculated and Real Azimuth

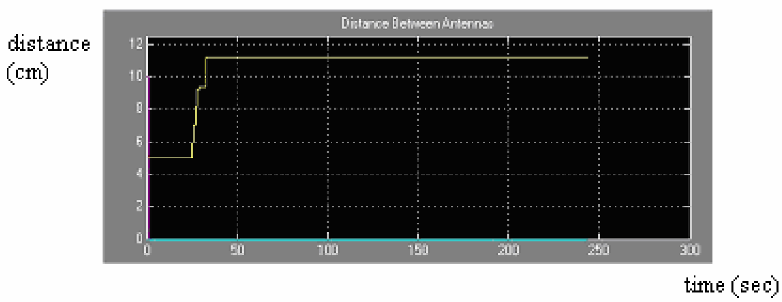

Figure 25**.** Distance between Antennas (cm)

3.5.2 Simulation Results 2

In this simulation results, system outputs and errors are discussed for various cases in general. Wavelength is about 20 cm for L1 signal.

For cases 1, 2 and 3, multipath error is not added. Since effect of baseline length is intended to be discussed. Error sources are only pseudorange measurements and precision limitation of computer.

Case 1: baseline=0.2 meter, input azimuth angle=11°, $\sigma^2_{multipath\_error}(cycle) = 0$

Integers [-1 0 1] are appointed, since baseline length is within one wavelength. For this case, iteration number is 27, as there are three GPS satellites and three integers due to baseline length.

Iteration number= $(3)^3$=27

Suitable integer set = [1 0 0]

Index number of integer set=23

[Calculated azimuth angle; value of cost function] = [10.9877°; 0.0000]

Error between real and calculated azimuth angle = 0.0123°

Case 2: baseline=0.5 meter, azimuth angle=11 degree, $\sigma^2_{multipath\_error}(cycle) = 0$

Integers [-2 -1 0 1 2] are appointed, since baseline length is within two wavelength. For this case, iteration number is 125, as there are three GPS satellites and five integers due to baseline length.

Iteration number= $(5)^3$=125

Suitable integer set = [2 -1 1]

Index number of integer set=109

[Calculated azimuth angle; cost value] = [10.9928°; 0.0000]

Error between real and calculated azimuth angle = 0.0072°

Case 3: baseline=0.76 meter, azimuth angle=11°,

$\sigma^2_{multipath\_error}(cycle) = 0$

Integers [-4 -3 -2 -1 0 1 2 3 4] are appointed, since baseline length is within four wavelength. For this case, iteration number is 729, as there are three GPS satellites and nine integers due to baseline length.

Iteration number= $(9)^3$=729

Suitable integer set = [3 -2 1]

Index number of integer set= 591

[Calculated azimuth angle; cost value] = [10.9928°; 0.0000]

Error between real and calculated azimuth angle = 0.0072°

All these results are seen in Table 1.

Table 1. Results of Cases 1, 2, and 3 for $\sigma^2_{multipath\_error}(cycle)$ =0

Case Number	Baseline (meter)	Number of Iteration	$\sigma^2_{multipath\_error}(cycle)$	Calculated Azimuth (degree)	Error (degree)
1	0.2	27	0	10.9877	0.0123
2	0.5	125	0	10.9928	0.0072
3	0.76	729	0	10.9928	0.0072

For cases 4, 5 and 6, multipath error is added. In addition, baseline length is changed for each case to see the reduction effect of baseline length. Error sources such as pseudorange measurements and precision limitation of computer is considered, too.

Case 4: baseline=0.2 meter, azimuth angle=11°,

$\sigma^2_{multipath\_error}(cycle) = (0.5\text{cm}/20\text{cm})^2$

Iteration number= $(3)^3$=27

Suitable integer set = [1 0 0]

Index number of integer set= 23

[Calculated azimuth angle; cost value] = [10.5715^o; 0.0000]

Error between real and calculated azimuth angle = 0.4285^o

Case 5: baseline=0.5 meter, azimuth angle=11^o,

$\sigma^2_{multipath\_error}(cycle) = (0.5\text{cm}/20\text{cm})^2$

Iteration number= $(5)^3$=125

Suitable integer set = [2 -1 1]

Index number of integer set=109

[Calculated azimuth angle; cost value] = [10.7027^o; 0.0000]

Error between real and calculated azimuth angle = 0.2973^o

Case 6: baseline=0.76 meter, azimuth angle=11^o,

$\sigma^2_{multipath\_error}(cycle) = (0.5\text{cm}/20\text{cm})^2$

Iteration number= $(9)^3$=729

Suitable integer set = [3 -2 1]

Index number of integer set= 591

[Calculated azimuth angle; cost value] = [11.1149^o; 0.0000]

Error between real and calculated azimuth angle = 0.1149^o

All these results are seen in Table 2.

Table 2. Results of Cases 4, 5 and 6 for $\sigma^2_{multipath\_error}(cycle) = (0.025)^2$

Case Number	Baseline (meter)	Number of Iteration	$\sigma^2_{multipath\_error}(cycle)$	Calculated Azimuth (degree)	Error (degree)
4	0.2	27	$(0.025)^2$	10.5715	0.4285
5	0.5	125	$(0.025)^2$	10.7027	0.2973
6	0.76	729	$(0.025)^2$	11.1149	0.1149

As seen from the cases, error decreases, as the baseline length is longer. However, iteration number increases. So, more computational effort is exhausted. In addition, using longer baseline reduces multipath effect as declared in Equation 3.21.

3.6 Summary

In this chapter, GPS based northfinding algorithm with integer search, single-phase difference, and cycle ambiguity resolution are discussed. Errors on this method are defined. In this method, measurement of single-phase difference between a pair of antennas is used. To solve cycle ambiguity problem, integer search is applied.

To test GPS based northfinding algorithm, GPS emulator is used. Azimuth finding system gets GPS emulator outputs such as carrier phase measurements, satellite positions and pseudorange measurements and calculates the azimuth by means of aforementioned techniques. This algorithm detects the north angle within 0.42^{o} precision that is seen from the case results. However, this precision highly depends on baseline length. For 0.76 meter, the north angle precision is within 0.11^{o}.

It is possible to obtain centimeter level accuracy in minutes, especially in good conditions, e.g. lots of satellites and low multipath using search techniques. In addition, measurements are collected at one instant. Afterwards, post-processing is applied to the measurements using aforementioned techniques. However, there are some additional shortcomings of this method. At one instant, there may be more than one integer set solution in practice. Therefore, this algorithm is not reliable and sometimes gives wrong results. Moreover, computational effort is very high for long baselines. In addition, GPS based northfinding techniques use the external signals. If these signals are blocked or jammed, then these techniques could not work.

Let us look other northfinding systems and compare them with GPS based northfinding technique with exhaustive search. In the past, attitude determination problem was solved using techniques based on inertial elements. Such techniques were associated with complex algorithms and control mechanisms. In addition, an IMU is typically very expensive, heavy, power hungry, requires long settling times and is degraded at high latitudes. An attitude determining GPS receiver does not have these shortcomings [45].

Attitude determination using GPS receivers is characterized by being simple, economic, more compact and less complex than other techniques [46]. This new GPS technology has many potential applications, such as replacing large and costly IMUs on ships, or at least to allow use of lower cost IMUs. It could provide heading information in the polar region where inertial systems cannot. It could provide rapid and precise sensor-pointing, etc [45]. Furthermore, the elimination of many different sensor devices and their interfaces can yield a substantial benefit in system reliability.

The magnetic compass has two disadvantages compared to GPS. First, the earth's magnetic field varies locally and the poles themselves move slightly over time. Second, the presence of magnetic material on a vessel disrupts the operation of the magnetic compass. The GPS is immune to these problems and gives the nearly same accuracy in the calculation of north angle [47].

CHAPTER 4

GPS BASED NORTHFINDING TECHNIQUE WITH KALMAN FILTER

In this chapter, GPS based northfinding technique with Kalman filter is introduced. Similar to the technique with exhaustive search, same GPS observables are used in this technique [23]. However, the processing of these measurements is different. Unlike the technique with exhaustive search, in the technique with Kalman filter carrier phase measurements at each antenna are differenced three times to find initial attitude estimate and two times to solve integer ambiguity and calculate the north angle of the vehicle [24].

In this chapter, GPS based northfinding technique with Kalman Filter is presented. Firstly, algorithm and set-up are described. Observations used in this algorithm are introduced. Single-phase difference, double phase difference and triple phase difference (time difference) concepts are presented. Then, phase ambiguity resolution technique used in this technique is explained. Afterwards, Kalman filter to solve integer ambiguity and estimation of attitude are examined [48, 49]. Errors on this algorithm are discussed. Simulation results are shown and an overview of this technique is given.

4.1 Concept of GPS Based Northfinding Algorithm with Kalman Filter

4.1.1 Set Up

Northfinding is performed by processing of carrier phase difference measurements between two or more antennas mounted on a vehicle. Noise that is common to the satellites or the receiver can be removed by phase differencing. The receiver can measure only the fractional part of the full carrier phase difference, not the number of full carrier cycles between antennas. This unmeasured integer is called the integer ambiguity, and resolving the ambiguity is the main problem in the attitude determination. All these definitions are same as in Chapter 3 and same Set-Up in Figure 16 is used for this technique too.

The receiver measures the relative range of the two antennas to the GPS satellite. The antenna baseline is defined as the relative position vector from one antenna to the other. The relative range is equal to the projection of the antenna baseline vector onto the line of sight vector to the GPS satellite. Equation 4.1 describes the carrier phase measurement.

$$\Phi = \Delta r + K\lambda + v = Hx + K\lambda + v \quad (4.1)$$

Where:

Φ : Vector of phase difference,

Δr : Relative range vector of the two antennas to the satellite,

H : Line of sight unit vector to the satellite,

x: Antenna baseline vector (meter),

K: Vector of unknown integer,

λ : Carrier wavelength,

v: Phase Measurement noise.

This definition can be seen in Figure 17. H and s are in the same meaning. In addition, all parameters in Equation 3.6 are multiplied with λ to constitute Equation 4.1.

4.1.2 Phase Differences and Algorithm

The cancellation of common mode noise is the primary reason for using differencing techniques. All errors are common to each GPS satellite signal are removed by the action of differencing the phase measurements from that GPS satellite between two different antenna phase centers. These errors include all GPS satellite clock prediction errors and short-term oscillator noise, all GPS satellite ephemeris radial prediction errors, and, for closely spaced antenna phase centers, most of the highly correlated ionospheric errors [25].

Single phase differencing measurements involve one GPS satellite and two antenna phase centers as in Figure 17, whereas double difference measurements involve two GPS satellites and two antenna phase centers separated by a baseline whose length and orientation are to be determined as in Figure 26.

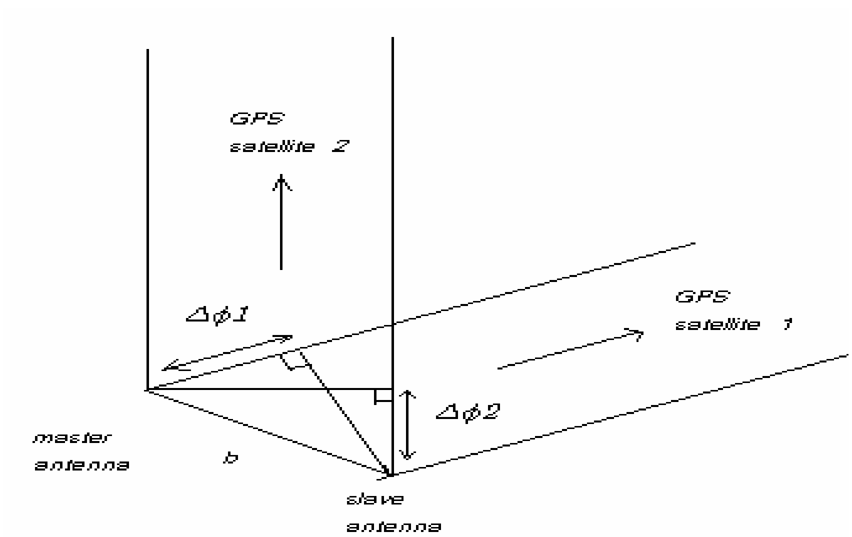

Figure 26. Double Difference Measurement Observation

The relation between the carrier phase and satellite range is given by [23, 24, 25, 48].

$$R_A^i = r_A^i(t-t_0) + b_A^i(t_0) + ct_i + ct_A \qquad (4.2)$$

Where:

R_A^i : Range from antenna A to satellite *i*,

$r_A^i(t-t_0)$: Integrated carrier Doppler from time t_0 (meter),

$b_A^i(t_0)$: Unknown initial carrier range bias (meter),

c : Velocity of light,

t_i : Satellite (*i*) clock error,

t_A : Antenna (A) phase delay and clock error,

The basic measurements in a GPS based attitude determination scenario are the carrier phase single difference observations constructed from two antennas with respect to a single GPS satellite. The carrier phase single difference for antenna *A* and *B*, and satellite *i* is given by Equation 4.3.

$$R_{AB}^i = R_A^i - R_B^j$$

$$R_{AB}^i = r_A^i(t-t_0) + b_A^i(t_0) + ct_i + ct_A - (r_B^i(t-t_0) + b_B^i(t_0) + ct_i + ct_B)$$

$$R_{AB}^i = r_{AB}^i(t-t_0) + b_{AB}^i(t_0) + c(t_A - t_B) \qquad (4.3)$$

The equation for path single difference for antenna *A* and *B* for a carrier signal originating from the GPS satellite *i* is given by:

$$D^i = X_{AB}.h^i \qquad (4.4)$$

Where:

D^i : Path difference between antenna A and B for a signal from satellite i,

X_{AB} : Baseline vector,

h^i : Unit direction vector pointing from the baseline AB to the satellite i.

The second difference across satellites of the single difference measurements is called double difference. Double difference eliminates receiver error sources such as receiver clock errors and common multipath bias errors. However, phase ambiguity remains.

The phase double difference for antenna A and B, and satellite i and j is given in Equation 4.5.

$$R_{AB}^{ij} = R_{AB}^{i} - R_{AB}^{j}$$

$$R_{AB}^{ij} = r_{AB}^{i}(t - t_0) + b_{AB}^{i}(t_0) + c(t_A - t_B) - (r_{AB}^{j}(t - t_0) + b_{AB}^{j}(t_0) + c(t_A - t_B))$$

$$R_{AB}^{ij} = r_{AB}^{ij}(t - t_0) + b_{AB}^{ij}(t_0) \qquad (4.5)$$

The path double difference for antenna A and B, and satellite i and j is given in Equation 4.6.

$$D^{ij} = X_{AB}.h^i - X_{AB}.h^j = X_{AB}.(h^i - h^j) \qquad (4.6)$$

A triple difference can be made by carrying out the difference between the double difference observables for two different instants of time, which are t_m and t_n. The triple difference yields an unambiguous phase observable in Equation 4.7. Therefore, the triple difference removes the phase ambiguity.

$$\Delta R_{AB}^{ij}(t) = R_{AB}^{ij}(t_n) - R_{AB}^{ij}(t_m)$$

$$\Delta R_{AB}^{ij}(t) = r_{AB}^{ij}(t_n - t_0) + b_{AB}^{ij}(t_0) - (r_{AB}^{ij}(t_m - t_0) + b_{AB}^{ij}(t_0))$$

$$\Delta R_{AB}^{ij}(t) = r_{AB}^{ij}(t_n - t_m) = r_{AB}^{ij}(t - t_0) \qquad (4.7)$$

The triple path difference is:

$$\Delta D^{ij} = D^{ij}(t) - D^{ij}(t_0) \qquad (4.8)$$

Path double difference and phase double difference are equal for known integer ambiguity. Therefore, using Equations 4.5 and 4.6, the fundamental equation for the phase double difference ambiguity is given by:

$$r(t) + K = \frac{H(t)X_{AB}}{\lambda} \qquad (4.9)$$

Where:

$r(t)$: Vector of phase double difference (cycle),

K : Vector of ambiguity integers (cycle),

$H(t)$: Double differenced observation vector matrix,

X_{AB} : Baseline vector (meter),

λ : GPS carrier wavelength.

4.2 Phase Ambiguity Resolution

Phase ambiguity problem is solved using triple difference. Initial attitude can be estimated, since triple difference eliminates integer ambiguities as in Equation 4.10.

$$\Delta r(t) = \Delta H^T(t) X_{AB} \qquad (4.10)$$

$$X_{AB} = \left[\Delta H(t) \Delta H^T(t)\right]^{-1} \Delta H(t) \Delta r(t) \qquad (4.11)$$

Where:

$\Delta r(t) = r(t) - r(t_0)$,

$\Delta H(t) = H(t) - H(t_0)$.

This initial attitude is used in the next loop (integer estimator), which yields the integer value by solving the phase ambiguity equation in Equation 4.9. Once the integer value is obtained, the final attitude solution is obtained by again solving Equation 4.9. Integer estimation and attitude estimation use the same equation for Kalman filter but using different initial condition and states.

4.3 Kalman Filter

Due to noisy observations of the GPS satellite signals and states that change in time, the attitude determination can be optimized using a stochastic approach. The Kalman filter is an ideal approach to this optimal estimation problem [26].

The discrete Kalman filter equations are summarized below. For a discrete linear system, the general system model is:

$$x_{k+1} = \Phi_k x_k + w_k \qquad (4.12)$$

Where:

x_k : System state vector at time t_k,

Φ_k : State transition matrix relating x_k to x_{k+1} in the absence of a forcing function

w_k : Process noise vector with covariance matrix Q_k

The measurement (observation) model is given by:

$$z_k = H_k x_k + v_k \qquad (4.13)$$

Where:

z_k : Measurement vector at time t_k,

H_k: Observation matrix relating the measurement with the state vector in noiseless condition,

v_k : Measurement error vector with covariance matrix R_k,

The vectors w_k and v_k are assumed to be white noise sequences uncorrelated with each other and the initial state vector.

The propagation of the error covariance and the state estimate is:

Error covariance: $P_{k+1}^{-} = \Phi_k P_k \Phi_k^T + Q_k$ (4.14)

State estimate: $x_{k+1}^{-} = \Phi_k x_k$ (4.15)

The state estimate and the error covariance are updated with a measurement z_k :

Error covariance: $P_k^{-} = (P_k^{-})^{-1} + H_k^T R_k^{-1} H_k$ (4.16)

State estimate: $x_k = x_k^{-} + K_k (z_k - H_k x_k^{-})$ (4.17)

Kalman gain: $K_k = P_k^{-} H_k^T (H_k P_k^{-} H_k^T + R_k)^{-1}$ (4.18)

Equations from 4.14 to 4.18 constitute the recursive processes of the Kalman filter. Below, the Kalman filter formulations for the integer estimation and the attitude estimation respectively are presented.

4.3.1 Integer Estimator

The GPS measurement model for a Kalman filter, where the initial integers are treated as random constants, is formulated as:

$$\begin{bmatrix} z_1 \\ z_2 \\ z_3 \end{bmatrix} = \frac{1}{\lambda} \begin{bmatrix} h_x^{12} & h_y^{12} & h_z^{12} & \lambda & 0 & 0 \\ h_x^{23} & h_y^{23} & h_z^{23} & 0 & \lambda & 0 \\ h_x^{34} & h_y^{34} & h_z^{34} & 0 & 0 & \lambda \end{bmatrix} \begin{bmatrix} x \\ y \\ z \\ K_1 \\ K_2 \\ K_3 \end{bmatrix} + \begin{bmatrix} v_1 \\ v_2 \\ v_3 \end{bmatrix} \quad (4.19)$$

Where:

z_1, z_2, z_3 : Double difference measurements,

h_x^{ij} , h_y^{ij} , h_z^{ij} : Differenced unit direction vector between i and j satellites,

x, y, z: Pointing vector (baseline vector),

K_1, K_2, K_3: Integer ambiguity vector,

v_1, v_2, v_3 : Measurement noise vector,

λ : GPS signal wavelength.

All elements of the state are random constants so the process has no input but has a random initial condition. Therefore, the Q matrix is zero and Φ is the identity matrix. The corresponding discrete process model is described by:

$$x_{k+1}^{-} = x_k \qquad (4.20)$$

The covariance matrix for the differenced measurement error vector v_k is time invariant and is given by:

$$R = \begin{bmatrix} 2r & -r & 0 \\ -r & 2r & -r \\ 0 & -r & 2r \end{bmatrix} \qquad (4.21)$$

Where:

r: Variance of single difference measurement error

Equation 4.21 can be derived as follows:

$$d_1 = (s_1 - s_2) + (s_{e1} - s_{e2})$$

$$d_2 = (s_2 - s_3) + (s_{e2} - s_{e3}) \qquad (4.22)$$

$$d_3 = (s_3 - s_4) + (s_{e3} - s_{e4})$$

Where:

s_i: Single phase difference for satellite i,

d_j: Double phase difference between two different satellite and antennas,

s_{ei}: Single difference measurement error for satellite i, uncorrelated with each other.

$$E\{d_1d_1\} = E\{(s_{e1} - s_{e2})(s_{e1} - s_{e2})\} = E\{s_{e1}{}^2\} + E\{s_{e2}{}^2\} = 2r$$

$$E\{d_1d_2\} = E\{(s_{e1} - s_{e2})(s_{e2} - s_{e3})\} = E\{s_{e2}{}^2\} = -r \qquad (4.23)$$

$$E\{d_1d_3\} = E\{(s_{e1} - s_{e2})(s_{e3} - s_{e4})\} = E\{s_{e2}{}^2\} = 0$$

$$R = \begin{bmatrix} E\{d_1d_1\} & E\{d_1d_2\} & E\{d_1d_3\} \\ E\{d_2d_1\} & E\{d_2d_2\} & E\{d_2d_3\} \\ E\{d_3d_1\} & E\{d_3d_2\} & E\{d_3d_3\} \end{bmatrix} \qquad (4.24)$$

A random constant can be thought of as consisting of a normal zero mean random variable with infinity variance. Initial conditions for the a priori estimate and error covariance are:

$$x_0^- = (x_0, y_0, z_0, 0,0,0) \qquad (4.25)$$

$$P_0^- = \infty I \qquad (4.26)$$

The initial pointing vector (x_0 ,y_0, z_0) is obtained by initializing the process where phase ambiguities are eliminated using a triple difference.

Using models and parameters described before, the Kalman filter loop comprised of Equations 4.14 to 4.18 will produce integer values recursively. Actually, the solution, K vector, will not have real integer value components. Forcing K to the nearest set of integers will obtain integer values.

4.3.2 Attitude Estimator

The measurement model for attitude estimation is given by:

$$\begin{bmatrix} z_1 \\ z_2 \\ z_3 \end{bmatrix} + \begin{bmatrix} K_1 \\ K_2 \\ K_3 \end{bmatrix} = \frac{1}{\lambda} \begin{bmatrix} h_x^{12} & h_y^{12} & h_z^{12} \\ h_x^{23} & h_y^{23} & h_z^{23} \\ h_x^{34} & h_y^{34} & h_z^{34} \end{bmatrix} \begin{bmatrix} x \\ y \\ z \end{bmatrix} + \begin{bmatrix} v_1 \\ v_2 \\ v_3 \end{bmatrix} \tag{4.27}$$

Where:

z_1, z_2, z_3 : Double difference measurements,

h_x^{ij} , h_y^{ij} , h_z^{ij} : Differenced unit direction vector between *i* and *j* satellites,

x, y, z: Pointing Vector,

K_1, K_2, K_3: Integer ambiguity vector,

v_1, v_2, v_3 : Measurement noise vector,

λ : GPS signal wavelength.

In this attitude estimator the integer values are not states but constants. The integers (obtained from the integer estimator) are put into the measurement equations. In addition, it is assumed that the antenna system is stationary with respect to the body-fixed reference coordinate and all sets of the attitude states can be modelled as random constants. Therefore, the Q matrix is zero and Φ is the identity matrix. The covariance matrix of measurement errors R is the same as the integer estimator case. The error covariance matrix has a value of infinity [48].

Let us systematically overview the technique:

Step 1: Take the pseudorange measurements, carrier phase measurements, satellite positions from GPS Emulator for two distinct instants.

Step 2: Calculate double phase and path difference using Equations 4.5 and 4.6 for these two distinct instants.

Step 3: Construct the triple phase and path difference using Equations 4.7 and 4.8 and calculate the initial estimate of the pointing vector.

Step 4: Use this estimated pointing vector as initial condition for integer estimator. In addition, zero vector of integers are used as initial condition for integer estimator. Initial conditions are in Equation 4.25.

Step 5: Calculate integer ambiguities using Kalman filter Equations from 4.14 to 4.18 and integer estimation Equation 4.19. For each iteration or instant, take GPS Emulator outputs and calculate necessary information for integer estimator such as line of sight vectors, carrier phase differences.

Step 6: Use **c**alculated integers as constants not as states in attitude estimator. Same initial attitude estimate calculated from triple difference is used.

Step 7: Calculate pointing vector using Kalman Filter Equations from 4.14 to 4.18 and Equation 4.27. For each iteration or instant, take GPS Emulator outputs and calculate necessary information for attitude estimator such as line of sight vectors, carrier phase differences.

4.4 System Accuracy and Errors

Similar to GPS based northfinding with exhaustive search in Chapter 3; GPS based northfinding with Kalman filter is affected from the same errors such as multipath. Better accuracy requires a longer antenna baseline. Double differencing, antenna pattern shaping, and multipath calibration methods can be used to minimize multipath errors [24].

4.5 Simulation Results

In this section, some simulation results are given. For all cases azimuth (heading)=11.0^{o}. For this method, four satellites are used for both pseudorange measurements and carrier phase measurement. A vector consist of three parts are constructed taking four satellites differences, and three unknowns which are pointing vector components are solved.

Firstly, baseline effect is examined to solve attitude.

Case 1: baseline=1 meter, $\sigma^2_{multipath\_error} = (0.1 \text{ rad})^2$

Real integer value of double difference for satellite 1 and 2 is K_{12}=6. It is constant for iteration period.

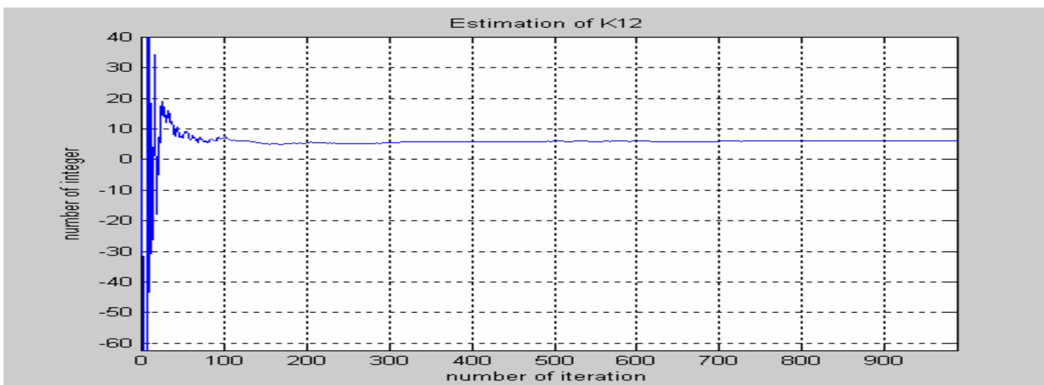

Figure 27. Estimation of Integer Value of Double Difference for Satellite 1 and 2

In Figure 27, convergence of integer estimator for satellite 1 and 2 is presented. Although, it becomes stable after iteration 400, process continues for 1000 iteration to be comparable with other cases.

Real integer value of double difference for satellite 2 and 3 is K_{23}= -5. It is constant for iteration period.

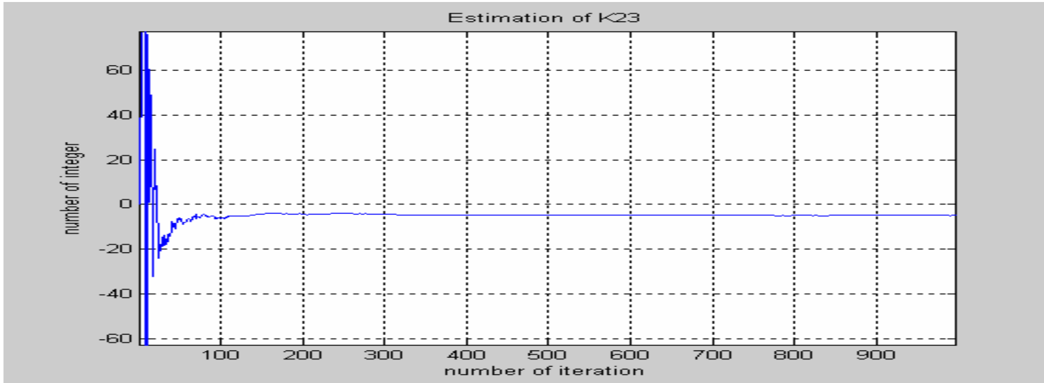

Figure 28. Estimation of Integer Value of Double Difference for Satellite 2 and 3

In Figure 28, convergence of integer estimator for satellite 2 and 3 is presented. It becomes stable after iteration 400.

Real integer value of double difference for satellite 3 and 4 is K_{34}= 6. It is constant for iteration period.

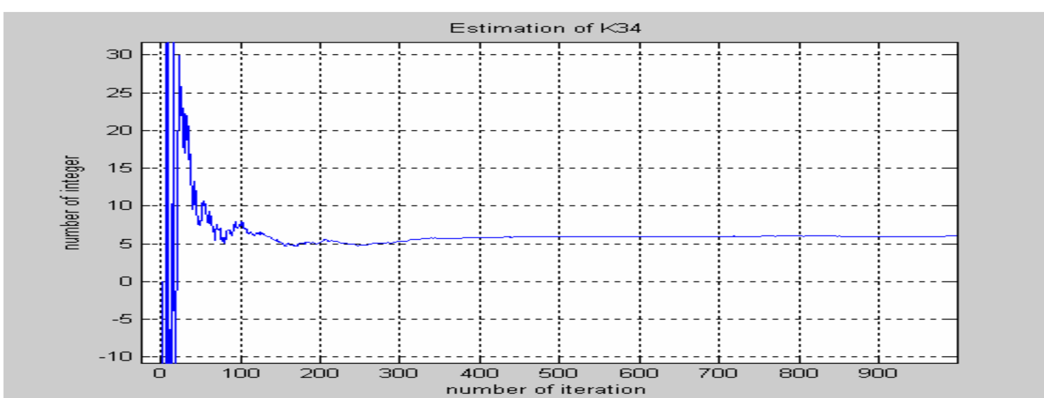

Figure 29. Estimation of Integer Value of Double Difference for satellite 3 and 4

In Figure 29, convergence of integer estimator for satellite 3 and 4 is presented. It becomes stable after iteration 500.

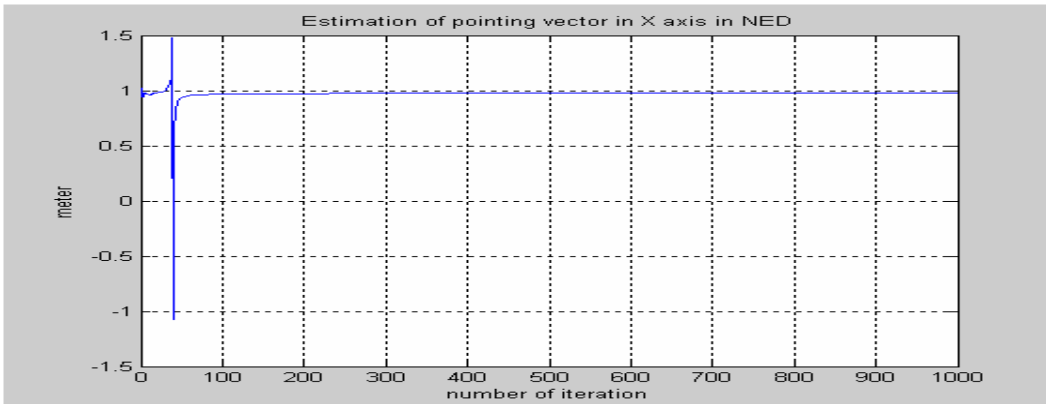

Figure 30. Estimation of Pointing Vector in x-axis of NED

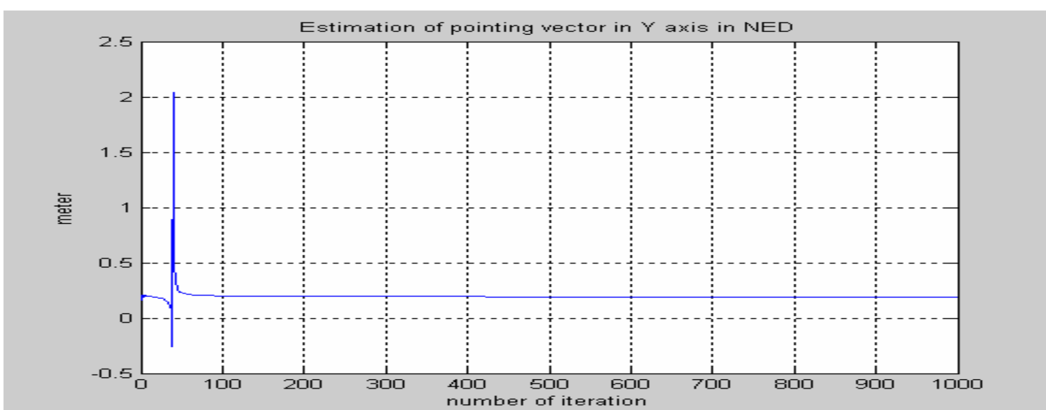

Figure 31. Estimation of Pointing Vector in y-axis of NED

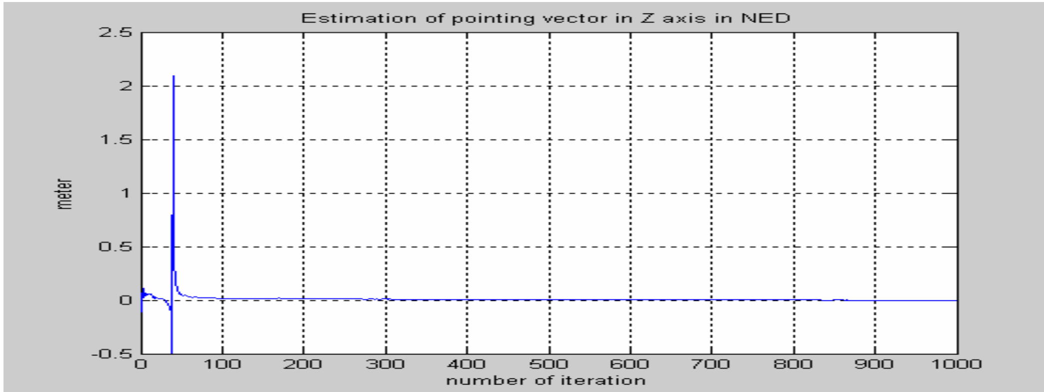

Figure 32. Estimation of Pointing Vector in z-axis of NED

In Figure 30, Figure 31, Figure 32, convergence of pointing vector for three axis. After nearly 400 iteration, all of them converge to real values.

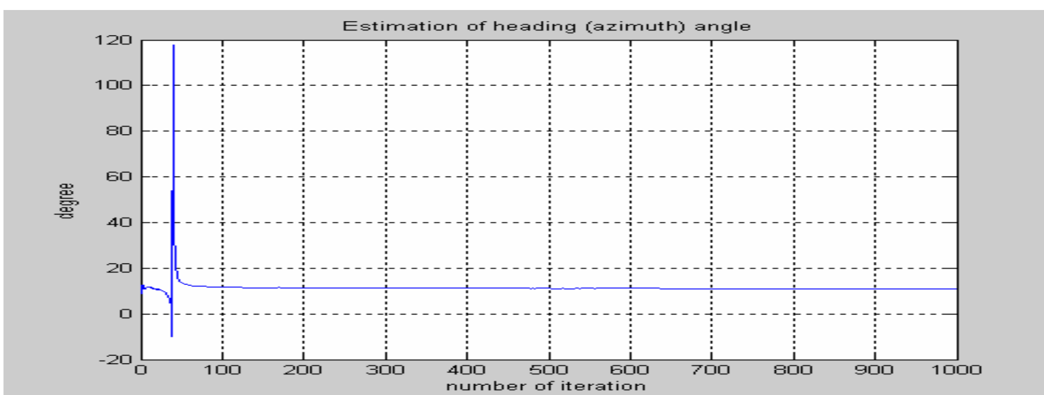

Figure 33. Estimation of Heading (azimuth) Angle

In Figure 33, convergence of heading angle is seen. After 400 iteration, it converges to real heading value.

Estimated heading value, error between real heading and estimated heading are as follows:

Heading = 11.0369^o, error=0.0369^o

Real pointing vector at three axes and estimated pointing vector at three axes are as follows respectively:

x_b = 0.9816 m, y_b = 0.1908 m, z_b = 0

x_b^e = 0.9811 m, y_b^e = 0.1914 m, z_b^e = -0.0013 m

Case 2: baseline=0.5 meter, $\sigma^2_{multipath\_error}$ = (0.1 rad)^2

Real integer value of double difference for satellite 1 and 2 is K_{12}=3. It is constant for iteration period.

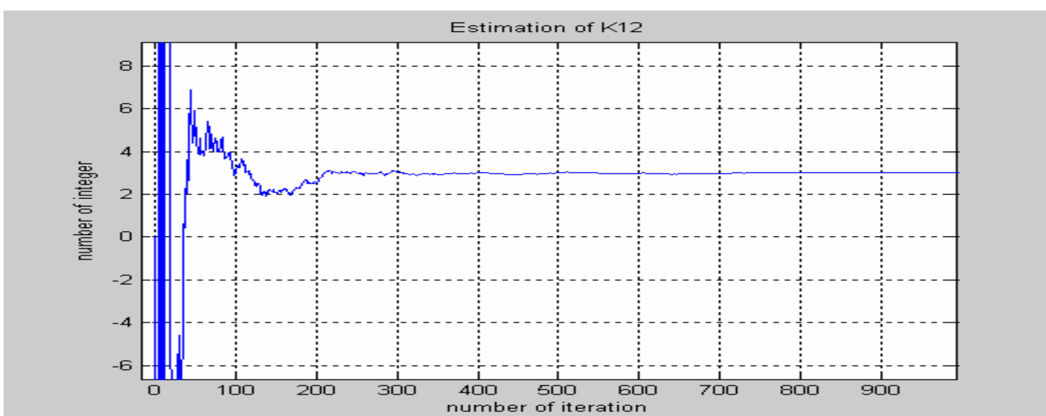

Figure 34. Estimation of Integer Value of Double Difference for Satellite 1 and 2

In Figure 34, convergence of integer estimator for satellite 1 and 2 is presented. It becomes stable after iteration 500.

Real integer value of double difference for satellite 2 and 3 is K_{23}=-3. It is constant for iteration period.

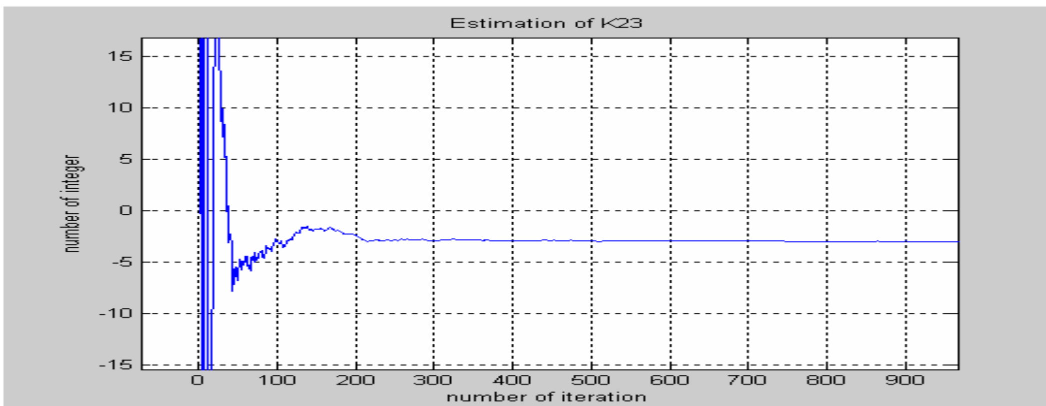

Figure 35. Estimation of Integer Value of Double Difference for Satellite 2 and 3

In Figure 35, convergence of integer estimator for satellite 2 and 3 is presented. It becomes stable after iteration 500.

Real integer value of double difference for satellite 3 and 4 is K_{34}=3. It is constant for iteration period.

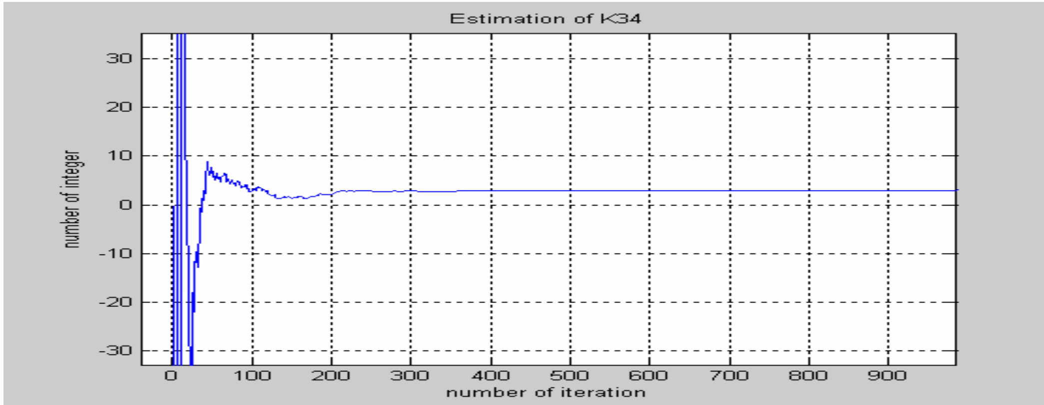

Figure 36. Estimation of Integer Value of Double Difference for Satellite 3 and 4

In Figure 36, convergence of integer estimator for satellite 3 and 4 is presented. It becomes stable after iteration 500.

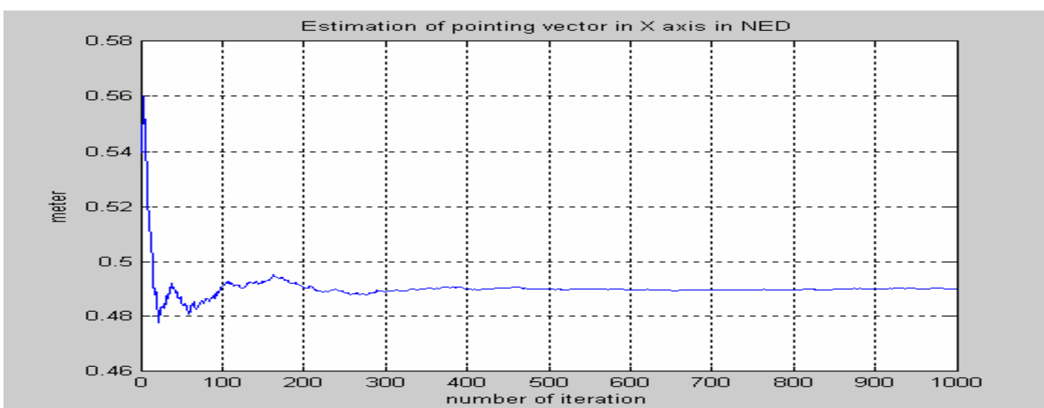

Figure 37. Estimation of Pointing Vector in x-axis of NED

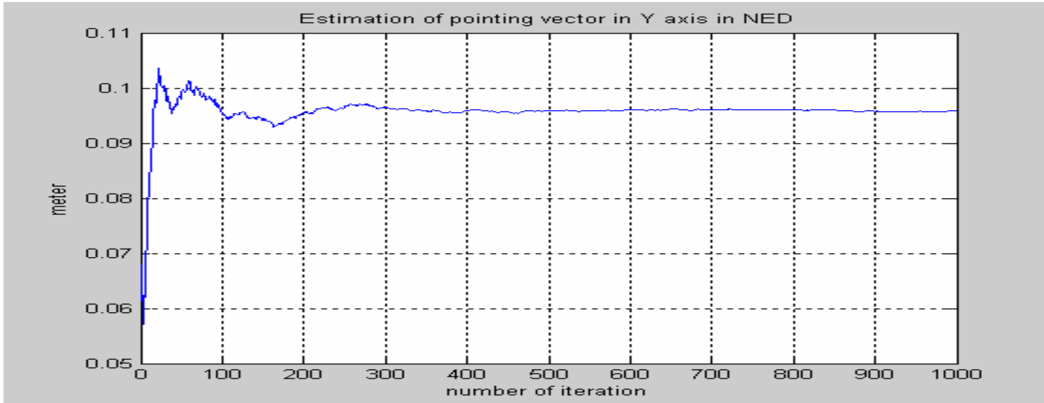

Figure 38. Estimation of Pointing Vector in y-axis of NED

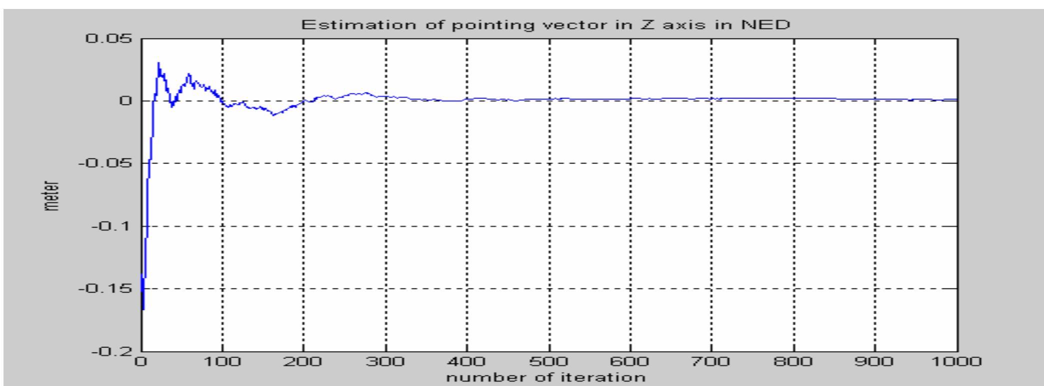

Figure 39. Estimation of Pointing Vector in z-axis of NED

In Figure 37, Figure 38, Figure 39, convergence of pointing vector for three axis. After nearly 600 iteration, all of them converge to real values.

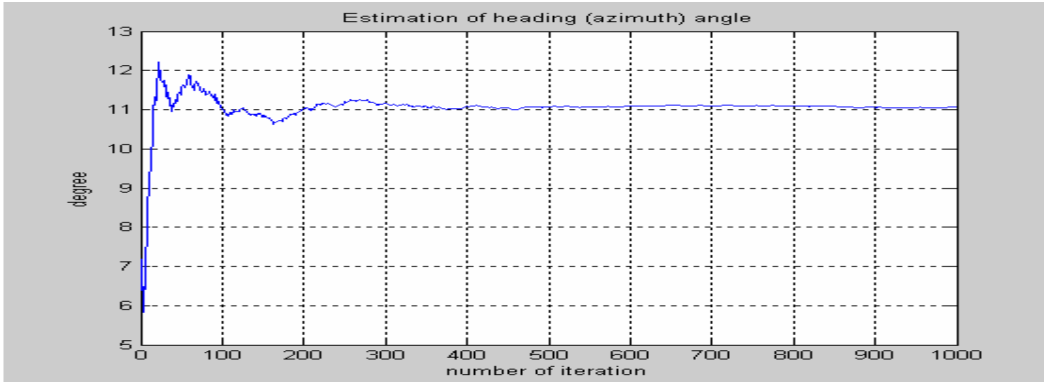

Figure 40.Estimation of Heading (azimuth) Angle

In Figure 40, convergence of heading angle is seen. After 600 iteration, it converges to real heading value.

Estimated heading value, error between real heading and estimated heading are as follows:

Heading = 11.056^o, error=0.056^o

Real pointing vector at three axes and estimated pointing vector at three axes are as follows:

x_b =0.4908 m, y_b = 0.0954 m, z_b =0

x_b^e =0.4902 m, y_b^e = 0.0958 m, z_b^e =9.8572e-004 m

Examining Cases 1 and 2, as baseline length is longer, both convergence time and error become smaller.

Secondly, multipath effect examined.

Case 3: baseline=1 meter, $\sigma^2_{multipath\_error}$ = (0.2 rad)^2

Real integer value of double difference for satellite 1 and 2 is $K_{12}=6$. It is constant for iteration period.

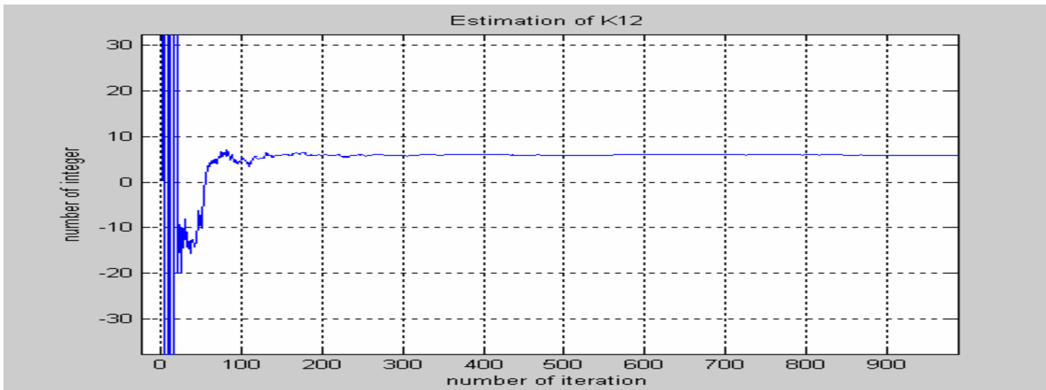

Figure 41. Estimation of Integer Value of Double Difference for Satellite 1 and 2

In Figure 41, convergence of integer estimator for satellite 1 and 2 is presented. It becomes stable after iteration 600.

Real integer value of double difference for satellite 2 and 3 is $K_{23}= -5$. It is constant for iteration period.

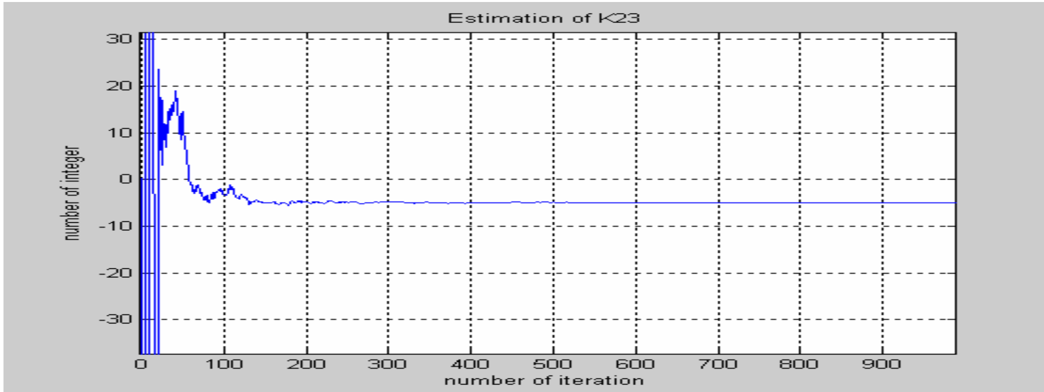

Figure 42. Estimation of Integer Value of Double Difference for Satellite 2 and 3

In Figure 42, convergence of integer estimator for satellite 2 and 3 is presented. It becomes stable after iteration 500.

Real integer value of double difference for satellite 3 and 4 is K_{34}= 6. It is constant for iteration period.

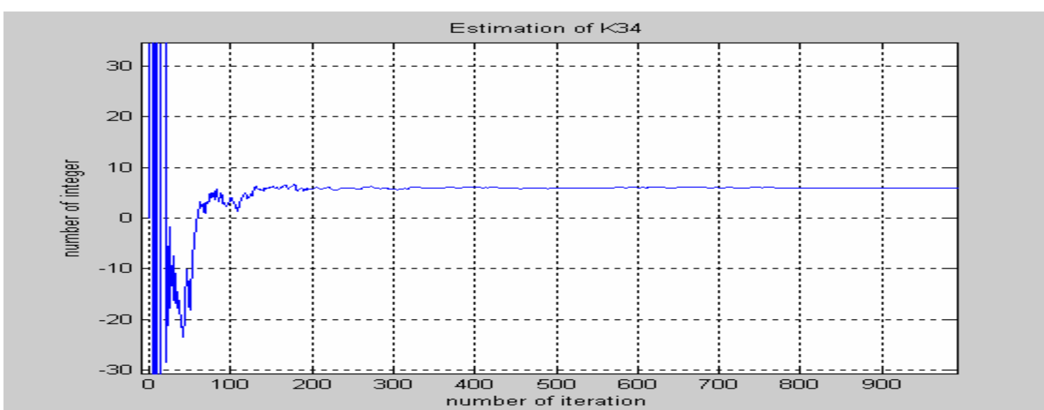

Figure 43. Estimation of Integer Value of Double Difference for Satellite 3 and 4

In Figure 43, convergence of integer estimator for satellite 3 and 4 is presented. It becomes stable after iteration 600.

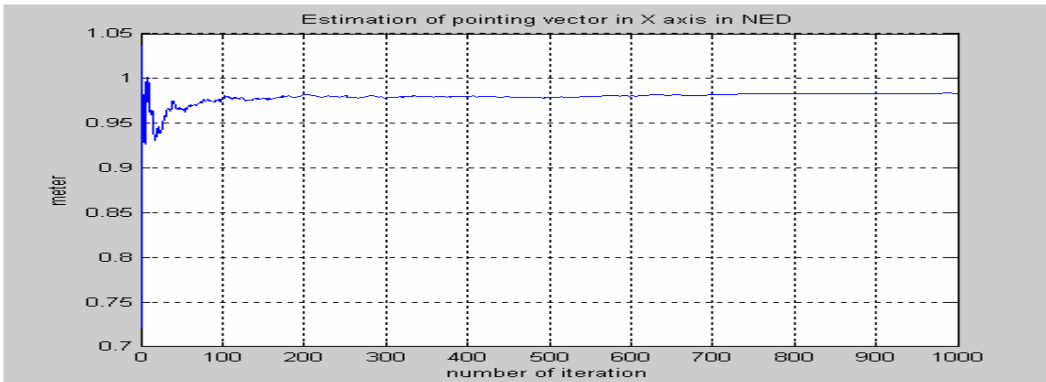

Figure 44. Estimation of Pointing Vector in x-axis of NED

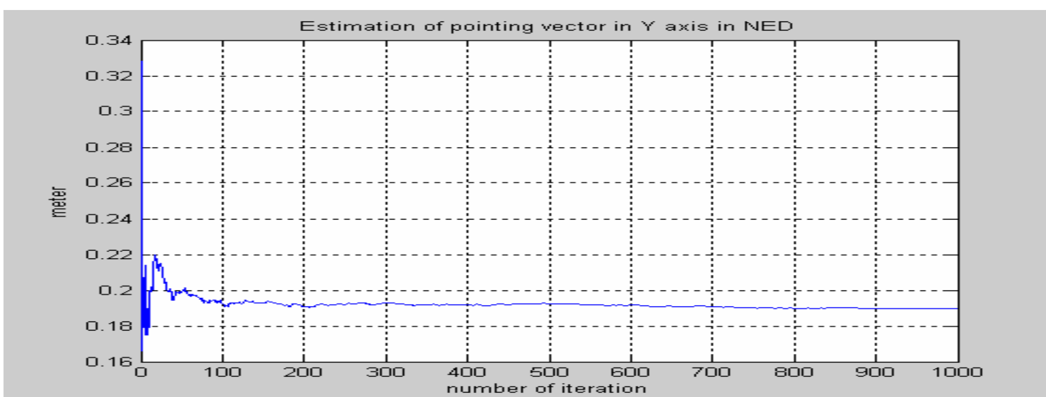

Figure 45. Estimation of Pointing Vector in y-axis of NED

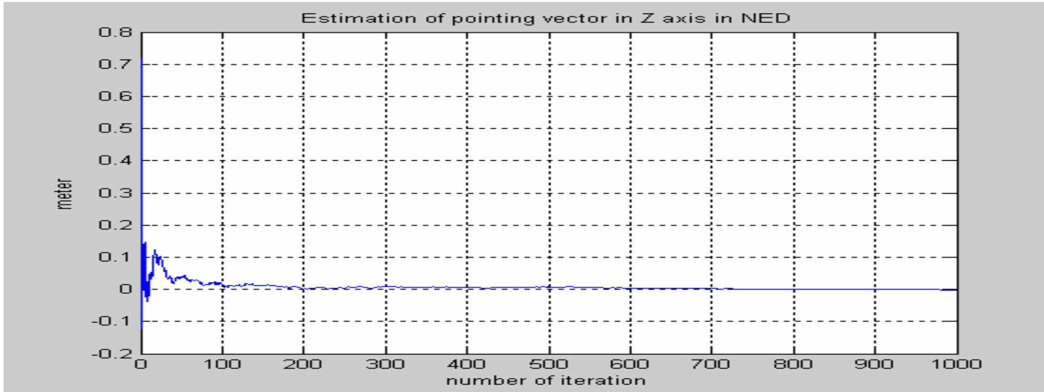

Figure 46. Estimation of Pointing Vector in z-axis of NED

In Figure 44, Figure 45, Figure 46, convergence of pointing vector for three axes is presented. After nearly 600 iteration, all of them converge to real values.

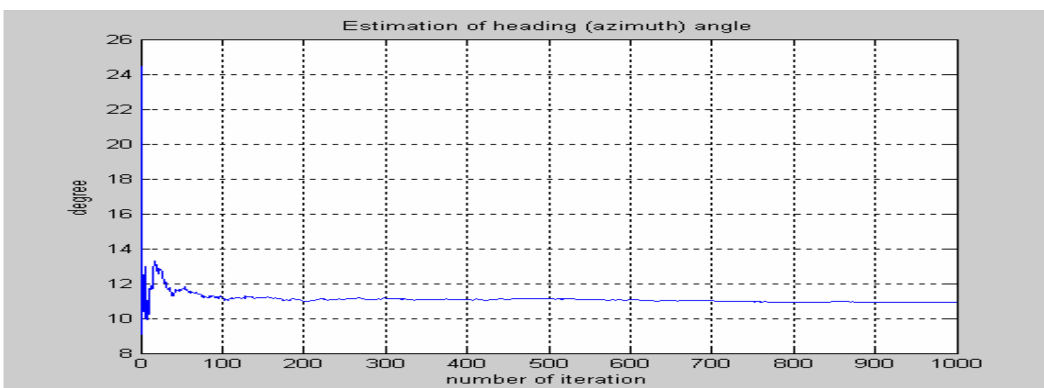

Figure 47. Estimation of Heading (azimuth) Angle

In Figure 47, convergence of heading angle is seen. After 600 iteration, it converges to real heading value.

Estimated heading value, error between real heading and estimated heading are as follows:

Heading=10.9168°, error= 0.0832°

Estimated pointing vector at three axes are as follows:

x_b^e = 0.9836 m, y_b^e = 0.1897 m, z_b^e = -0.0016 m

Examining results of Case 1 and 3, as multipath effect increases, both iteration time and error increase.

In Table 3, results of GPS based northfinding technique with Kalman filter can be seen. As seen from the results, as the baseline length increases, accuracy of the system increases. In addition, effect of multipath can be observed. As the multipath is higher, accuracy decreases.

Table 3. Results of GPS Based Northfinding Technique with Kalman Filter

Case Number	Baseline (meter)	$\sigma^2_{multipath\_error}(rad)$	Calculated Heading (degree)	Error (degree)
1	1	$(0.1)^2$	11.0369	0.0369
2	0.5	$(0.1)^2$	11.056	0.0560
3	1	$(0.2)^2$	10.9168	0.0832

4.6 Summary

In this chapter, GPS based nortfinding algorithm which is double difference technique with Kalman Filter is discussed. Observations central to this technique are measurements of the carrier phase of the GPS signal. Initial rough attitude is solved taking triple difference of observations. Attitude and integers are estimated with Kalman Filter applied on double difference of observations. Sources of measurement errors are identified. It was recognized that the multipath effects are potentially the dominant source of error in carrier phase measurements. A simple model for multipath phase errors is developed.

To test GPS based northfinding algorithm with Kalman filter, GPS emulator is used. Azimuth finding system gets GPS emulator outputs such as carrier phase measurements, satellite positions and pseudorange measurements and calculates the azimuth by means of aforementioned techniques. This algorithm detects the north angle within 0.08^o precision, which is seen from the case results. However, this precision highly depends on the baseline length. For one meter baseline and $(0.1\ rad)^2$ multipath error variance, the north angle precision is within 0.03^o.

To collect the data, a specific time must be waited for this method. However, after this time, iteration of this algorithm is computationally very easy as compared to GPS based northfinding technique with exhaustive search. Using longer baselines and getting more accurate solution are possible in technique with Kalman filter as compared to the technique with exhaustive search. In addition, differencing techniques reduce the noise components better than search techniques. Also even in bad condition, solutions do not go to wrong results.

As compared with other techniques, attitude determination using GPS receivers is characterized by being simple, economic, more compact and less complex than other techniques. All the advantages and disadvantages of GPS based northfinding systems are given in Chapter-3.

CHAPTER 5

ACCELEROMETER BASED NORTHFINDING TECHNIQUE

Accelerometer is an apparatus, which senses inertial reaction of the free mass to measure linear and angular acceleration. This chapter includes the detailed information about the accelerometers and the accelerometer based northfinding technique. Firstly, accelerometer structure, its working principles and accelerometer types are presented. Afterwards, accelerometer based northfinding algorithm and mechanism to detect the north with accelerometer are introduced. Accelerometer based northfinding technique is implemented in MATLAB and necessary inputs to test the algorithm are also created. Simulation results are explained clearly. Finally, comments on accelerometer based northfinding technique are given in order to give a general idea to the reader.

5.1 Accelerometers

A fundamental requirement in aerospace system design and operation is the measurement of vehicular acceleration with respect to inertial space. Sensors commonly known as accelerometers provide these measurements. Therefore, accelerometers also referred as specific force sensors are fundamental sensors of inertial navigation systems. They have been used since 17th century. At the beginning, besides linear accelerometers, angular accelerometers were used. Nevertheless, in the course of time, gyroscopes replace angular accelerometers since gyroscopes have good performance of measuring angular rate [50].

5.1.1 Accelerometer Structure and Its Operation

Accelerometers provide acceleration information in the input axis direction as electrical quantity. By using this information, position and velocity information are obtained. Input-output relation of accelerometers is in Figure 48 and usage of accelerometers can be seen in Figure 49.

Figure 48. Input-Output Relation of Accelerometers

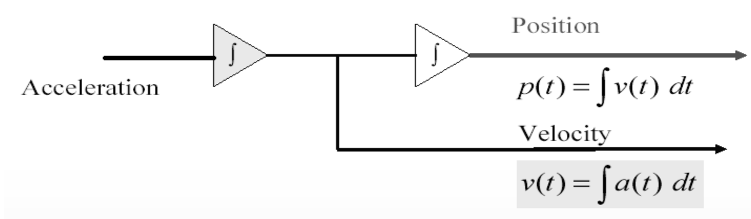

Figure 49. Usage of Accelerometers

For a moving vehicle, specific force implies the total net Newtonian force acting on the vehicle divided by its mass as follows:

$$a=F/m \qquad (5.1)$$

Where:

a : Specific force

F : Total Newton force

m : Vehicle Mass

a is commonly resolved along the body-axes of the vehicle x, y, z, so that $a = \begin{bmatrix} a_x & a_y & a_z \end{bmatrix}^T$. Since accelerometers are single input-axis devices, each axis requires the dedication of at least one accelerometer.

Force causes changing tension of a spring, deviation of a string or vibration frequency of a mass. To start out at this point, main principles of accelerometers can be explained. In most primitive form, accelerometer is assumed as a box formed by a spring and a mass that is tied to that spring. That is to say, accelerometer is described as an apparatus consists of a moving mass, a suspension mechanism, a pickoff working as capacitive, inductive or resistive as shown in Figure 50 and formalization of this is seen in Equation 5.2.

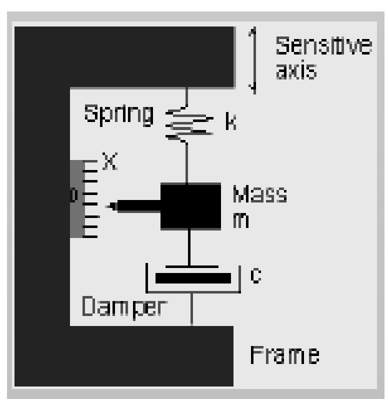

Figure 50. Inner Structure of Accelerometers

$$F = m\frac{d^2x}{d^2t} + c\frac{dx}{dt} + kx \qquad (5.2)$$

In Figure 51, Compact form of MEMS (Micro-Electro-Mechanical Systems) accelerometer photographs are shown.

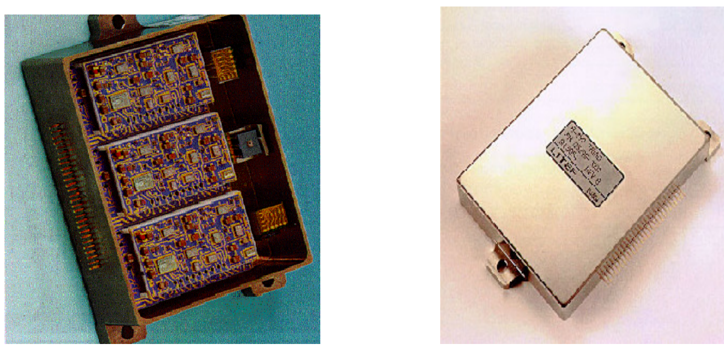

Figure 51. B290 MEMS Accelerometer

5.1.2 Accelerometers Types

Accelerometers are classified in three groups, which are pendulous accelerometers, vibrating beam accelerometers, MEMS accelerometers.

5.1.2.1 Pendulous accelerometers

Pendulous accelerometers are the first designed accelerometers and they are produced to measure gravity. Pendulous accelerometers are comprised from proof mass, suspension, pickoff and forcer.

5.1.2.2 Vibrating beam accelerometers

H.C. Hays invented vibrating beam accelerometers in 1928. This mechanism works according to the principle same as guitar string. Spring vibration frequency is proportional to square root of string stretch. In other words, frequency of vibrating string is affected and is changed by up and down mass motion due to applied acceleration.

Most accelerometers are analog apparatus. Accelerometers provide electrical output, which is voltage or current proportional to the applied acceleration. However, like most of the applications digital output is preferred. For this reason, vibration beam accelerometers with frequency output get popular.

5.1.2.3 MEMS accelerometers

MEMS structures are integration of mechanic components, sensors, switches and electronic staffs on silicon surface by means of micro-fabrication technology.

Nowadays MEMS accelerometers usage increases. This production technique of accelerometers decreases accelerometer cost, greatly. Moreover, with this technology, accelerometers are smaller and much functional. In addition, they are lighter and more reliable.

5.2 System and Algorithm

Accelerometer based northfinding technique is based on the reading of a rotating, vertically placed accelerometer. Vertically placed accelerometer on a rotating platform is used to measure the horizontal component of Earth rotation rate with the help of Coriolis effect. The functional relationship between the measured specific force and the azimuth information is derived in this section.

5.2.1 Coriolis Effect

Coriolis acceleration is sensed at a point moving in a rotating coordinate system. When a point mass is moving at a velocity ***V*** with respect to a coordinate system that rotates at an angular velocity *w*, then that point experiences a Coriolis acceleration whose value is $2wxV$ [32, 51]. Suppose that the point rotates at the rate of turn Ω_o on a circle whose radius is *r*. Then, the translatory velocity ***V*** is equal to $\Omega_o xr$. Consequently, the Coriolis acceleration is as seen in Equation 5.3.

$$f_{coriolis} = 2wx(\Omega_o xr) \qquad (5.3)$$

Where:

w: Angular velocity of the coordinate system

r: Circle's radius

Ω_o: Circle's rate of turn

5.2.2 System

In this thesis, accelerometer based northfinding system is composed of vertically placed accelerometer on a rotating table. This rotating table, which rotates at a constant angular velocity Ω, is horizontally placed on the Earth's surface as shown in Figure 52 [5, 6, 7].

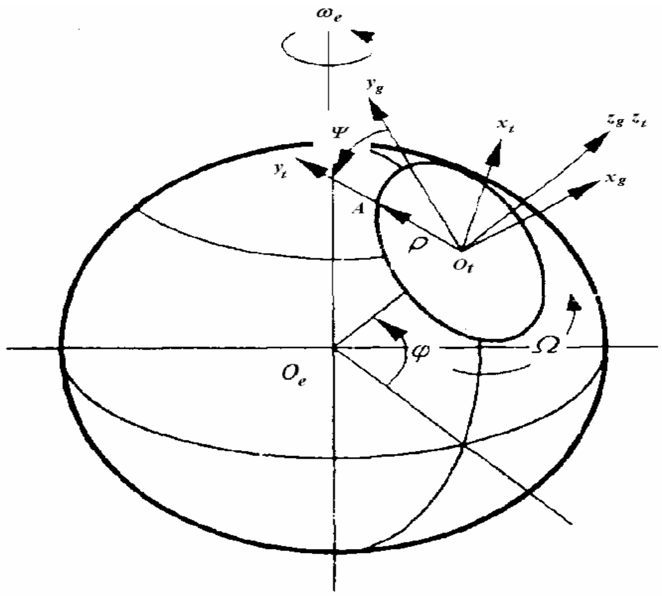

Figure 52. System Model of Accelerometer Based Northfinding

Where:

O_e: Earth' center,

φ: Latitude at which the spinning table positioned,

O_t: Center of the rotating table,

A: Point mass on the platform surface,

ρ : Distance from point A to O_t.

The two coordinate frames shown in Figure 52 are used in deriving the algorithm. In positions corresponding to t=0, these coordinate frames are

a) The locally level coordinate system [g] O_t-$x_g y_g z_g$, with its axis x_g, y_g and z_g pointing to the direction of local East, North and Up, respectively;

b) The rotating table coordinate system [t] O_t - $x_t y_t z_t$, with its axis y_t aligned with line $O_t A$, and axis z_t is perpendicular to the table.

5.2.3 Algorithm

According to the well-known Coriolis Effect, the total acceleration measurable at point mass A with respect to the inertial space expressed as projections along the axes of coordinate frame [g] will be

$$\overline{a}^g = \overline{G} + \frac{d^2\overline{r}}{dt^2} + 2\overline{w}_e x \frac{d\overline{r}}{dt} + \overline{w}_e x(\overline{w}_e x\overline{r}) \qquad (5.4)$$

Where:

$\overline{G}$: Vector of local gravity,

$$\overline{G} = \begin{bmatrix} 0 \\ 0 \\ -g \end{bmatrix} \qquad (5.5)$$

$\overline{r}$: Instantaneous displacement vector of point A from its center of revolution O_t, with respect to coordinate frame [g],

$$\overline{r} = \begin{bmatrix} -\rho\sin(\Omega t + \Psi) \\ \rho\cos(\Omega t + \Psi) \\ 0 \end{bmatrix} \qquad (5.6)$$

Ψ : Initial azimuth of vector $\overline{r}$ from true north,

$\overline{w}_e$: Earth rotation vector,

$$\overline{w}_e = \begin{bmatrix} 0 \\ w_N \\ w_H \end{bmatrix} = \begin{bmatrix} 0 \\ w_e\cos\varphi \\ w_e\sin\varphi \end{bmatrix} \qquad (5.7)$$

w_N : Horizontal component of Earth rotation,

w_H : Vertical component of Earth rotation,

Ω : Rate of turn of the rotating platform.

Assuming $\Omega >> w_e$ and using Equations 5.5, 5.6 and 5.7, Equation 5.4 becomes

$$\bar{a}^g = \begin{bmatrix} \Omega^2 \rho \sin(\Omega t + \psi) \\ -\Omega^2 \rho \cos(\Omega t + \psi) \\ -g \end{bmatrix} + \begin{bmatrix} 2\Omega w_H \rho \sin(\Omega t + \psi) \\ -2\Omega w_H \rho \cos(\Omega t + \psi) \\ 2\Omega w_N \rho \cos(\Omega t + \psi) \end{bmatrix} \qquad (5.8)$$

Re-express above acceleration as projections along the axes of coordinate frame [t], since accelerometers sense acceleration in body or vehicle frame,

$$\bar{a}^t = C_g^t \bar{a}^g = \begin{bmatrix} 0 \\ -\Omega^2 \rho - 2\Omega w_H \rho \\ -g \end{bmatrix} + \begin{bmatrix} 0 \\ 0 \\ 2\Omega w_N \rho \cos(\Omega t + \psi) \end{bmatrix} \qquad (5.9)$$

Where:

C_g^t: Direction cosine matrix from frame [g] to frame [t].

$$C_g^t = \begin{bmatrix} \cos(\Omega t + \psi) & \sin(\Omega t + \psi) & 0 \\ -\sin(\Omega t + \psi) & \cos(\Omega t + \psi) & 0 \\ 0 & 0 & 1 \end{bmatrix} \qquad (5.10)$$

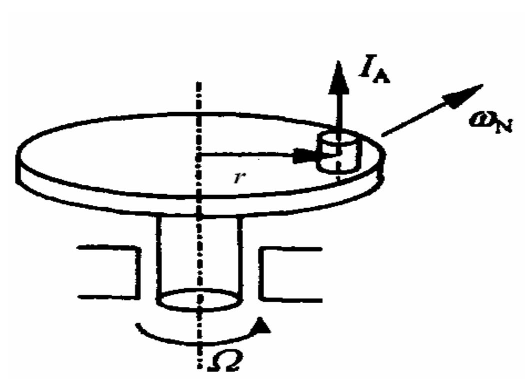

Figure 53. Vertically Placed Accelerometers on a Rotating Platform

If a linear accelerometer is mounted at point A with its sensitive axis strictly vertical as seen in Figure 53, it will read acceleration in Equation 5.11 from equation 5.9.

$$f = a_o - g + 2\Omega w_N \rho \cos(\Omega t + \psi) + n_r \qquad (5.11)$$

Where,

a_o: Null bias of the accelerometer,

n_r: Random high frequency noise of the accelerometer.

AC component of the signal is in Equation 5.12

$$f_{AC} = 2\Omega w_N \rho \cos(\Omega t + \psi) + n_r \qquad (5.12)$$

and this term holds the information of the initial azimuth of the accelerometer with respect to the direction of true North. Direction of true North can be determined by appropriate signal processing procedures applied to Equation 5.12 as follows

$$A = \int_0^T f_{AC} \operatorname{sgn}(\cos \Omega t) dt \qquad (5.13)$$

$$B = -\int_0^T f_{AC} \operatorname{sgn}(\sin \Omega t) dt \qquad (5.14)$$

Where:

T: Period of the complete revolution of the rotating table, $T = 2\pi/\Omega$

$$A = 8 w_N \rho \cos\psi \qquad (5.15)$$

$$B = 8 w_N \rho \sin\psi \qquad (5.16)$$

$$\hat{\psi}_d = tg^{-1} \frac{B}{A} \ \text{(for } A >> B\text{)} \qquad (5.17)$$

$$\hat{\psi}_d = ctg^{-1}\frac{A}{B} \text{ (for } A<B) \qquad (5.18)$$

Let us systematically present the accelerometer based northfinding technique:

Step 1: Place a very accurate accelerometer vertically on a rotating platform with high rotation rate.

Step 2: Let it sense the Earth rotation rate by means of Coriolis acceleration.

Step 3: Take the AC component of the signal sensed by the accelerometer.

Step 4: Apply signal processing to obtained signal by using Equations from 5.13 to 5.16.

Step 5: Take the inverse tangent of the ratio of these terms.

5.2.4 Errors

There are two main sources of errors. One of them is accelerometer noise and the other one is base inclination. In the following section, these error sources are examined.

5.2.4.1 Accelerometer Noise:

The standard deviation of the azimuth calculation may be estimated as [33]

$$\sigma_{\psi} = \frac{\sigma_{n_r}}{w_e \cos\varphi\sqrt{n}} \qquad (5.19)$$

Where:

σ_{n_r} : Standard deviation of the accelerometer (converted into angular rate),

n : Number of repeating periods.

As seen in Equation 5.19, standard deviation of the azimuth is proportional to standard deviation of the accelerometer, directly. It is obvious that to reduce the effect of the accelerometer noise, more samples should be taken. Other limit to the accuracy of an accelerometer based northfinder is the latitude at which it is operating. Northfinding at the equator is the easiest; moving north (or south) makes the process more difficult. As the northfinder is moved away from the equator, the magnitude of the measured rotation becomes smaller and smaller, decreasing the signal to noise ratio of the measurement.

5.2.4.2 Base Inclination:

It is intended that the base of the system be placed locally level in order to keep the sensitive axis of the accelerometer strictly vertical. Because of the geometry between the system base and the Earth's spin axis, north-heading error $\Delta\psi$ depends on the local latitude φ, the inclination angle θ and the inclination axis azimuth ψ [34].

$$\Delta\psi \approx tg^{-1}(\theta . tg\varphi . \cos\psi) \qquad (5.20)$$

Where:

θ : Inclination angle

5.3 Simulation Results

Real data could not be used to drive accelerometer based northfinding algorithm in this thesis. Making such a mechanism is difficult. One of the difficulties is to get a very accurate accelerometer, which has 10^{-6} g random high frequency noise. Moreover, the spinning table should rotate at a constant angular velocity of 600 rpm, which is 3600°/s. Nevertheless, the three-axis motion simulator, which is introduced in chapter six, rotates at a constant angular velocity at most 1000°/s. Therefore, simulation input signals are implemented in MATLAB to derive the accelerometer based northfinding algorithm.

In following case results, effects of latitude, repeating periods or in other words number of samples, base inclination angle and accelerometer noise are examined.

Firstly, the following parameters have been assumed on simulation, which has no error term:

$\Omega = 600 rpm = 20 * \pi$ rad/sec,

ψ =60^{o}=0.3333*pi rad,

$\rho = 0.05\, m$,

$\sigma_{n_r} = 0$,

$\varphi = 40^{o} = 0.2222 * \pi$ rad,

$\theta = 0 rad$,

$w_e = 15.041 * pi/(180 * 3600)$ rad/sec,

$n=10$

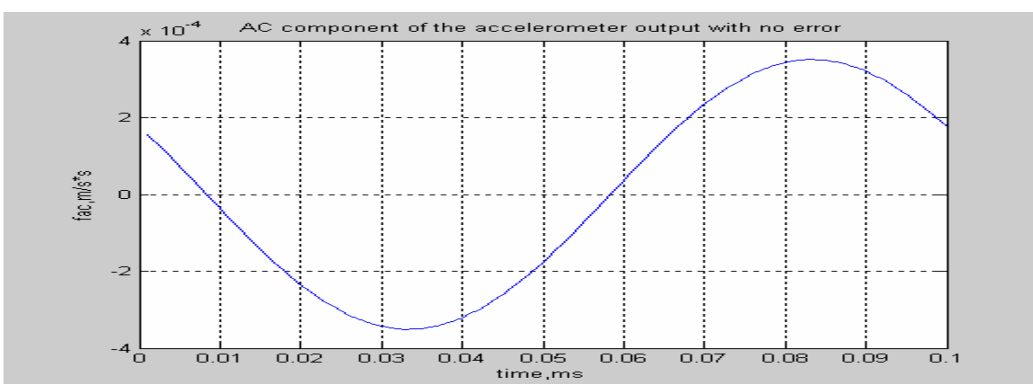

Figure 54. AC Component of the Accelerometer Output with No Error

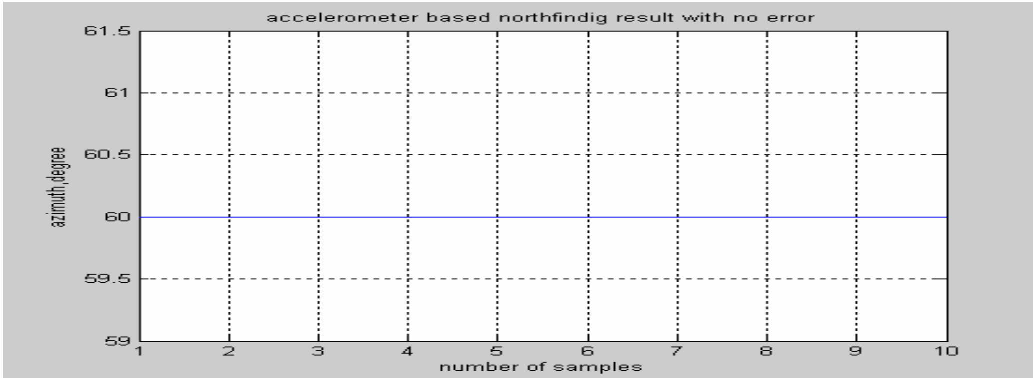

Figure 55. Accelerometer Based Northfinding Result with No Error

Signal sensed by the accelerometer is seen in Figure 54. In Figure 55, accelerometer based northfinding technique result without error is seen.

5.3.1 Effect of Latitude

In this section, effect of latitude is examined. In each step of the case, all of the above quantities are same but latitude changes. These quantities are as follows:

$\Omega = 600 rpm = 20 * \pi$ rad/sec,

$\psi = 60^o = 0.3333 * \pi$ rad,

$\rho = 0.05 m$,

$\sigma_{n_r} = 10^{-5}$ m/s^2,

$\theta = 0 rad$,

$w_e = 15.041 * pi/(180 * 3600)$ rad/sec,

n=10

Case 1: $\varphi = 40^o = 0.2222 * \pi$ rad.

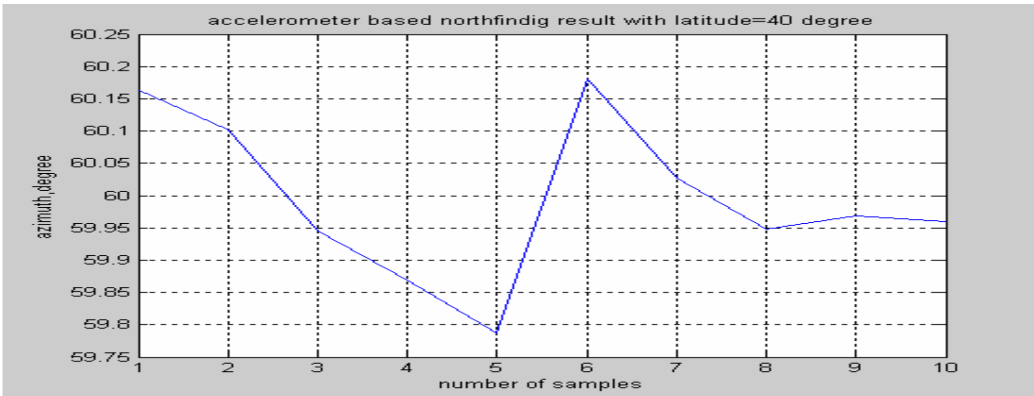

Figure 56. Accelerometer Based Northfinding Result with Latitude=40°

Accelerometer based northfinding result for 40° latitude is shown in Figure 56. Standard deviation of azimuth error for this case is $\sigma_\psi = 0.1252$ °

Case 2: For $\varphi = 30^o = 0.1667 * \pi$ rad.

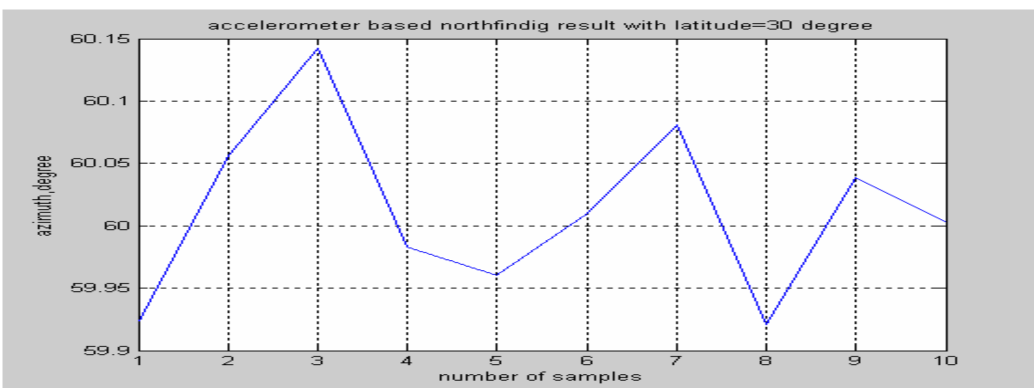

Figure 57. Accelerometer Based Northfinding Result with Latitude=30°

Accelerometer based northfinding result for 30° latitude is shown in Figure 57. Standard deviation of azimuth error for this case is $\sigma_{\psi} = 0.0699$ °

Case 3: For $\varphi = 20^{o} = 0.1111 * \pi$ rad.

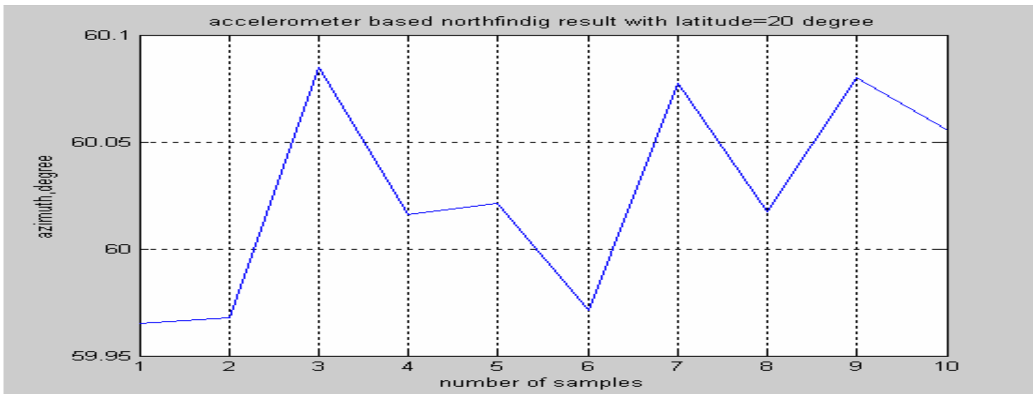

Figure 58. Accelerometer Based Northfinding Result with Latitude=20°

Accelerometer based northfinding result for latitude 20° is shown in Figure 58. Standard deviation of azimuth error for this case is $\sigma_{\psi} = 0.0474$ °

Theory of accelerometer based northfinding suggests that as the latitude gets smaller, standard variation of azimuth error becomes smaller, because at small latitudes accelerometer senses or measures bigger signal which is horizontal component of earth rotation vector. When the above figures and standard deviations of azimuth errors are investigated, same result is reached.

5.3.2 Effect of Number of Samples

In this section, effect of number of samples is investigated. In each step of the case, all the above quantities are same but number of samples changes.

$\Omega = 600rpm = 20 * \pi$ rad/sec,

$\psi = 60^o = 0.3333 * \pi$ rad,

$\rho = 0.05\,m$,

$\sigma_{n_r} = 10^{-5}$ m/s^2,

$\theta = 0 rad$,

$\varphi = 40^o = 0.2222 * \pi$ rad,

$w_e = 15.041 * pi/(180 * 3600)$ rad/sec,

Case 1: For *n=3*.

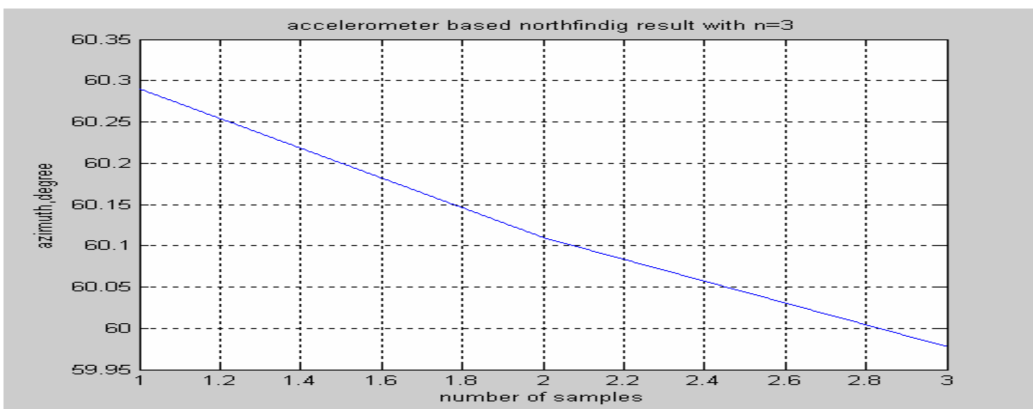

Figure 59. Accelerometer Based Northfinding Result with *n*=3

Accelerometer based northfinding result for *n*=3 is shown in Figure 59 and standard deviation of azimuth for this case is $\sigma_\psi = 0.1569^{\circ}$

Case 2: For *n=10*.

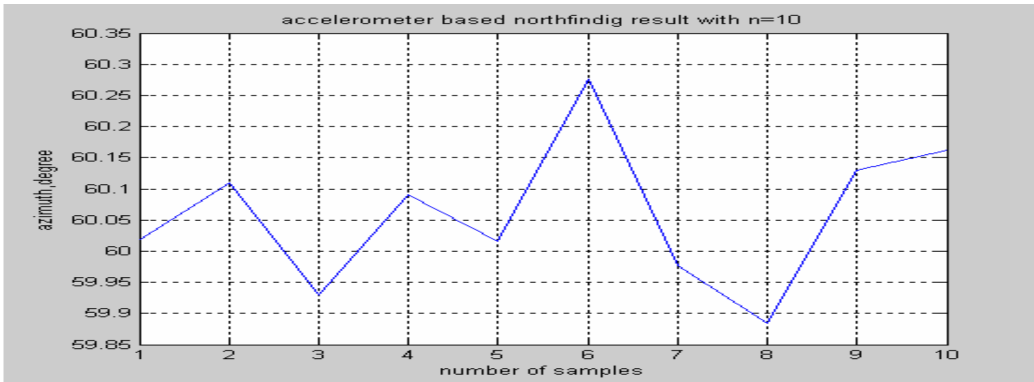

Figure 60. Accelerometer Based Northfinding Result with *n*=10

Accelerometer based northfinding result for *n*=10 is shown in Figure 60. Standard deviation of azimuth error for this case is $\sigma_{\psi} = 0.1172^{\circ}$.

Case 3: For *n=20*.

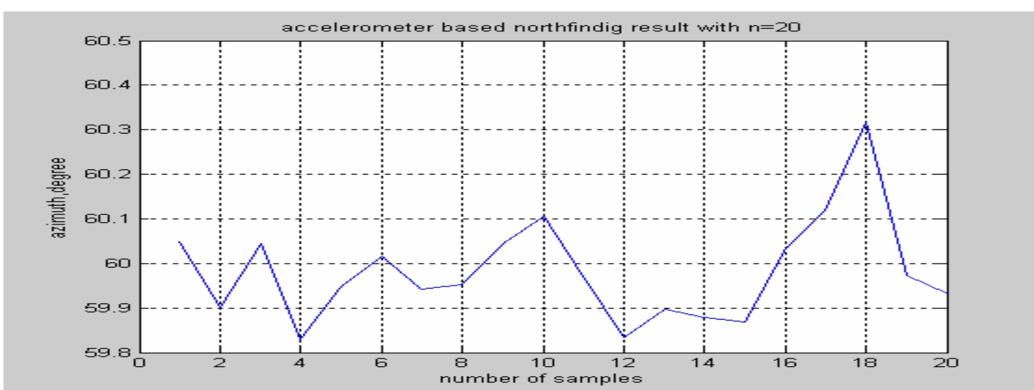

Figure 61. Accelerometer Based Northfinding Result with *n*=20

Accelerometer based northfinding result for n=20 is shown in Figure 61. Standard deviation of azimuth error for this case is $\sigma_{\psi} = 0.1147^{\circ}$

Case 4: For *n=30*,

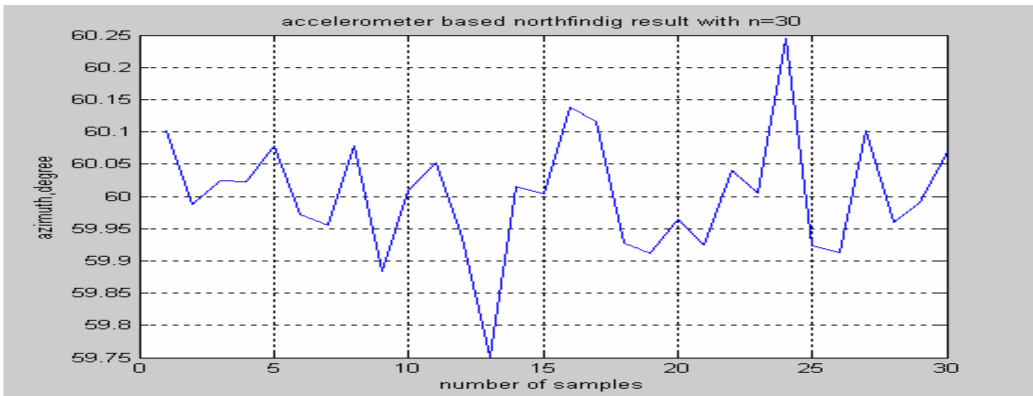

Figure 62. Accelerometer Based Northfinding Result with n=30

Accelerometer based northfinding result for n=30 is shown in Figure 62 and standard deviation of azimuth error for this case is $\sigma_{\psi} = 0.0936^{\circ}$

Theory of accelerometer based northfinding suggests that as the number of samples gets bigger, standard variation of azimuth becomes smaller, because by taking many sample, azimuth is estimated much accurately. When the above figures and standard deviations of azimuths are examined, same result is reached.

5.3.3 Effect of Base Inclination

In this section, effect of base inclination is investigated. In each step of the case, all the above quantities are same but angle of base inclination changes.

$\Omega = 600rpm = 20 * \pi$ rad/sec,

$\psi = 60^o = 0.3333 * \pi$ rad,

$\rho = 0.05\,m$,

$\sigma_{n_r} = 10^{-5}$ m/s^2,

n=5

$\varphi = 40^o = 0.2222 * \pi$ rad,

$w_e = 15.041 * pi/(180 * 3600)$ rad/sec,

Case 1: For $\theta = 0 rad$, accelerometer based northfinding algorithm result is the mean value of the calculated azimuth for each sample as follows.

Mean of calculated azimuths: $\psi = 59.9712^{\circ}$

$\sigma_{\psi} = 0.1091^{\circ}$

$\Delta\psi = 0.0288^{\circ}$

Case 2: For $\theta = 0.2^o = 0.0011 * \pi rad$, accelerometer based northfinding algorithm result is the mean value of the calculated azimuth for each sample as follows.

Mean of calculated azimuths: $\psi = 59.8886^{\circ}$

$\sigma_{\psi} = 0.0989^{\circ}$

$\Delta\psi = 0.1114^{\circ}$

Case 3: For $\theta = 2^o = 0.011 * \pi rad$, accelerometer based northfinding algorithm result is the mean value of the calculated azimuth for each sample as follows.

Mean of calculated azimuths: $\psi = 59.1168^{\circ}$

$\sigma_{\psi} = 0.0887^{\circ}$

$\Delta\psi = 0.8832^{\circ}$

Case 4: For $\theta = 5^{o} = 0.0278 * \pi rad$, accelerometer based northfinding algorithm result is the mean value of the calculated azimuth for each sample as follows.

$\psi = 57.8003^{\circ}$

$\sigma_{\psi} = 0.0806^{\circ}$

$\Delta\psi = 2.1997^{\circ}$

Theory of accelerometer-based northfinding suggests that as the angle of base inclination gets bigger, error in azimuth becomes bigger. Since horizontal component of earth rotation vector is sensed harder. When the above results and mean values are examined, same result is reached.

5.4 Summary

In this section, accelerometer based northfinding technique is presented. At the beginning, the answers of the questions about what the accelerometer is and where they are used are researched. Afterwards, a detailed description of the apparatus for azimuth finding, which is based on the measurements of an accelerometer that is placed vertically on a rotating plate, is given. The measured acceleration is the Coriolis acceleration generated when the accelerometer travels on a circular path with respect to moving navigation frame. Formulas for extracting the azimuth are developed. Moreover, errors of accelerometer based northfinding technique are examined.

Over the past century, new techniques have been exploited for inertial navigation to produce low cost and high performance northfinding systems used in both military and civil fields. All systems rely on detecting the direction of the horizontal component of the Earth's spin rate. Conventional northfinding systems employ expensive gyroscopes as basic inertial sensors to detect the Earth's rotation; it is therefore highly desirable to devise an inertial northfinder without gyroscopes. As a result of the above discussions, it is seen that by applying accelerometer's basic principle to the measurement of the Earth's spin rate, true north can be found with an inexpensive linear accelerometer. The system can serve as a substituting counterpart to the traditional gyroscopic northfinders due to its low cost and fast response. In addition to that, the apparatus is light, small, and consumes little power.

Its most obvious error comes from the inclination of platform as to earth's surface. However, this can be improved by good leveling techniques. Another problematic matter is the construction of the apparatus. Although, accelerometers are relatively cheap, for this technique very precise accelerometer is needed. In addition, platform must be rotated very fast to sense Earth rotation rate. Nevertheless, to give such fast rotation is not an easy job. Lastly, during the northfinding process, working machines, moving people around the system can cause disturbance.

CHAPTER 6

IMU BASED NORTHFINDING TECHNIQUE

IMU (Inertial Measurement Unit) is a module, which consists of accelerometers and gyroscopes to calculate the vehicles inertial motions. In this chapter, IMU based northfinding technique is presented. Firstly, IMU structure, its operation and IMU types are introduced in detail. Then, IMU based northfinding algorithm is explained. The algorithm is implemented in MATLAB programming. This program inputs are real IMU outputs. IMU is put in a three-axis motion simulator and its data is collected. The environment of the set-up is described in this chapter. Moreover, program results are presented. Finally, comments of IMU based northfinding technique are considered in order to give a general idea to the reader.

6.1 IMU (Inertial Measurement Unit)

IMU is the critical segment of the INS (Inertial Navigation Systems) since this unit produces the measurements. IMU simply measures acceleration and angular rate of a vehicle. One can update the vehicle's initial position and attitude by using these inertial measurements of IMU and therefore obtain the vehicles current position and attitude. In order to analyze the IMU, its structure, operation and types should be introduced.

6.1.1 IMU Structure

Roughly, navigation can be described as a process of transferring the vehicle from one point to another point in the space. The most important problem of a navigated vehicle is determining its position and attitude. Systems that calculate the position, velocity and attitude of a navigated vehicle in a known coordinate system are named as navigation systems. Inertial Navigation Systems determine information about position and attitude by internal means; that is to say, no need to external signals. In general, inertial navigation is described as measuring accelerations of the vehicle and taking integral of these measurements to find position and velocity in a defined coordinate system.

The compact assembly formed by the three rate gyros and the three accelerometers is called as an IMU (Inertial Measurement Unit) and forms the hearth of any INS (Inertial Navigation Unit). An IMU consists of three orthogonally arranged single-axis accelerometers to determine the acceleration vector and of three orthogonally arranged single-axis gyroscopes to determine the angular rate vector of the vehicle in 3-dimensional space. In Figure 63, IMU structure and placement of inertial sensors are illustrated.

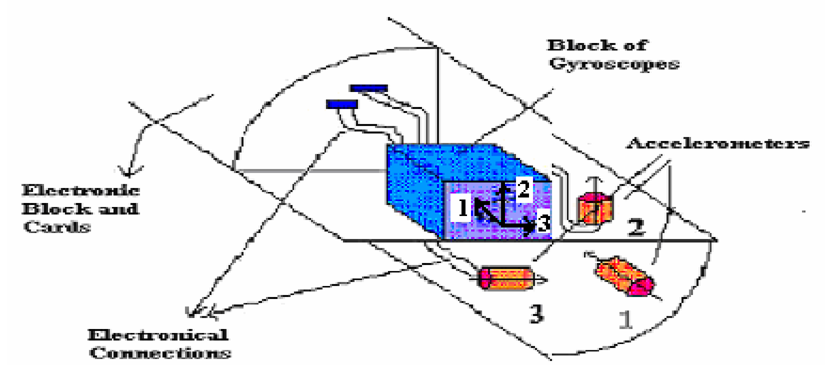

Figure 63. IMU Structure

6.1.2 IMU Operation

In IMU operation, the most important issue to be considered is the reference coordinate frame of the outputs of the gyroscopes and the accelerometers. Thus, navigation computer is needed in order to provide coordinate transformations. Rotations sensed by the gyroscopes are in coordinates fixed to the body. The body referenced accelerometer outputs are transformed from the body to the navigation frame in the navigation computer using the transformation matrix. This transformation matrix is generated in the navigation computer by combining the rate outputs from the body fixed gyroscopes and the navigation frame rates created by the vehicle's velocity.

6.1.3 IMU Types

Different IMU types can be considered when the reference frames of the sensors of the IMU are investigated and it can be found that two distinct implementation approaches for inertial systems are possible: gimballed inertial navigation systems and strapdown systems.

6.1.3.1 Gimballed Inertial Navigation System:

In gimballed inertial navigation system, the inertial sensors are mounted on an actuated platform. The gimbal angles are commanded to maintain the platform-frame alignment with a specified navigation coordinate system. This is achieved by feeding gimbals using the gyroscope outputs so that platform will be isolated from vehicle rotational motion. If this is achieved, then the platform does not experience any rotation relative to the navigation frame, in spite of vehicle motion. In this approach, accelerometers aligned with the platform measure the specific force along the navigation coordinate system axes. Scaling and integration of this measured acceleration yield the desired navigation frame position and velocity vectors. Vehicle attitude is determined by measurement of the relative angles between the vehicle and the platform axes. This design makes easy to calculate position and velocity, on the other hand the mechanical structure gets complicated.

In Figure 64, structure of gimballed inertial navigation is shown. In Figure 65, working principles of gimballed inertial navigation is well understood. One can notice that there is not any coordinate transformation operation in Figure 65, since the gimballed IMU keeps the inertial sensors, which are gyroscope, and accelerometers on the navigation coordinate frame.

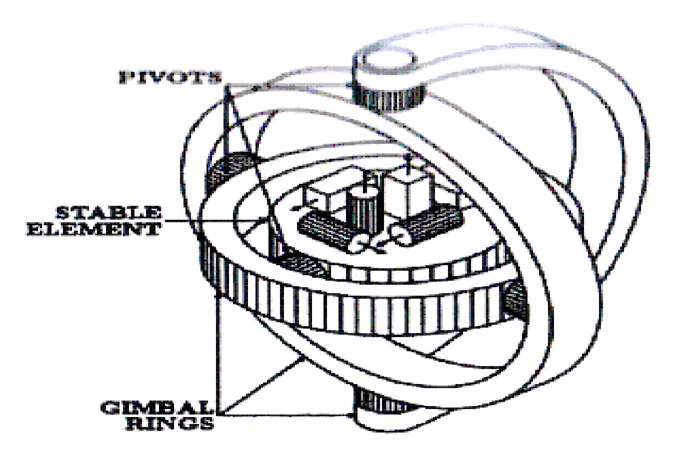

Figure 64. Structure of Gimballed Inertial Navigation System

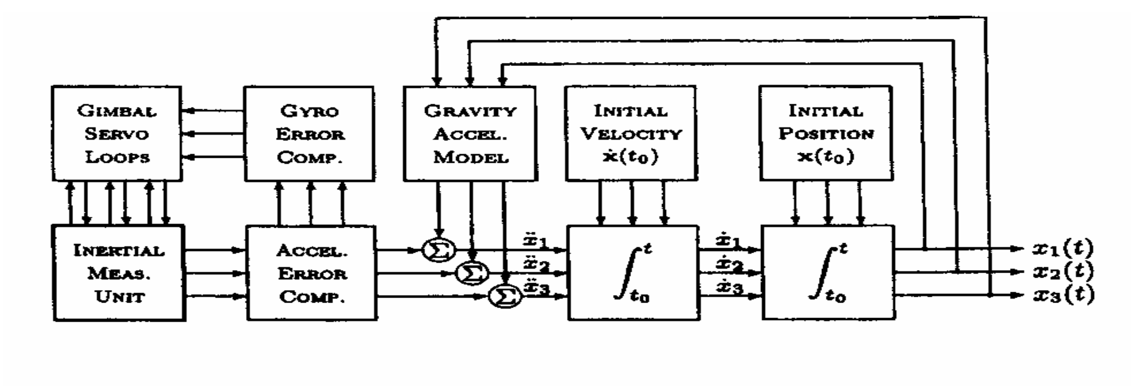

Figure 65. Principles of Gimballed Inertial Navigation System

6.1.3.2 Strapdown Inertial Navigation System:

Strapdown systems attach the inertial sensors directly to the vehicle frame. In this approach, the sensors experience the full dynamic motion of the vehicle. Therefore, higher bandwidth (possibly noisier) rate gyros with a higher dynamic range are required. Because of the increased dynamic range, gyro scale-factor error and nonlinearity become increasingly important. In addition, the relationship among vehicle, navigation, and inertial coordinate frames must be maintained computationally. This increases the on-board computational load relative to that of a gimballed system [37]. In Figure 66, structure of strap-down inertial navigation is seen.

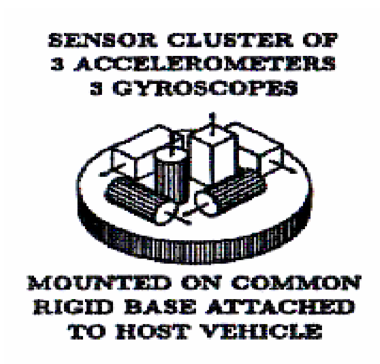

Figure 66. Structure of Strapdown Inertial Navigation System

In Figure 67, working principles of strapdown inertial navigation are presented. Accelerometers sense accelerations in vehicle or body frame but measurements must be transformed from body frame to inertial navigation system to calculate velocity and position of the vehicle in inertial navigation frame. Gyroscope outputs, which are angular rate of body frame with respect to inertial navigation frame, are used to calculate transformation matrix between two frames. Then, using this transformation matrix, accelerometers outputs are transformed from body frame to inertial navigation frame. Lastly, taking first and second integral of accelerometer outputs, velocity and position of the vehicle are calculated respectively.

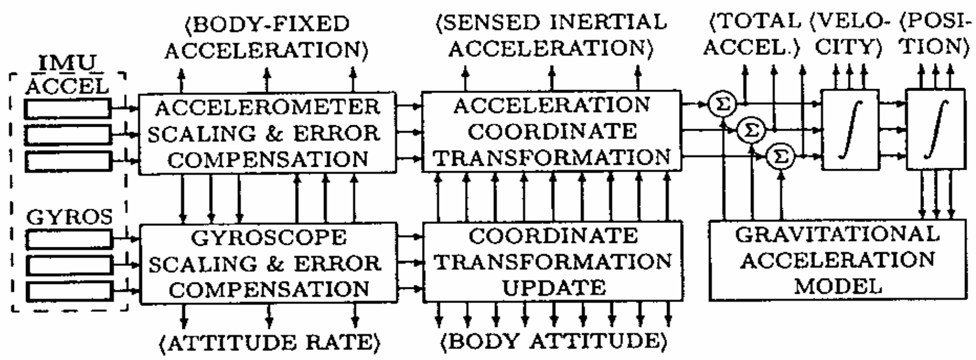

Figure 67. Principles of Strap-down Inertial Navigation System

Strapdown system is the used IMU type in the IMU based northfinding technique in this thesis.

6.2 Algorithm and Errors

As mentioned before, in this chapter northfinding algorithm is implemented by using the IMU outputs. Up to now, IMU is explained and it is declared that strapdown IMU is used in this study. In this part, algorithm and errors on IMU based northfinding are presented.

6.2.1 Algorithm

In a strapdown system, attitude information is stored as a direction cosine matrix. The objective of the northfinding process is to determine the direction cosine matrix, which defines the relationship between the inertial sensor axes and the local geographic frame. The azimuth or the north angle, which can be defined as a misalignment between the body axis roll vector and local geographic frame north vector, is calculated easily from direction cosine matrix [35, 36].

The body mounted sensors measure components of the specific force needed to overcome gravity and components of Earth rotation rate, denoted by the vector quantities $\underline{g}^b$ and $\underline{w}^b_{i/e}$ respectively. These vectors are related to the gravity and Earth's rate vectors specified in the local geographic frame, $\underline{g}^n$ and $\underline{w}^n_{i/e}$ respectively, in accordance with the following Equations 6.1 and 6.2.

$$\underline{g}^b = C_n^b \underline{g}^n \qquad (6.1)$$

$$\underline{w}^b_{i/e} = C_n^b \underline{w}^n_{i/e} \qquad (6.2)$$

Where:

$\underline{g}^b$ (3x1): Accelerometers output in body frame in three axes,

$\underline{g}^n$ (3x1): Gravity vector in navigation frame in three axes,

$\underline{w}^b_{i/e}$ (3x1): Gyroscopes output in body frame in three axes,

$\underline{w}^n_{i/e}$ (3x1): Earth rotation vector in navigation frame in three axes,

C_n^b (3x3): Direction cosine matrix from navigation frame to body frame.

$$C_b^n = \begin{bmatrix} \cos(p)*\cos(az) & -\cos(r)*\sin(az)+\sin(r)*\sin(p)*\cos(az) & \sin(r)*\sin(az)+\cos(r)*\sin(p)*\cos(az) \\ \cos(p)*\sin(az) & \cos(r)*\cos(az)+\sin(r)*\sin(p)*\sin(az) & -\sin(r)*\cos(az)+\cos(r)*\sin(p)*\sin(az) \\ -\sin(p) & \sin(r)*\cos(p) & \cos(r)*\cos(p) \end{bmatrix}$$

(6.3)

Where:

p: Pitch angle

r : Roll angle

az : Azimuth angle or north angle

All these above information can be combined in a single matrix product in Equation 6.4

$$\left\lfloor \underline{g}^{b} \middle| \underline{w}_{i/e}^{b} \middle| \underline{g}^{b} x \underline{w}_{i/e}^{b} \right\rfloor = C_{n}^{b} \left\lfloor \underline{g}^{n} \middle| \underline{w}_{i/e}^{n} \middle| \underline{g}^{n} x \underline{w}_{i/e}^{n} \right\rfloor \tag{6.4}$$

Or, above matrix product is transposed and this transposing is expressed in Equation 6.5

$$\left[\underline{g}^{b} \middle| \underline{w}_{i/e}^{b} \middle| \underline{g}^{b} x \underline{w}_{i/e}^{b} \right]^{T} = \left[\underline{g}^{n} \middle| \underline{w}_{i/e}^{n} \middle| \underline{g}^{n} x \underline{w}_{i/e}^{n} \right]^{T} C_{b}^{n} \tag{6.5}$$

To express C_{b}^{n} in terms of the other terms, the 3x3[]^{T} matrix on the right side is inverted and premultiplied at both sides. This process results in Equation 6.6

$$C_{b}^{n} = \left[\underline{g}^{n} \middle| \underline{w}_{i/e}^{n} \middle| \underline{g}^{n} x \underline{w}_{i/e}^{n} \right]^{-T} \left[\underline{g}^{b} \middle| \underline{w}_{i/e}^{b} \middle| \underline{g}^{b} x \underline{w}_{i/e}^{b} \right]^{T} \tag{6.6}$$

Assuming a local level geographic N-E-D frame as navigation frame, gravity and Earth rotation vectors are expressed in Equations 6.7 and 6.8 as follows.

$$\underline{g}^{n} = \begin{bmatrix} 0 \\ 0 \\ -g \end{bmatrix} \tag{6.7}$$

$$\underline{w}_{i/e}^{n} = \begin{bmatrix} w_{i/e} \cos\phi \\ 0 \\ -w_{i/e} \sin\phi \end{bmatrix} \tag{6.8}$$

Equation 6.9 gives the cross product of these two vectors

$$\underline{g}^n x \underline{w}^n_{i/e} = \begin{bmatrix} 0 \\ g w_{i/e} \sin\phi \\ 0 \end{bmatrix} \qquad (6.9)$$

Where:

ϕ: Latitude of the vehicle,

$w_{i/e}$: Earth rotation rate

Substituting Equations 6.7, 6.8 and 6.9 into 6.6, the initial C_b^n direction cosine matrix is computed. As a result, the north or azimuth angle of the vehicle is calculated from this initial direction cosine matrix or transformation matrix easily from Equation 5.10.

$$az = \tan^{-1}(C_b^n(2,1) / C_b^n(1,1)) \qquad (6.10)$$

Now, let us summarize the IMU based northfinding algorithm systematically.

Step 1: Get the outputs of inertial sensors, which are placed, in IMU. Accelerometers measure linear accelerations at each axis in body coordinate system. Gyroscopes measure rotation or angular rates of each body frame axis with respect to each navigation frame axis.

Step 2: Assume local geographic frame N-E-D as navigation frame. In addition, relate gravity vector described in Equation 6.7 and Earth rotation vector described in Equation in 6.8 to accelerometer outputs and gyroscope outputs by using Equations 6.1 and 6.2 respectively.

Step 3: Using Equations 6.4, 6.5 and 6.6 to get direction cosine matrix, which describe the attitude of body coordinate frame with respect to navigation frame.

Step 4: Calculate azimuth or north angle of vehicle from direction cosine matrix by using Equation 6.10.

6.2.2 Errors on IMU Based Northfinding Technique

A stationary strapdown inertial navigation unit provides sensed gravity and Earth rotations by its accelerometers and gyroscopes. These sensors' outputs contain errors. Sensed specific force and gyroscope rate errors are represented in Equations in 6.11 and 6.12 as follows

$$\underline{\bar{f}}^{b} = \underline{g}^{b} + \delta \underline{\bar{f}}^{b} \qquad (6.11)$$

$$\underline{\overline{w}}^{b}_{i/b} = \underline{\overline{w}}^{b}_{i/e} + \delta \underline{w}^{b} \qquad (6.12)$$

Thus, C_b^n matrix computed as outlined in section 6.2.1 contains error, and C_b^n matrix with error is represented in Equation 6.13.

$$\overline{C}_b^{n} = \left[\underline{g}^{n} \middle| \underline{w}^{n}_{i/e} \middle| \underline{g}^{n} x \underline{w}^{n}_{i/e}\right]^{-T} \left[\underline{\bar{f}}^{b} \middle| \underline{\overline{w}}^{b}_{i/b} \middle| \bar{f}^{b} x \underline{\overline{w}}^{b}_{i/b}\right]^{T} \qquad (6.13)$$

Assuming small attitude errors in each axis, C_b^n matrix with errors is assumed as follows

$$\overline{C}_b^{n} = [I - (\underline{\phi} x)] C_b^n \qquad (6.14)$$

Put Equations 6.14, 6.11 and 6.12 into Equation 6.13,

$$[I - (\underline{\phi} x)] C_b^n = []^{-T} \left(\left[\underline{g}^{b} \middle| \underline{w}^{b}_{i/e} \middle| \underline{g}^{b} x \underline{w}^{b}_{i/e}\right]^{T} + \left[\delta \underline{f}^{b} \middle| \delta \underline{w} \middle| \delta(\underline{f}^{b} x \underline{w}^{b})\right]^{T} \right) \qquad (6.15)$$

Making some operation on 6.15,

$$-(\underline{\phi} x) C_b^n = []^{-T} \left[\delta \underline{f}^{b} \middle| \delta \underline{w} \middle| \delta(\underline{f}^{b} x \underline{w}^{b})\right]^{T} \qquad (6.16)$$

Equation 6.16 can be used to relate navigation frame tilt errors to body referenced sensor errors for any navigation frame mechanization.

In order to illustrate this relationship, the local geographic frame is used for the navigation frame. Frame misalignment (attitude errors at each axis) is described by the cross product skew symmetric matrix equivalent to Equation 6.17

$$-(\underline{\phi} x) = \begin{bmatrix} 0 & \phi_d & -\phi_e \\ -\phi_d & 0 & \phi_n \\ \phi_e & -\phi_n & 0 \end{bmatrix} \qquad (6.17)$$

Where:

ϕ_d : Misalignment (error) at down axis

ϕ_e : Misalignment (error) at east axis

ϕ_n : Misalignment (error) at north axis

Assume that the navigation system is nominally aligned with the geographic frame such that

$$C_b^n \equiv I \qquad (6.18)$$

Putting Equations 6.18 and 6.17, into 6.16 and making some operation on Equation 6.16 yield the following navigation frame misalignments

$$\phi_n = -\frac{\delta f_y}{g} \qquad (6.19)$$

$$\phi_e = \frac{\delta f_x}{g} \qquad (6.20)$$

$$\phi_d = [\frac{\delta f_y}{g} \tan\phi + \frac{\delta w_y}{w_{ile} \cos\phi}] \qquad (6.21)$$

ϕ : Latitude of the vehicle

δw_y : Gyroscope rate bias stability

δf_y : Accelerometer bias stability

$w_{i/e}$: Earth rotation rate

Equations 6.19, 6.20 and 6.21 demonstrate that misalignment errors are introduced as a result of accelerometer and gyroscope errors when using IMU based northfinding. The magnitude of azimuth alignment error is dependent on latitude of the vehicle, gyroscope error and accelerometer error.

6.3 Simulation Environment

In order to test IMU based northfinding technique, real IMU outputs are needed. Strapdown IMU is placed into the three-axis motion simulator, which is located in TUBITAK-SAGE. Then the motion simulator is run with eight different attitudes. Then, IMU based northfinding algorithm gets data from IMU and calculates the azimuth of the motion simulator for each attitude.

In this section, characteristics of the three-axis motion simulator are explained. Furthermore, properties of the inertial sensors that are used in the tests are introduced.

6.3.1 Three-Axis Motion Simulator

Three-Axis Motion Simulator features three servo controlled orthogonal axes. This allows precision positioning of an inertial guidance component or system to any attitude. Smooth rates over a wide dynamic range and precision positioning accuracy are key characteristics of this system.

Three-axis motion simulator possesses three degree of freedom in its motion and it can realize all rotational motion in three-dimensional space. In Figure 68, photograph of motion simulator is seen. Characteristics of motion simulator can be learned from Table 4. With this characteristics motion simulator can emulate all F16 maneuvers.

Figure 68. Three-Axis Motion Simulator

Table 4. Characteristics of Motion Simulator

Degree of Freedom	3 (gimbal)
Position Precision	0.0003^{o}
Highest Velocity	$1000^{o}/s$ (inner axis) $750^{o}/s$ (middle axis) $500^{o}/s$ (outer axis)
Highest Acceleration	$1660^{o}/s^{2}$(inner axis) $590^{o}/s^{2}$(middle axis) $660^{o}/s^{2}$(outer axis)
Measurement Mechanization Precision	3 min (rough) 1 sec (precise)

6.3.2 Inertial Sensors

Testing of IMU based northfinding approach requires high-quality gyros with precision and accuracy sufficient to measure earth rate as it has a small value. However, accelerometers can be worse since it measures larger value, which is gravitational force. In this method, IMU, which consists of three Fiber Optic Gyroscopes (FOG) and three MEMS accelerometers, is used. In Table 5, performance characteristics of FOG are shown and in Table 6, performance characteristics of MEMS accelerometers are seen.

Table 5. Performance Characteristics of FOG

Rate Bias	$\leq 1^o / h$ (1σ)
Random Walk	$\leq 0.1^o / \sqrt{h}$
Scale Factor Error	$\leq 500 ppm$ (1σ)
Maximum Measurement Range	$\pm 1000^o / s$
Axis Misalignment	$\pm 10 mrad$ (absolute) $\pm 1 mrad$ (stability)
Initialization Time	$\leq 120 ms$

Table 6. Performance Characteristics of MEMS Accelerometer

Measurement Range	±10 g
Scale Factor **Repeatability (day to day) (1 σ)** **Stability(short term)**	 500 ppm 200 ppm
Bias **Repeatability (day to day)(1 σ)** **Stability(short term)**	 1 mg 0.2 mg
Noise Equivalent Acceleration	<250μg/ $\sqrt{s}$

6.4 Simulation Results

In this study, eight experiments have been realized for IMU based northfinding algorithm. Strapdown IMU is placed into three-axis motion simulator. Afterwards, motion simulator is operated at eight different attitudes. At each attitude, inertial sensors in strapdown IMU sense accelerations and angular rates at each axis of the body, which is the motion simulator. Then, inertial sensors outputs are processed in IMU based northfinding algorithm to find azimuth of the vehicle for each attitude. Assuming a local level geographic N-E-D frame as navigation frame, eight different attitudes of motion simulator are in Table 7 as follows.

Table 7. Attitude of Motion Simulator for Each Experiment

Experiment Number	X-Axis of Motion Simulator Points at local geographic navigation frame	Y-Axis of Motion Simulator Points at local geographic navigation frame	Z-Axis of Motion Simulator Points at local geographic navigation frame
1	West	North	Down
2	North	East	Down
3	East	South	Down
4	South	West	Down
5	West	Up	North
6	North	Up	East
7	East	Up	South
8	South	Up	West

As a result, IMU based northfinding algorithm calculation outputs are in Table 8 for each experiments.

Table 8. Calculated Azimuth and True Azimuth for Each Experiment

Experiment Number	Calculated Roll of Motion Simulator (degree)	Calculated Pitch of Motion Simulator (degree)	Calculated Azimuth of Motion Simulator (degree)	True Azimuth of Motion Simulator (degree)
1	-0.1211	-0.0394	-93.1806	-90
2	-0.1058	-0.0051	-1.8492	0
3	-0.0704	-0.0142	94.9229	90
4	-0.0808	-0.0472	175.8582	180
5	-90.1449	-0.0103	-91.3591	-90
6	-90.1328	0.0217	1.0726	0
7	-90.0984	0.0106	88.8216	90
8	-90.1093	-0.0221	-179.8368	-180

These experiment results are a bit different from true azimuth. This is due to gyroscope rate bias, accelerometer bias and latitude of the vehicle as mentioned above. Considering these experiments are conducted at latitude of 39 ^{o} 55", gyroscope rate bias is as shown in Table 5 and accelerometer bias is as seen in Table 6, following error range is expected for azimuth calculation:

$$\phi_d = [\frac{\delta f_y}{g}\tan\phi + \frac{\delta w_y}{w_{i/e}\cos\phi}] \qquad (6.22)$$

$$\phi_d \leq 4.9615^{o}$$

Where:

ϕ : Latitude of the vehicle, $39^o 55^{''}$

δw_y : Gyroscope rate bias stability, $\leq 1^o / h$ (1σ),

δf_y : Accelerometer bias stability, 1 mg,

$w_{i/e}$: Earth rotation rate, 15.041^o/h,

g : Gravity.

Looking to the results, IMU based northfinding technique calculates the azimuth of the vehicle within 5^o. However, this error can be improved by using more accurate inertial sensors. Nevertheless, as the accuracy of the inertial sensor gets better, cost of the sensor is higher. In addition, if the azimuth error equation 6.21 is examined, IMU based northfinding algorithm results are better near the equator where latitude is nearly 0^o but worse near the poles where latitude 90^o. Explanation to this is that, as goes to poles Earth rotation rate and gravity force cancel each other and measured signals are smaller. Therefore, signal to noise ratio is smaller.

6.5 Summary

As a conclusion, in this chapter, IMU based nortfinding algorithm is introduced. Simulation environment and simulation results are discussed. In addition, some error sources and effects of them are examined.

Briefly discussing the algorithm, measurements of inertial sensors, which are placed vehicle's three body coordinate axes, are taken and related with known gravity vector and earth rotation rate vector at navigation frame by means of direction cosine matrix. Then, these relations are exploited to find direction cosine matrix. Finding north is an easy task if direction cosine matrix is known.

Let us discuss advantages and disadvantages of finding north with IMU.

Advantages of the system are

1. Finding north by using strapdown IMU is straightforward.

2. It is unlike GPS azimuth determination implementation, which is subjected to signal blockage and jamming. The IMU based northfinder is inherently un-blockable and un-jammable.

3. Unlike a magnetic compass measurement, it is not subject to external influences and does not point to magnetic north. IMU based northfinder provides an azimuth reference relative to true north.

4. IMU based northfinder can provide an alignment in heavily wooded areas, mountainous areas, in cities, in buildings, underground in tunnels and mines or drilled shifts and under water.

5. If better inertial sensors are used, systems that are more accurate can be implemented.

However, there are various limits to the accuracy of IMU based northfinder. Disadvantages of the system are

1. Latitude at which it is operating is a problem. Near equator, system immune to noise is very good but near poles, it is worse.

2. Another significant limit is the noise of the gyroscopes being used for the measurement.

3. Accelerometer bias stability affects the accuracy.

4. IMU consists of three accelerometers and three gyroscopes so it is a very expensive system as compared to the others.

5. IMU consumes more power and heavier as compared to other systems.

6. Gyroscope precision is more important. Since it senses small value, which is Earth rotation rate. Looking equation 6.22, worse accelerometers can be used since gravity force is very big with respect to accelerometer bias.

CHAPTER 7

CONCLUSION

In this chapter, we will make an overall assessment of the thesis work.

In this thesis, importance of northfinding is discussed and four different techniques, which are GPS based northfinding with exhaustive search, GPS based northfinding with Kalman filter, accelerometer based northfinding and IMU based northfinding techniques, are implemented. The performances, advantages and disadvantages of these four techniques are examined. The comparisons of them are given. In addition, a realistic GPS Emulator is designed to provide raw navigation data to GPS based northfinding techniques.

7.1 Summary of Chapters

To test the GPS based northfinding techniques, a realistic stochastic model for a general-purpose GPS receiver is developed. Twenty-four satellite tracks are simulated and the GPS emulator reports the satellites that are detectable in a real time scenario. Two basic criteria for satellite detection are defined; other constraints can also be implemented in the emulator. Moreover, realistic errors of GPS are considered on pseudorange measurements and carrier phase measurements.

GPS based northfinding technique with exhaustive search is introduced. In this technique, single differences of GPS signal carrier phases are used as observables. The critical problem of GPS based northfinding techniques is the carrier phase ambiguity since the receiver measures only the fractional part of carrier phase and integer part remains unknown. Integer search technique, which relies on checking all possible integer sets for each satellites and antenna combination, is developed to solve this problem. In addition, main error sources of this technique are discussed and performance of the technique is presented. It is seen that accuracy of the technique depends on baseline length and multipath effect.

GPS based nortfinding technique with Kalman filter is presented. Double differences of GPS carrier phases are the main observables central to this technique. To solve the integer ambiguity and to detect the north, Kalman filter is used. Initial rough attitude is found by taking triple difference of observations. Then, this rough initial attitude is used as initial condition at integer estimator. With known integer set and found initial condition, attitude estimator based on application of Kalman filter on double phase differences calculates the north angle. In addition, main error sources of this technique are discussed and performance of the technique is presented. It is seen that accuracy of the technique depends on baseline length and multipath effect.

If we compare the two GPS based techniques, they both use the same GPS signals. However, both data collection and processing of this data are different for two techniques. For the technique with exhaustive search, data is collected at one instant. On the contrary, data is collected in an adequate time period for the technique with Kalman filter. Therefore, as compared according to data collection time, exhaustive search technique is superior. Nevertheless, in processing this data, as the baseline gets longer, computational effort of exhaustive search is much bigger since number of integer sets increases exponentially with the baseline length. For the technique with Kalman filter, computational load does not change significantly as the baseline length changes. Both techniques are affected mainly by multipath error. However, taking double differences of carrier phase measurements between antennas and satellites reduces receiver, satellite and common multipath errors in the technique with Kalman filter. Therefore, technique with Kalman filter can tolerate errors much better. In addition, sometimes algorithm with exhaustive search can go to wrong results in practice since there may be more than one possible integer sets at that instant. Considering the all the above comments and experiment results, technique with Kalman filter is superior as compared to the technique with exhaustive search.

Accelerometer based northfinding technique is the other technique which is presented in this thesis. This technique relies on measurements of vertically placed linear accelerometer on a rotating platform. The observable in this technique is Coriolis acceleration generated when the accelerometer travels on a circular path with respect to a moving frame. Formulas for extracting the azimuth from this measurement are developed. Moreover, errors of accelerometer based northfinding technique are examined. Its most obvious errors come from the inclination of the platform and the accelerometer bias. In addition, at the time of northfinding process, working machines, moving people around the system can distort the operation of the system. It is seen that accelerometer based northfinding technique is cheap. However, its practical implementation is difficult, since a platform that rotates at high speed is required and very accurate accelerometer is needed. Nevertheless, if these shortcomings are overcome, it presents an advantage in terms of the system cost.

IMU based northfinding technique uses measurements of inertial sensors such as gyroscopes and accelerometers, which are placed at vehicle's three body coordinate axes. To find north, measurements of the two vectors of Earth are needed. They are gravity vector, which is sensed by accelerometers and Earth rotation rate vector that is sensed by gyroscopes. If another vector is constructed perpendicular to them, the direction cosine matrix, which establishes the relation of body and navigation frame, is calculated by using these three vectors. Finding north is an easy task if the direction cosine matrix is known. The accuracy of IMU based northfinding technique depends on accelerometer bias stability, gyroscope bias stability and the latitude of the vehicle. However, gyroscope precision is more important, since it senses a smaller quantity, which is Earth rotation rate. Although, it is an easy task to find the north angle with IMU, it is very expensive since it requires three accelerometers and three high precision gyroscopes. In addition, as compared to GPS cases, its north angle error is larger.

7.2 Comparison of the Northfinding Techniques

In the past, attitude determination or northfinding problem was solved using techniques based on inertial elements. Such techniques were associated with complex algorithms and control mechanisms. In addition, an IMU is typically very expensive, heavy, power hungry, requires long settling times and is degraded at high latitudes. Accelerometer based northfinding is a new and inexpensive method but its practical implementation is difficult for the present. However, both of these methods are not affected from external means since they measure the north angle by means of their inertial elements. Attitude determination or northfinding using GPS receivers is characterized by being simple, economic, more compact and less complex than other techniques. This new GPS technology has many potential applications, such as replacing large and costly IMU on ships, or at least to allow the use of lower cost IMU. It could provide heading information in the polar region where inertial systems fail. It could provide rapid and precise sensor pointing. Furthermore, the elimination of many different sensor devices and their interfaces can yield a substantial benefit in system reliability. In addition, its accuracy is better than the other techniques. GPS based northfinding method with Kalman filter is superior than GPS based northfinding technique with exhaustive search, since its accuracy is higher and computational load is smaller. However, GPS based northfinding technique measurements are external signals that can be blocked or jammed. The whole results and comparisons of four northfinding techniques, which are implemented in this thesis, can be seen in Table 9 .

Table 9. Comparison of Four Northfinding Techniques

	GPS based with Kalman Filter	GPS with Exhaustive Search	Accelerometer based	IMU based
Components	2 GPS Antennas	2 GPS Antennas	1 Accelerometer & platform	3 acc & 3 gyro
Accuracy	0.08°	0.5°	0.2°	5°
Cost	inexpensive	inexpensive	expensive	expensive
Practical Usage	Yes	Yes	Not Yet	Yes
Dependency	External signals	External signals	Internal means	Internal means
Geographic Coverage	Depends on signal reception	Depends on signal reception	Degraded at high latitudes	Degraded at high latitudes
Computational complexity	Low	High	Low	Low

In northfinding subject, there are not many adequate sources. This thesis is a good collection of references of northfinding. In addition, realistic implementations and comparisons of different northfinding techniques are done to make integrated northfinding systems possible.

7.3 Future Work

In this thesis, implementations and comparisons of four northfinding techniques are given. In the future, integration of different techniques can be considered, especially GPS and IMU based northfinding techniques. Since, they have the potential to compensate each other's errors.

In the future, implementation of GPS based northfinding techniques can be done with real GPS receivers. While studying on this thesis, real data is collected from two Trimble GPS receivers. However, synchronization problems pose a main obstacle. Since a dedicated electronic and mechanical design is required. Therefore, a dual-antenna GPS receiver can be used to overcome the synchronization problem. For example, Trimble produces MS860, which is a rugged dual antenna GPS receiver for precise heading and position. With this dual antenna GPS receiver and the GPS northfinding techniques implemented in this study, real GPS based northfinding systems can be constructed.

REFERENCES

[1] Ellis, J.F. and G.A. Creswell, "Interferometric Attitude Determination with the Global Positioning System" Journal of Guidance and Control, 2(6):522-527, Nov.-Dec., 1979.

[2] Joseph, K. M. and P.S. Deem, "Precision Orientation: A new GPS Application," International Telemetering Conference, San Diego, California, Oct., 1983.

[3] Kruczynski, L.R., P.C. Li, A.G. Evans and B.R. Hermann, "Using GPS to determine Vehicle Attitude: U.S.S. Yorktown Test Results," Proceedings of ION GPS-1989, Colorado, Sept. 1989.

[4] Chesley, B. and P. Axelrad, "An Integrated GPS Attitude Determination System for JAWSAT," Proceedings of ION GPS-94, Salt Lake City, Utah, Sept. 20-23,1994, pp. 1251-1261.

[5] Wolf, R.G. Hein, B. Eissfeller and E. Loehnert, "An Integrated Low Cost GPS/INS Attitude Determination and Position Location System," Proceedings of ION GPS-96, Kansas City, Missouri, Sept. 17-20, 1996, pp.975-981.

[6] Schwarz, K.P., El-Mowafy and M. Wei, "Testing a GPS Attitude System in Kinematic Mode," Proceedings of ION GPS-92, Albuquerque, New Mexico, Sept. 16-18, 1992, pp.801-809.

[7] Mercer, J.A., R.R. Ryan and H.A. Kolve, "United States Navy Applications of a GPS Attitude and Position Measurement System," Albuquerque, New Mexico, Sept. 16-18, 1992, pp.783-791.

[8] Diefes, D.L., G.G. Hazel and D.F. Greenlee, "GPS Attitude Determining System for Marine Navigation," Proceedings of ION GPS-93, Salt Lake City, Utah, Sept. 22-24, 1993, pp.649-655.

[9] Spalding, J. and M. Lunday, "Results of Testing on a GPS-Based Compass," Proceedings of ION GPS-95, Palm Springs, California, Sept. 12-15, 1995, pp. 941-948.

[10] Cohen, C.E. and B. W. Parkinson, "Aircraft Application of GPS Based Attiude Determination," Proceedings of ION GPS-92, Albuquerque, New Mexico, Sept. 16-18, 1992, pp.775-782.

[11] Cannon, M.E. and H. Sun, "Assessment of a Non-Dedicated GPS Receiver Sytem for Precise Airborne Attitude Determination," Proceedings of ION GPS-94, Salt Lake City, Utah, Sept. 20-23,1994, pp. 645-654.

[12] Kruczynski, L.R., J. Delucchi and T. Iacobacci, "Results of DC-10 Tests Using GPS Attitude Determination," Proceedings of ION GPS-1995, Palm Spring, California, Sept. 12-15, 1995. pp. 1743-1750.

[13] Cohen, C.E., E.G. Lightsey, B. W. Parkinson and W.A. Feess, "Space Flight Tests of Attitude Determination Using GPS: Preliminary Results," Proceedings of ION GPS-93, Salt Lake City, Utah, Sept. 22-24, 1993, pp.625-632.

[14] Brock, K., R. Fuller, S. Hur-Dias and J. Rodden, "GPS Attiude and Orbit Determination for Space" Proceedings of ION GPS-94, Salt Lake City, Utah, Sept. 20-23, 1994, pp. 1243-1250.

[15] Cohen, C.E., "Attitude Determination Using GPS," Ph. D. Dissertation, Stanford University, Dec. 1992.

[16] Yunchun Yang, Hatch R. R. and Sharpe R.T., "Minimizing the Integer Ambiguity Search Space for RTK", 2003.

[17] Crassidis L. John, Markley F. Landis, Lightsey E. Glenn, "Fast Integer Ambiguity Resolution for GPS Attitude Determination", AIAA-99-3967.

[18] Sutton Eric, "Integer Cycle Ambiguity Resolution Under Conditions of Low Satellite Visibility", IEEE 2002.

[19] Zazzera F. Bernelli, Molina M., Vanotti M., Vasile m., "New Algorithm for Attitude Determination Using GPS Signals", XVI Congresso Nazionale AIDAA, 24-28 Settembre 2001, Palermo.

[20] Crassidis L. John, Markley F. Landis, Lightsey E. Glenn, "Global Positioning System Integer Ambiguity Resolution without Attitude Knowledge", AIAA Journal of Guidance, Control and Dynamics, Vol. 22, No. 2, March-April 1999, pp. 212-218.

[21] Lopes Roberto, "Integer Ambiguity Resolution for Spacecraft Attitude Determination Using GPS", ION GPS 2002 Portland, OR

[22] Chu Q. P., Woerkom Van P. Th. L. M. "GPS for Low-Cost Attitude Determination: A review of concepts, In-Flight Experiences, and Current Developments", Acta Astronautica Vol. 41, 1997.

[23] Ron Brown, Phil Ward, "A GPS Receiver with Built-in Precision Pointing Capability", IEEE 1990.

[24] M. Martin-Neira, R. Lucas, M.A. Martinez, "Attitude Determination with GPS: Experimental Results", IEEE AES Magazine, September 1990.

[25] J. Rath, P. Ward, "Attitude Estimation Using GPS", presented to National Technical Meeting of the Institute of Navigation, San Mateo, CA , January 1989.

[26] Graas Van Frank, Braasch Michael, "GPS Interferometric Attitude and Heading Determination: Initial Flight Test Results", Journal of the Institute of Navigation, Vol.38, No. 4, Winter 1991-92.

[27] Juang Jyh-Ching and Huang Guo-Shing, "Development of GPS-Based Attitude Determination Algorithms," IEEE Transactions on Aerospace and Electronic Systems, Vol. 33, No. 3, July 1997.

[28] Kruczynski, L.R., A.G. Evans, "Using GPS to determine Vehicle Attitude," Proceedings of ION Int. Tech. Mtg., 1988, p139-145.

[29] Brown A. Ronald. "Instantaneous GPS Attitude Determination", IEEE AES Magazine, June 1992.

[30] Richard D. Jurgens and Rodgers E. Charles, "Advances in GPS Attitude Determining Technology as Developed for the Strategic Defense Command", Proc. ION Int. Mtg., 1991, pp 45-51

[31] Richard D. Jurgens and Rodgers E. Charles and Fan C. Leopold, "GPS Azimuth Determining System (ADS) Cycle Resolution, System Design, and Army Test Results," Proc. ION Int. Mtg., 1991, pp 991-999.

[32] BAR-ITZHACK Itzhack Y., REINER Jacob, NARODITSKY Michael, "New Inertial Azimuth Finder Apparatus", Journal of Guidance, Control and Dynamics, Vol. 24, No.2, March-April 2001.

[33] GU Qitai, SUN Guofu, "Accelerometer Based North Finding System", IEEE Transaction, 2000.

[34] Lİ Benliang, GU Qitai, LİU Xuebin, "Study and Simulation on Dynamic Gyroless North Finder", IEEE Transaction, 2000.

[35] Rogers M. Robert, "Applied Mathematics in Integrated Navigation Systems", AIAA, 2000.

[36] Tittreton D.H., Weston J.L, "Strapdown Inertial Navigation Technology", 1997.

[37] Farrell A. JAY, Barth Matthew, "The Global Positioning System and Inertial Navigation", McGraw-Hill, 1999.

[38] Mohinder S.Grewal, Lawrence R.Weill, Angus P.Andrews, Global Positioning Systems, Inertial Navigation, and Integration, A John Wiley & Sons, Inc. Publication, 2001.

[39] Gunaydın E., Oguz P., Sonmez T., "Implementing a GNSS Emulator for Navigation Systems," 6^{th} International ESA Conference on Guidance, Navigation & Control Systems, 17 – 20 October 2005.

[40] Robert M. Rogers, Applied Mathematics in Integrated Navigation Systems, AIAA Education Series, 2000.

[41] James Bao, Yen Tsui, Fundamentals of Global Positioning System Receivers- A Software Approach, Wiley Interscience Publication, 2000, New York, NY.

[42] GPS Interface Control Document, ICD-GPS-200C-004, 12 April 2000.

[43] Bradford W. Parkinson, James J. Spilker Jr., Global Positioning System: Theory and Applications Volume II, American Institute of Aeronautics and Astronautics, Inc., 1996, Washington, DC.

[44] Yu Wenbo, Gao Guojiang, ZhaoYan and Lin Minmin, "An Accurate Kinematic Relative Positioning Algorithm Based on the Single Frequency Carrier Phase", The Fifth Lab, Beijing University of Aeronautics and Astronautics *No. 37 of xueyuan road, Beijing 100083, China.*

[45] Mcmillan J. Chris. "A GPS Attitude Error Model for Kalman Filtering", Defense Research Establishment, 1994.

[46] Arslan T., Jiangning Xu, Wan Dejun, WANG Qing. "GPS Attitude Determination Algorithm", IEEE Transaction, 2002.

[47] Kelly Alonzo. "Modern Inertial and Satellite Navigation Systems", 1994.

[48] Jong Hoon Kim, "Design and Simulation of a Stand-Alone GPS Attitude Determination System", Dissertation 1994.

[49] Brown Robert Grover, Hwang Y.C. Patrick, "Introduction to Random Signals and Applied Kalman Filtering", John Wiley and Sons, Inc 1997.

[50] Samuel Merhav, Aerospace Sensor Systems and Applications, Springer, 1996.

[51] Pitman, G.P., “Inertial Guidance”, Wiley, New York, 1962,